*Author:*
**Plasting, Stephen Christopher**

*Title:*
**Turbulence has its limits : a priori estimates of transport properties in turbulent fluid flows**

# TURBULENCE HAS ITS LIMITS:

## *a priori* estimates of transport properties in turbulent fluid flows


Stephen Christopher Plasting

School of Mathematics

February 2004

A dissertation submitted to the University of Bristol
in accordance with the requirements of the degree
of Doctor of Philosophy in the Faculty of Science

# PAGE NUMBERING AS ORIGINAL

# Abstract

This thesis studies a variational approach to extract information about turbulent flows directly from the governing equations. We develop a numerical technique for solving the optimal equations of the background method of Constantin–Doering–Hopf. We use this to calculate the optimal solution for the problem of plane Couette flow and estimate that the energy dissipation rate $\epsilon \leq 0.008553$ as $Re \to \infty$ in units of $V^3/d$. Busse's assumption that the optimal solutions are independent of the streamwise coordinate is verified by a three-dimensional eigenvalue calculation. We extend the standard background method to include a linear stability constraint on the optimal mean profile. The Euler–Lagrange equations are deduced, a solution programme is described and preliminary findings are discussed.

Our numerical technique is then applied to finding the solution which maximises the heat transport to the infinite Prandtl number convection problem studied by Chan. Two boundary conditions are considered; no-slip and stress-free. We also use a method of Otero, with an enlarged set of test functions having non-zero channel-interior gradient, to calculate simple conservative estimates of the optimal asymptotic scaling of the global heat transport. We find that for the no-slip problem we can estimate the dimensionless heat transport $Nu \leq 0.139\, Ra^{1/3}$ as $Ra \to \infty$. For the stress-free problem we cannot discern the asymptotic scaling for the optimal solution but instead with the aid of the conservative estimate we can deduce that $Nu \leq c_2 Ra^{\gamma}$ as $Ra \to \infty$ where $2/5 \leq \gamma \leq 5/12$ and $c_2$ is a constant.

Our development of these two physical problems illuminates features of the duality relationship between the optimum theory of Howard–Busse and the background method of Constantin–Doering. We conclude that a worthy future direction for study of these variational problem, is in making extensions using additional constraints rigorously derived from the governing equations or based on empirical hypothesis.

For my parents

# Acknowledgements

Firstly I wish to thank my family and friends, particularly my parents, Susan and Phillip, for their continuous support and encouragement throughout my studies. Special thanks go to my long-time friends, John Malone–Lee and Martin, Kasia and Sophia East, and to Laura Bird who deserves a full page of thanks.

And also to my two scientific shepherds, my adviser Dr Richard Kerswell, for his suggestion of this topic and his never-failing ability to shed light on problems that I had thought insoluble; and Professor Glenn Ierley for his enthusiasm and for introducing me to the delights of numerical analysis.

I also wish to thank a number of scientists, Friedrich Busse, Charlie Doering and Jesse Otero, whose assistance during my work has challenged my thinking and contributed to my understanding. Thanks also to Martin Holthaus and Nikolay Vitanov for their help in clarifying points and sharing results.

I thank the support staff at Bristol University, in particular the Computing Officers, Ian Stewart and Jason Hogan–O'Neill for providing and supporting access to top quality computing facilities.

I also wish to thank Dr Colm Caulfield for his hospitality during my visit to UCSD and whose criticism has encouraged me in my work.

Thanks also go to my colleagues and friends in the Mathematics Department, in particular Kristín Hákonardóttir, Matt Leifer, Miguel Marques dos Santos, Brian Winn and Matt Nunes for the many memorable times spent as a graduate student.

Thanks also go to the organisers of the Geophysical Fluid Dynamics Program 2002, Woods Hole Oceanographic Institute, and to the many good friends made there.

Finally, I wish to gratefully acknowledge the financial support of EPSRC.

# Author's Declaration

I declare that the work in this thesis was carried out in accordance with the Regulations of the University of Bristol. The work is original except where indicated by special reference in the text and no part of the dissertation has been submitted for any other degree. Any views expressed in the dissertation are those of the author and do not necessarily represent those of the University of Bristol. The thesis has not been presented to any other university for examination either in the United Kingdom or overseas.

Stephen Christopher Plasting

Date: 16th January 2004

# Contents

# Notation

Space and time averages:

$$\overline{(\cdot)} = \lim_{L_x,L_y\to\infty} \frac{1}{4L_xL_y} \int_{-L_x}^{+L_x} \mathrm{d}x \int_{-L_y}^{+L_y} \mathrm{d}y(\cdot) \quad \text{horizontal space average}$$

$$\langle\cdot\rangle = \int_{-1/2}^{1/2} \overline{(\cdot)}\mathrm{d}z \quad \text{global space average}$$

$\|f\|^2 = \langle |f|^2 \rangle$ $L_2$ norm on scalar function

$\|\mathbf{g}\|^2 = \langle \mathbf{g}^* \cdot \mathbf{g} \rangle$ $L_2$ norm on vector function

$(\mathbf{a}, \mathbf{b}) = \langle \mathbf{a}^* \cdot \mathbf{b} \rangle$ complex inner product

Derivative operators:

$\mathrm{D} \equiv (\,)' \equiv \mathrm{d}/\mathrm{d}z$ $z$-derivative

$\boldsymbol{\nabla} = \left(\frac{\partial}{\partial x}, \frac{\partial}{\partial y}, \frac{\partial}{\partial z}\right)$ gradient operator

$\nabla^2 = \frac{\partial^2}{\partial x^2} + \frac{\partial^2}{\partial y^2} + \frac{\partial^2}{\partial z^2}$ Laplacian operator

$\nabla^4 = (\nabla^2)^2$ bilaplacian operator

$\frac{\delta \mathcal{L}}{\delta \mathbf{a}}$ : if $\mathcal{L} = \langle f(\mathbf{a}) \rangle$ define Fréchet derivative

$$\left\langle \frac{\delta \mathcal{L}}{\delta \mathbf{a}} \cdot \delta\mathbf{a} \right\rangle = \lim_{\epsilon\to 0} \frac{1}{\epsilon} \left( \langle f(\mathbf{a} + \epsilon\, \delta\mathbf{a}) \rangle - \langle f(\mathbf{a}) \rangle \right)$$

Vectors:

$\mathbf{a} = (a_1, a_2, a_3)$ three-tuple

$\boldsymbol{u} = (u, v, w)$ velocity vector

$\widehat{\boldsymbol{\nu}}$ vector with zero horizontal-mean

Eigenvalue problems:

$\mu$ commonly eigenvalue

$\overline{\mu}$ most positive eigenvalue

$a^*$ complex conjugate of $a$

$\Psi^\dagger$ adjoint eigenfunction of $\Psi$

Miscellaneous:

$\mathfrak{Re}()$ / $\mathfrak{Im}()$ real / imaginary part

$a_{opt}$ optimal value of $a$

$j$-$k$ or $j$-mode optimal solution will $j$ associated wavenumbers

# List of Figures

# Chapter 1

# Introduction

Scaling laws appear almost everywhere in the mathematical study of the macroscopic behaviour of physical systems. The details of a scaling law often gives insight into the underlying principles governing the fundamental mechanisms of a complex system. Scaling laws are studied in such diverse subjects as the biological sciences where, for example, scaling in cell populations is inferred from the underlying nutrients network in an organ; or in financial markets where price changes follow power-laws due to the aggregate effect of interacting agents. In a complex system experiencing both temporal and spatial fluctuations the small scale behaviour may look tremendously complicated; while aggregate properties follow a simple law such as a pure power law as a function of a control parameter. Turbulence in fluid flows is a phenomenon which exhibits strong spatial intermittency of local structure; flows have both spots of strong vorticity and of quiescence: while the global properties of the turbulence, the *turbulent statistics*, are believed to follow scaling laws as a function of the Reynolds number of the flow.

Classical turbulence research, with major contributors such as von Kármán, Kolmogorov, Prandtl and Taylor (for details see either Tennekes & Lumley (1972), Frisch (1995) or Pope (2000)) focuses mainly on statistical analysis of the small-scales of motion in a turbulent fluid. The canonical flow setup often investigated by turbulence researchers is unbounded three-dimensional flow with some form of body forcing to sustain a turbulent flow. Intuitive physical arguments and dimensional analysis, without mathematical foundation or analytical derivation, are used to es-

tablish power-laws for spectral statistics and correlation functions. Experimental data plays a key role in validating hypotheses. One of the most notable predictions (due to Kolmogorov and Obukhov) based on dimensional analysis is that the energy spectrum of a 3-D turbulent flow behaves as $k^{-5/3}$ over a wide range of wavenumbers $k$. The great Russian Mathematician A. N. Kolmogorov once said of turbulence "that there is no chance to develop a closed purely mathematical theory". Even so, he and several other eminent turbulence researchers suggested semi-empirical hypotheses which were based on expressions for mean velocity components derived from the Navier–Stokes equations and supplemented with a 'closure hypothesis' for the Reynolds stress. A notable achievement of semi-empirical analysis of large-scale properties of turbulence is the logarithmic friction law for shear flows which implies that the energy dissipation is not independent of viscosity $\nu$; the prediction is that it vanishes proportional to $[\log(1/\nu)]^{-2}$ as $\nu \to 0$ when all other parameters are held fixed.

In the past couple of decades, mathematicians, armed with the tools of functional analysis, have worked on rigorously deriving some of the results of turbulence earlier based on only phenomenological arguments, directly from the Navier-Stokes equations (henceforth denoted NSE); for example see Doering & Gibbon (1995) or Foias, Manley, Rosa & Temam (2001). This modern approach is a complementary technique to the statistical or dimensional analysis methods. Semi-empirical theories are obviously capable of making bolder predictions than rigorous analysis due to the use of uncontrolled approximations in the former, however, it is certainly interesting to see exactly what aspects of fluid turbulence can be derived from only rigorous analysis.

Much interest also surrounds the practical problems of fluid dynamics, such as thermal convection or shear flows. For mathematical simplicity, the flow domain is extended to an infinite layer; or equivalently horizontal periodicity for all flow fields is assumed. Engineering type questions associated with the global nature of a turbulent flow are studied by theoreticians. An example of such a question is: how does turbulence change the heat transport properties of a layer of fluid being heated from below? Theories may be based on integral moments of the governing equations — for example the *power constraints* which are the first moments of the NSE or of

the Boussinesq equations for convection — that describe the time evolution of global quantities. In the absence of a method for solving the NSE at high Reynolds number scientists have become adept at making hypotheses about such equations. Indeed, in the combined experimental and theoretical papers of Malkus (1954*a*,*b*), two important theories are postulated which are historically the original inspiration for the research area of "Bounds on Turbulent Transport" from which this thesis is borne. Malkus's theories relate to the mean properties of a turbulent flow, specifically convection in an infinite layer heated from below, without resolution of, or reference to, local details of the fluid flow. The first hypothesis is that amongst all possible solutions of the governing equation the realised flow is the one which maximises the heat transport across the layer. The second hypothesis is that the smallest scale of motion is determined by being just neutrally stable as an infinitesimal perturbation on the mean field. The maximum heat transport problem will hereafter be referred to as Malkus's *first* theory and the linear stability problem on the mean field will be referred to as Malkus's *second* theory.

Malkus's first theory can be reduced to a simplified hypothesis that solutions maximise the heat transport even amongst fields which satisfy only a small number of integral consequences of the governing equations. The validity of this reduction is based on the proposition that the critical elements of these equations are contained in the small set of integral constraints. Owing to the absence of analytical solutions to the governing equations, this reduced problem was felt to be a natural first step towards testing Malkus's first theory. Thus in the paper Howard (1963) the first mathematical formulation of the maximum heat transport problem was made, and a variational problem was solved for two different groups of constraint. First, Howard showed that amongst fields which satisfy the two power constraints of the Boussinesq equations, but without including incompressibility, the solution maximising the heat transport[1] has associated heat transport which scales as $Ra^{1/2}$. With the imposition of the differential incompressibility-constraint and the power constraints, Howard showed that for fields with a *single* horizontal mode[2] the maximum attainable heat

[1]This maximiser will often be referred to as the *optimal solution* of the Euler–Lagrange equations for the variational problem.

[2]Howard conjectured that the minimum of his variational functional $\mathscr{F}$, or equivalently the maximum heat transport, was achieved by a solution with a single horizontal modes. This conjecture was later found to be true only for a limited range of the Rayleigh number in Busse (1969*b*).

transport scales as $Ra^{3/8}$. Howard concluded that since the mean properties of the maximising flows were found to resemble mean properties of real flows then the results tended to support Malkus's first hypothesis. The subject of calculating upper bounds on global transport quantities at high Rayleigh numbers was thus born in Howard's 1963 theoretical paper.

Howard's variational problem which included the incompressibility constraint was further developed in Busse (1969*b*). Busse found that the assumption that the optimal solution has only a single horizontal wavenumber was not globally valid for all values of the Rayleigh number. Instead, the maximiser undergoes transition from a single wavenumber solution to a two wavenumber solution and so on *ad infinitum*, with many nested boundary layers for high Rayleigh numbers. This class of optimal solution with a multiple boundary-layer structure has since been termed the *multi-$\alpha$ solution* in the literature[3]. The upper bound on the heat transport attained by this enlarged solution set scales as $Ra^{1/2}$ in common with Howard's first exact result which disregarded incompressibility, albeit with a much lower numerical coefficient. Busse's theory is an asymptotic result involving matching of the Euler–Lagrange equations in the three different regions of each of the nested boundary layers. In his paper he states that: "there are strong reasons [...] that this class of solution describes the correct upper bound on the heat transport among all possible solutions of the Euler equations". This statement will be validated in Chapter 2 of this thesis by solving the Euler–Lagrange equations numerically. The realisation that the single-$k$ solution is the first member of the multi-$k$ class of solution implies that the exponent of the empirically measured heat transport must be a function of the Rayleigh number also: starting at 3/8 and rising to 1/2 with increasing Rayleigh number.

Over the next two decades, after Howard first formulated a theory to test Malkus's principles, research progressed swiftly. Busse coined the phrase *Optimum Theory* for the burgeoning field[4] and extended the theory to turbulent shear flows in Busse (1970), while Chan (1971) applied the multi-$k$ technique to infinite Prandtl number convection. Both Howard and Busse published review articles

[3]Note that Busse denoted the spanwise wavenumber by $\alpha$, while in this thesis we use $k$ and hence we use the terminology multi-$k$ instead.

[4]The underlying approach is also referred to as the Howard–Busse (or HB) method.

on the progress in the area; see Howard (1972) and Busse (1978). The consensus view on Malkus's first theory was that no maximum transport principle exists for heat transport, or analogously momentum transport for shear flows, but that instead turbulent flows should be interpreted in terms of the stability of the viscous boundary-layer. In Busse (1978) one can find a complete discussion of the state of the research area toward the end of the 1970s, with a nice discussion of the complex multi-$k$ solution technique and the problems to which it had been applied. Turbulence is often synonymous with a flow structure of many coupled modes and with discrete transitions particularly in turbulent convection. The multi-$k$ solutions show a strong resemblance to this picture of turbulence but not to a 'fully developed' turbulent state with a continuous spectrum of wavenumbers. Howard's review article is a rather graceful account of the application of variational calculus in fluid dynamics and of 'turbulence theories'. Instead of solving the Euler–Lagrange equations for the Howard–Busse problem in plane Couette flow he uses direct functional estimates to derive upper bounds on the single-$k$ and double-$k$ solutions, which support Busse's predictions, but without resulting to a 'boundary-layer' approach. The conclusion of Howard's paper, was that more comprehensive direct methods were needed in order to simplify the procedure of calculating upper bound estimates, and that a feasibility study of numerical methods for calculating the exact optimal solution was called for. The answer to these wishes came towards the end of the twentieth century in the form of the *background method* for calculating upper bounds on turbulent transport communicated by Doering and Constantin.

The so-called 'background method' was initially introduced in the letter Doering & Constantin (1992) as a method to upper bound the energy dissipation in plane Couette flow "making no *a priori* assumptions about the flow or its spectrum and using only elementary functional estimates". This constituted a radical shift in the subject of establishing maximum transport properties for turbulent flows. The analysis initially evolved out of research into the regularity properties of the Navier–Stokes equations. The method uses a decomposition of the velocity field due to Hopf (1941), which separates the velocity into a *background* field assuming the boundary conditions but otherwise free, and a *fluctuation* field satisfying homogeneous boundary conditions. The method is therefore also termed the Constantin-Doering-Hopf

method[5]. In the trio of papers: Doering & Constantin (1994); Constantin & Doering (1995); Doering & Constantin (1996), the background method is applied to plane Couette flow, Poiseuille flow and thermal convection. Using the background method Constantin and Doering were able to make rigorous estimates on Busse's multi-$k$ asymptotic upper bounds. For example, the multi-$k$ maximum heat transport scaling of $Ra^{1/2}$ for Howard's problem with incompressibility, was derived rigorously in Doering & Constantin (1996).

The essential difference between the two variational problems is that the HB method seeks to maximise a functional over divergence free fields satisfying Dirichlet boundary conditions — thus only the maximiser is a rigorous upper bound on the flow quantity — while the CDH method is a minimisation problem over a set of competitor fields (the background fields) and any member of this competitor fields yields a rigorous upper bound. It is elementary, using the CDH method, to find principle scaling laws by computing conservative estimates using trial function representatives for the background field and simple functional estimates. In the CDH formulation the competitor fields are those background fields which satisfy a constraint, termed the 'spectral constraint'[6], which is a function of the divergence free fluctuation fields. We will use the terminology that a background field is SC-stable if it satisfies the spectral constraint and SC-neutral if it only marginally satisfies the constraint; i.e. being on the boundary of the admissible set. It is the spectral constraint which makes possible both direct estimation of the optimal upper bound for the variational problem, and a neat programme for a numerical calculation of the optimal solution. The geometry of the spectral constraint, in terms of Hilbert space theory, implies that there is a unique solution to the Euler–Lagrange equations which is SC-neutral.

The CDH method was extended to include an additional optimisation parameter, called the *balance parameter*, by Nicodemus, Grossmann & Holthaus (1997*a*), which resulted in an improvement to the pre-factor of the upper bound published in Doering & Constantin (1994) by a factor of 27/32. The parameter was more significant than is evidenced from this slight improvement. With this extra balance

[5]This will be abbreviated to the CDH method in future.
[6]The term 'spectral constraint' will be abbreviated to SC in future chapters.

parameter the duality of the HB and CDH methods was proved by Kerswell (1997, 1998, 2001) for the case of shear flow and thermal convection with arbitrary Prandtl number. These papers consolidated all of the results and techniques available from the two individual methods: Howard's single-$k$ solutions; Busse's multi-$k$ solutions; Constantin and Doering's direct estimates of upper bounds using test functions; and latterly numerical techniques.

Numerical methods have previously been employed to solving the optimal equations of the HB method, and in determining conservative estimates of the optimal bound in the CDH method. In Vitanov & Busse (1997), a solution to the Euler–Lagrange equations of the HB method was computed for the thermal convection problem with stress-free boundaries. Solutions of the Euler–Lagrange equations with between one and three horizontal wavenumbers were computed and the solution with the largest associated heat transport was selected as optimal. We will see that the selection procedure for the optimiser can be put on a firmer footing within the framework of the CDH method with the aid of the spectral constraint.

The first paper to use numerical techniques to improve conservative estimates on the optimal bound via the CDH method was Nicodemus *et al.* (1998*a*). Enhancement to the original estimate in Doering & Constantin (1994) was made by considering a more general form of the background field, namely quadratic profiles of two parameters. Their numerical technique involved optimising over the two parameters in order to find the lowest value of the upper bound for which the test function was SC-stable. Implementation of the spectral constraint was a little complicated owing to the complexity of background fields. A more efficient method of determining the SC-stability, valid for piecewise-linear test functions, is given in Otero (2002).

It is clear that, while the Optimum Theory began in order to study the relevance of Malkus's first theory, with the discovered of the complementary background method the subject has flourished into diverse application. The methods have been used to set phenomenological predictions on a firmer footing and to complement direct numerical simulations and experimentation in practical fluid flows. Comparison of the optimal solution structure with empirical data has shown qualitative agreement with the turbulent mean profile and its fluctuations, even though quanti-

tatively solutions do not match with realised flows. Success has been found in using the method as a stage for testing theories of turbulence, for instance in Otero *et al.* (2002) the effect of reformulating the boundary conditions in thermal convection is considered, while in Kerswell (2000) the effects of imposing a minimum lengthscale parallel to the plates in a shear flow problem is investigated. First steps have also been made towards extending the standard variational method to include more constraints derived from the Navier–Stokes equations, thereby closing the gap between theory and reality, in Kerswell & Soward (1996), Nicodemus *et al.* (1999), Kerswell (2000), Ierley & Worthing (2001).

In this thesis, we take advantage of the CDH method to develop a numerical programme for solving the optimal equations of the background method which utilises the spectral constraint to enable bifurcation between solution branches. In Chapter 2 we apply this technique to the plane Couette flow variational problem[7] first considered in Busse (1970). In Chapter 3 we demonstrate that Busse's two-dimensionality hypothesis for the optimal fluctuation fields is indeed sound. Leading on from this, we show how to extend the standard PCF bounding problem to consider mean profiles which are only marginally stable to infinitesimal disturbances, in order to test Malkus's second hypothesis. Our discussion will include preliminary results of the full optimal solution and future outlook.

In Chapters 4 and 5, we will look at the problem of thermal convection at infinite Prandtl number. This problem has been studied both using the HB and CDH methods, but they disagree on the limiting exponent of the upper bound on the heat transport. We look at both no-slip and stress-free boundary conditions; most of the literature concerns the no-slip condition while the stress-free optimal scaling is unknown. We use the conservative bound techniques reported in Otero (2002) and draw comparison between optimal results and conservative estimates of the optimal bound. We will see that the conservative estimates nicely complement the optimal solutions.

In Chapter 6 we derive some miscellaneous theoretical results which shall provide general insight into the HB and CDH variational problems.

[7]Later we will abbreviate plane Couette flow to PCF. (Note that this problem is sometimes simply called shear flow, while plane Poiseuille flow is called channel flow.)

# Chapter 2

# Shear flow CDH problem: Optimal solution

---

**Improved upper bound on the energy dissipation rate in plane Couette flow: The full solution to Busse's problem and the Constantin–Doering–Hopf problem with one-dimensional background field**

S. C. Plasting and R. R. Kerswell

Department of Mathematics, University of Bristol, Bristol, BS8 1TW, UK

*Published in the Journal of Fluid Mechanics: Plasting & Kerswell (2003).*

We present an improved upper bound on the energy dissipation rate in plane Couette flow. This is achieved through the numerical solution of the 'background field' variational problem formulated by Constantin and Doering with a one-dimensional unidirectional background field. The upper bound presented here both exhausts the bounding potential of the one-dimensional background field problem and also solves the provably equivalent problem formulated by Busse. The solution is calculated up to asymptotically large Reynolds number where we can estimate that the energy dissipation rate $\varepsilon \leq 0.008553$ as $Re \to \infty$ (in units of $V^3/d$ where $V$ is the velocity difference across the plates separated by a distance $d$ and $Re = Vd/\nu$, $\nu$ kinematic viscosity). This represents a 21% improvement over the previous best value due to Nicodemus *et al.* Comparison is drawn between this numerical solution and the so-called multi-alpha asymptotic solutions discovered by Busse.

## 2.1 Introduction

One of the few tools open to the theoretician interested in high-Reynolds number turbulence is a variational approach which strives to produce rigorous inequality information directly from the governing equations. Although over 40 years old (Malkus, 1954*a*, 1956; Howard, 1963), the approach has enjoyed a resurgence of interest recently with the discovery of a new alternative technique (Doering & Constantin, 1992, 1994; Constantin & Doering, 1995; Doering & Constantin, 1996; Nicodemus, Grossmann & Holthaus, 1997*a*) based upon a mathematical device going back to Hopf (1941). This 'background method', as it has been christened, is now known to produce the complementary variational problem to the classical Euler–Lagrange approach pioneered by Howard (1963, 1972, 1990) and Busse (1968*a*,*b*, 1969*a*,*b*, 1970, 1978) (see Kerswell, 1997, 1998, 2001). This has been an important development since new rigorous bounds have emerged which have improved previous bounds (those not including incompressibility as a constraint, Howard, 1963; Busse, 1968*a*) and put other better bound estimates (incorporating incompressibility) on a firmer footing.

This is nowhere more true than in bounding the energy dissipation rate, $\epsilon$, in the canonical shear flow problem of plane Couette flow. Over thirty years ago, Busse (1970) set up an Euler–Lagrange problem to maximise the energy dissipation rate possible for a velocity field which satisfied the dynamical constraints of mean momentum balance and the global power balance together with the kinematic constraints of incompressibility and the boundary conditions. Since this proved analytically intractable, he developed a multiple-boundary-layer approach to estimate the asymptotically large Reynolds number limit. Working within the space of almost periodic functions, Busse considered a variational solution consisting of a countable number of Fourier modes with each mode having its own boundary layer structure. Then using considerable ingenuity, he secured the estimate $\epsilon_{Busse} \approx 1/99.7$ as $Re \to \infty$ of the true maximum $\epsilon_{bound}$ for these constraints (measured in inviscid units of $V^3/d$ where $V$ is the velocity difference across the plates separated by a distance $d$ and $Re = Vd/\nu$, $\nu$ kinematic viscosity). Although his problem was one of maximisation, Busse argued that this estimate was nevertheless a strict upper

bound on the true bound $\varepsilon_{bound}$ because the terms he neglected as being higher order would all tend to lower the dissipation estimate. Unfortunately, technical difficulties associated with his analysis (the nestled boundary layers do not separate asymptotically in the required distinguished limit) meant that it was unclear how good an estimate this was and in the absence of accompanying numerical solutions, the way forward was uncertain. This coupled with the complexity of the analysis meant interest in the approach waned.

However, twenty years later, in the first application of their new method, Doering & Constantin (1992) derived the first clearly rigorous upper bound $\varepsilon \leq 1/11.3$ (as $Re \to \infty$) in the plane Couette problem. This was later improved by Gebhardt, Grossmann, Holthaus & Löhden (1995) down to $\varepsilon \leq 1/12.7$ by using a better trial background field and to $\varepsilon \leq 1/15.1$ by Nicodemus *et al.* (1997*a*,*b*) who found a way of further optimising the formulation. Then Nicodemus *et al.* (1998*a*,*b*) developed a sophisticated trial function approach to explore the method for finite $Re$ and managed to lower the asymptotic value down even further to $\varepsilon \leq 1/92.0$ by extensive numerical calculations. At this point, it had become clear that the best bound that could emerge from the Constantin–Doering–Hopf one-dimensional background problem (optimised by Nicodemus *et al.*, 1997*a*) corresponded *exactly* with that available in Busse's original problem (Kerswell, 1997, 1998). With this realisation, the fact that Nicodemus *et al.*'s result was so close to Busse's provided some reassurance that his multiple-boundary-layer technique was effective.

To properly resolve this issue, however, requires a complete solution of the variational problem to find the asymptotic value of $\varepsilon_{bound}$. The main purpose of this paper is to describe this calculation. The optimal variational solution which emerges is compared with Busse's multiple-boundary-layer estimate in order to indicate how effective an analytic tool his approximation is. This has important implications for other variational problems where Busse's technique still offers the only theoretical way of gaining insight but where complementary numerical computations have not been done.

There are also other interesting issues that need to be addressed. Firstly, neither Busse's multiple-boundary-layer ansatz or the trial function approach adopted by Nicodemus *et al.* (1998*a*,*b*), which artificially restricted the form of the background

field profile and fluctuation field, were able to allow the precise form of the optimal flow to emerge. Of particular interest is identifying whether the optimal mean flow profile develops a logarithmic-type layer just outside the viscous sublayer near the boundaries thereby mimicking realised flows. One of the motivations behind constructing such variational problems above and beyond the bounds themselves is learning whether the corresponding optimal solution bears any resemblance to realised flows. If it does in the case of plane Couette flow, then it is reasonable to speculate that the flow may be trying to maximise the energy dissipation or equivalently the momentum transport across the plates. The fact that asymptotically both Busse's trial solution and the Nicodemus *et al.* solution develop a $\frac{1}{4}$-shear across the interior of the flow is highly suggestive that the true optimal solution does also, but neither can say anything about the potentially delicate structure of the optimal solution at the boundary. This issue has recently become more prominent with the realisation that the optimal background field for the maximal energy dissipation rate problem also solves a whole suite of neighbouring variational problems addressing more general functionals of the dissipation and its component parts (see Kerswell, 2002).

Secondly, it is unclear which of the features of the upper bound for finite $Re$ that emerged in the work of Nicodemus *et al.* (1998*a*) are true to the optimal bound solution. Most notable amongst these is the surprising global minimum in their bound at $Re \approx 740$ (see figure 8 Nicodemus *et al.*, 1998*a*). Busse's asymptotic solution indicates that the optimal solution should contain an ever increasing number of wavenumbers in the fluctuation part of the velocity field as $Re$ increases whereas Nicodemus *et al.* allow only two. The influence of this limitation warrants investigation.

Given these motivations, then, we describe how to solve the full one-dimensional background field variational problem completely up to asymptotically large Reynolds numbers. This calculation finally solves an important variational problem first formulated over 30 years ago by Busse (Busse, 1970).

## 2.2 Formulation of the variational problem

We wish to consider the system of plane Couette flow in which a fluid layer is sheared by two parallel plane plates a distance $d$ apart with constant relative velocity $V$. The dimensional governing equations are

$$\frac{\partial u^*}{\partial t^*} + u^* \cdot \nabla^* u^* + \nabla^* p^* = \nu \nabla^{*2} u^*, \qquad (2.1)$$
$$\nabla^* \cdot u^* = 0, \quad u^*(x^*, y^*, \pm\tfrac{1}{2}d) = \mp\tfrac{1}{2}V\widehat{x}$$

where the starred variables are dimensional variables, $\nu$ is the kinematic viscosity, $\widehat{x}$ denotes the unit vector in the $x$-direction and the parallel plates are positioned at $z^* = \pm\frac{1}{2}d$. The domain of the fluid is the infinite layer $(x^*, y^*, z^*) \in \mathbb{R}^2 \times [-\frac{1}{2}d, \frac{1}{2}d]$ where $x$ is the streamwise, $y$ the spanwise and $z$ the wall-normal coordinate. All variables are assumed periodic in the horizontal directions.

We non-dimensionalise distances by the plate separation $d$ and time by the viscous diffusion time scale $d^2/\nu$ so that the equations become

$$\mathcal{N} := \frac{\partial u}{\partial t} + u \cdot \nabla u + \nabla p - \nabla^2 u = 0, \qquad (2.2)$$
$$\nabla \cdot u = 0, \quad u(x, y, \pm\tfrac{1}{2}) = \mp\tfrac{1}{2}Re\widehat{x},$$

where $Re := Vd/\nu$. Defining bulk averaging and horizontal averaging as

$$\langle\!\langle (\cdot) \rangle\!\rangle := \int_{-1/2}^{+1/2} \mathrm{d}z\, \overline{(\cdot)} := \int_{-1/2}^{+1/2} \mathrm{d}z \lim_{L_x, L_y \to \infty} \frac{1}{4L_x L_y} \int_{-L_x}^{+L_x} \mathrm{d}x \int_{-L_y}^{+L_y} \mathrm{d}y\, (\cdot), \qquad (2.3)$$

the non-dimensionalised, long-time-averaged energy dissipation rate per unit mass may be written as

$$\mathcal{E} := \frac{d^4}{\nu^3} \lim_{T\to\infty} \frac{1}{T} \int_0^T \nu \langle |\nabla^* u^*|^2 \rangle \,\mathrm{d}t = \lim_{T\to\infty} \frac{1}{T} \int_0^T \langle |\nabla u|^2 \rangle \,\mathrm{d}t. \qquad (2.4)$$

In terms of inviscid units, where we non-dimensionalise distance by $d$ and time by $d/V$, this quantity is just

$$\varepsilon := \frac{d}{V^3} \lim_{T\to\infty} \frac{1}{T} \int_0^T \nu \langle |\nabla^* u^*|^2 \rangle \,\mathrm{d}t = \frac{\mathcal{E}}{Re^3}. \qquad (2.5)$$

We derive the Constantin–Doering–Hopf variational problem (henceforth abbreviated to CDH) by considering the Lagrangian functional

$$\mathcal{L} := \lim_{T\to\infty} \frac{1}{T} \int_0^T \mathrm{d}t \left\{ \langle |\nabla u|^2 \rangle - \left\langle a\nu \cdot \left[ \frac{\partial u}{\partial t} + u \cdot \nabla u + \nabla p - \nabla^2 u \right] \right\rangle \right\} \qquad (2.6)$$

where the field $a\boldsymbol{\nu}$ is a Lagrange multiplier which imposes the governing equations and the real constant $a$ is included for comparison with earlier work on the background field method. The objective is to find the maximum stationary value of $\mathcal{L}$ over $\boldsymbol{u}$, $\boldsymbol{\nu}$ and $a$ which corresponds to the maximum dissipation rate over all possible solutions to the governing equations. In the CDH problem the Lagrange multiplier field $\boldsymbol{\nu}$ and the velocity field $\boldsymbol{u}$ are connected via a background field $\phi$

$$\phi(z)\widehat{\boldsymbol{x}} := \boldsymbol{u}(\boldsymbol{x},t) - \boldsymbol{\nu}(\boldsymbol{x},t) \tag{2.7}$$

where $\phi$ is a one-dimensional function independent of time which takes up the boundary conditions, $\phi(\pm\frac{1}{2}) = \mp\frac{1}{2}Re$. It should be stressed that $\phi$ is not necessarily equal to the horizontal average of $\boldsymbol{u}$. This decomposition of $\boldsymbol{u}$ into a 'background field' satisfying the boundary conditions and a 'fluctuation field' that is incompressible and satisfies homogeneous boundary conditions is known as the Hopf decomposition (Hopf, 1941). By forcing this relationship between $\boldsymbol{u}$ and $\boldsymbol{\nu}$, the constraints imposed by $\boldsymbol{\nu}$ are now only the total power balance and horizontally averaged momentum balance in the $\widehat{\boldsymbol{x}}$-direction. This can be seen by substituting $\boldsymbol{\nu} = \boldsymbol{u} - \phi\widehat{\boldsymbol{x}}$ into (2.6) and rearranging to get

$$\mathcal{L} = \lim_{T\to\infty}\frac{1}{T}\int_0^T \mathrm{d}t\left[\langle|\nabla\boldsymbol{u}|^2\rangle - a\langle\boldsymbol{u}\cdot\boldsymbol{\mathcal{N}}\rangle + \int_{-\frac{1}{2}}^{\frac{1}{2}} a\phi\overline{\mathcal{N}_1}\,\mathrm{d}z\right];$$

$\boldsymbol{\mathcal{N}}$ denotes the Navier–Stokes equations (see 2.2) with first component $\mathcal{N}_1$, $a$ is the Lagrange multiplier for the total power balance integral for the Navier–Stokes equations and $\phi$ is the Lagrange multiplier for the horizontally-averaged momentum balance in the $\widehat{\boldsymbol{x}}$ direction.

With the change of variables $\boldsymbol{u} = \phi\widehat{\boldsymbol{x}} + \boldsymbol{\nu}$, $\mathcal{L}$ can be written as

$$\mathcal{L} = \langle\phi'^2\rangle - \lim_{T\to\infty}\frac{1}{T}\int_0^T \langle a\nu_1\nu_3\phi' + (a-1)|\nabla\boldsymbol{\nu}|^2 - (a-2)\nu_1\phi''\rangle\,\mathrm{d}t \tag{2.8}$$

(where implicitly $\nabla\cdot\boldsymbol{\nu} = 0$). At this stage the key observation is that if $\phi$ can be chosen such that $\mathcal{L}$ has a maximum over all $\boldsymbol{\nu}$, then this value will bound the true dissipation rate $\epsilon$ since any realisable $\boldsymbol{u}$ which satisfies the Navier–Stokes equations can still be reached by some $\boldsymbol{\nu}$. Minimising the maximum over allowable $\phi$ then produces the best such upper bound. It turns out that this is equivalent to finding the largest saddle point value of $\mathcal{L}$ (see Kerswell, 1998) which can be accomplished

by considering only stationary solenoidal fluctuation fields $\boldsymbol{\nu}$. With $\lim_{T\to\infty}(1/T)$ dropped from (2.8), the Euler–Lagrange equations for $a$, $\phi$ and $\boldsymbol{\nu}$ are

$$\frac{\delta\mathcal{L}}{\delta a} := -\langle|\nabla\boldsymbol{\nu}|^2 + \phi'\nu_1\nu_3 - \phi''\nu_1\rangle = 0, \tag{2.9}$$

$$\frac{\delta\mathcal{L}}{\delta\phi} := -2\phi'' + a\overline{\nu_1\nu_3}' + (a-2)\overline{\nu_1}'' = 0, \tag{2.10}$$

$$\frac{\delta\mathcal{L}}{\delta\boldsymbol{\nu}} := 2(a-1)\nabla^2\boldsymbol{\nu} - a\phi'\begin{bmatrix}\nu_3\\0\\\nu_1\end{bmatrix} + \nabla p + (a-2)\phi''\widehat{\boldsymbol{x}} = \mathbf{0}. \tag{2.11}$$

If we take the mean part of equation (2.11) and use the incompressibility condition on $\boldsymbol{\nu}$ we discover that the fluctuation field can be split into a mean part $\overline{\nu_1}(z)\widehat{\boldsymbol{x}}$ and a mean-less part $\widehat{\boldsymbol{\nu}}$ ($\overline{\widehat{\boldsymbol{\nu}}} = \mathbf{0}$). Equation (2.11) then splits into two, one homogeneous and one inhomogeneous equation, namely

$$\frac{\delta\mathcal{L}}{\delta\widehat{\boldsymbol{\nu}}} := 2(a-1)\nabla^2\widehat{\boldsymbol{\nu}} - a\phi'\begin{bmatrix}\widehat{\nu}_3\\0\\\widehat{\nu}_1\end{bmatrix} + \nabla\widehat{p} = 0, \tag{2.12}$$

$$\frac{\delta\mathcal{L}}{\delta\overline{\nu_1}} := 2(a-1)\overline{\nu_1}'' + (a-2)\phi'' = 0. \tag{2.13}$$

This latter equation can be integrated twice to

$$\overline{\nu_1} = -\frac{a-2}{2(a-1)}[\phi + Rez] \tag{2.14}$$

after applying the boundary conditions for $\phi$ and $\boldsymbol{\nu}$, so that the mean flow of the optimal field and the background field are connected as follows

$$\overline{\boldsymbol{u}} = \left[\frac{a}{2(a-1)}(\phi + Re\,z) - Re\,z\right]\widehat{\boldsymbol{x}}. \tag{2.15}$$

Defining a new parameter $\lambda := a/(a-1)$ and rescaling the pressure field $\widehat{p} \to (a-1)\widehat{p}$ we can transform the remaining equations for the optimal field (2.9),(2.10) and (2.12)

to

$$\lambda = 2 - \frac{\langle |\nabla \widehat{\nu}|^2 \rangle}{Re\langle \widehat{\nu}_1 \widehat{\nu}_3 \rangle}, \tag{2.16}$$

$$\frac{\lambda}{2}(\phi' + Re) = \overline{\widehat{\nu}_1 \widehat{\nu}_3} - \langle \widehat{\nu}_1 \widehat{\nu}_3 \rangle, \tag{2.17}$$

$$2\nabla^2 \widehat{\nu} - \lambda \phi' \begin{bmatrix} \widehat{\nu}_3 \\ 0 \\ \widehat{\nu}_1 \end{bmatrix} + \nabla \widehat{p} = 0, \tag{2.18}$$

$$\nabla \cdot \widehat{\nu} = 0, \tag{2.19}$$

where (2.16) has been written for optimal numerical conditioning (see Appendix A for the derivation). Substituting (2.14) into the expression for $\mathcal{L}$ gives

$$\mathcal{L} = \frac{\lambda^2}{4(\lambda - 1)} \langle (\phi' + Re)^2 \rangle + Re^2 - \frac{1}{\lambda - 1} \mathcal{H}_{\phi,\lambda}(\widehat{\nu}) \tag{2.20}$$

where $\mathcal{H}_{\phi,\lambda}(\widehat{\nu}) := \langle |\nabla \widehat{\nu}|^2 \rangle + \lambda \langle \widehat{\nu}_1 \widehat{\nu}_3 \phi' \rangle$. A stationary value of $\mathcal{L}$ is an upper bound on $\varepsilon$ if the minimum of the quadratic form $[1/(\lambda - 1)]\mathcal{H}_{\phi,\lambda}(\widehat{\nu}) = (a - 1)\langle |\nabla \widehat{\nu}|^2 \rangle + a\langle \widehat{\nu}_1 \widehat{\nu}_3 \phi' \rangle$ exists over the set $\mathcal{V} := \{\nu \,|\, \nabla \cdot \nu = 0,\ \overline{\nu} = 0,\ \nu(x, y, \pm\tfrac{1}{2}) = 0\}$. This means that both $a > 1$ and the so-called 'spectral' constraint

$$\mathcal{H}_{\phi,a}(\widehat{\nu}) \geq 0 \qquad \forall \widehat{\nu} \in \mathcal{V} \tag{2.21}$$

must be satisfied if the stationary value of $\mathcal{L}$, calculated through solving Equations (2.16–2.19), is to be an upper bound on $\varepsilon$. The Euler–Lagrange equation for $\widehat{\nu}$, (2.18), implies that $\mathcal{H}_{\phi,a}(\widehat{\nu}) = 0$ at every stationary point of $\mathcal{L}$ but only the largest (unique) stationary value satisfies the spectral constraint (see Section 2.4 of Kerswell, 1998).

Hence the upper bound which emerges from the CDH problem is

$$\mathcal{E} \leq \mathcal{E}_{max} := \frac{\lambda^2}{4(\lambda - 1)} \langle (\phi' + Re)^2 \rangle + Re^2 \tag{2.22}$$

where $\phi$ and $\lambda$ along with an associated fluctuation field $\widehat{\nu}$ satisfy (2.16–2.19) together with the spectral constraint.

## 2.3 Solution Technique

In all studies to date no solution of the full set of Euler–Lagrange equations has been attempted. Instead test functions for $\phi$ have been constructed and functional inequalities on $\mathcal{H}_{\phi,a}$ used to verify the spectral constraint (Doering & Constantin, 1992; Gebhardt *et al.*, 1995; Nicodemus *et al.*, 1997*a*). One notable exception to this is the work by Nicodemus *et al.* (1998*a*) which employs a sophisticated background trial profile with several degrees of freedom and solves the spectral constraint numerically allowing fluctuation fields with up to two spanwise wavenumbers. It remains unclear how close their solution is to the full solution.

In this section we will discuss how a numerical solution to equations (2.16–2.19) can be made using the method of pseudo-spectral collocation (see Boyd, 2001) and how the all important spectral constraint is enforced. We assume as in previous studies that the optimal solution has no streamwise variation, $\partial_x = 0$ (Busse, 1969*a*, 1970). The solution to the linear equations (2.18–2.19) takes the form

$$\widehat{\boldsymbol{\nu}} = \sum_{m=1}^{M} \begin{bmatrix} \widehat{\nu}_1^{(m)} \cos(k_m y) \\ \widehat{\nu}_2^{(m)} \sin(k_m y) \\ \widehat{\nu}_3^{(m)} \cos(k_m y) \end{bmatrix}, \qquad \widehat{p} = \sum_{m=1}^{M} \widehat{p}^{(m)} \cos(k_m y),$$

where the hatted variables are $z$-dependent functions. We expand each of these functions together with the background field in Chebyshev polynomials as follows

$$\phi(z) = -Re\, z + \sum_{n=1}^{N} \widehat{\phi}_n U_{2n}(2z) \tag{2.23a}$$

and

$$\widehat{\nu}_i^{(m)} = \sum_{n=1}^{N} \widehat{\nu}_{i,n}^{(m)} U_n(2z) \quad \text{for } i \text{ from 1 to 3,} \tag{2.23b}$$

$$\widehat{p}^{(m)} = \sum_{n=1}^{N} \widehat{p}_n^{(m)} T_{n-1}(2z) \tag{2.23c}$$

where $T_n(z)$ is the Chebyshev polynomial, $T_n(z) = \cos(n \cos^{-1} z)$, and $U_n(z)$ is the modified Chebyshev polynomial defined by $U_n(z) = T_{n+1}(z) - T_{n-1}(z)$. Every $U_n$ satisfies homogeneous boundary conditions by construction

$$U_n(\pm 1) = 0 \qquad \forall n \in \mathbb{N} \tag{2.24}$$

so this basis is a natural choice for both $\phi$ and $\widehat{\nu}$. Under the assumption that the background field is odd in $z$, $\phi$ is expanded in the odd basis $\{U_{2n}\}$. Also twice as much resolution is put in $\phi$ than $\widehat{\nu}$ because $\phi'$ is forced by a quadratic in $\widehat{\nu}$ (see equation 2.17). The equations are collocated over the interior Chebyshev grid $\{z_i = \frac{1}{2}\cos(\pi(2i-1)/(2N)), i = 1,\ldots,N\}$.

Horizontal modes do not mix because of the linearity of the optimal equation for $\widehat{\nu}$ (2.18) and the incompressibility constraint (2.19). Therefore these constraints separate into constraints on each subfield $[\widehat{\nu}^{(m)}, \widehat{p}^{(m)}]$ as follows

$$\frac{\delta\mathcal{L}}{\delta\widehat{\nu}^{(m)}} := 2(\widehat{\nu}^{(m)''} - k_m^2\widehat{\nu}^{(m)}) - \lambda\phi' \begin{bmatrix} \widehat{\nu}_3^{(m)} \\ 0 \\ \widehat{\nu}_1^{(m)} \end{bmatrix} + \begin{bmatrix} 0 \\ -k_m\widehat{p}^{(m)} \\ \widehat{p}^{(m)\prime} \end{bmatrix} = 0, \tag{2.25a}$$

and

$$k_m\widehat{\nu}_2^{(m)} + \widehat{\nu}_3^{(m)\prime} = 0. \tag{2.25b}$$

where $(\,)' \equiv \mathrm{d}/\mathrm{d}z$. An extra equation describing the variation of $\mathcal{L}$ with horizontal wavenumber $k_m$ is now required to close the system of optimal equations. Expression (2.20) with the incompressibility constraint explicitly included is:

$$\mathcal{L} = \frac{\lambda^2}{4(\lambda-1)}\langle(\phi' + Re)^2\rangle + Re^2 - \frac{1}{\lambda-1}\left[\mathcal{H}_{\phi,\lambda}(\widehat{\nu}) + \langle\widehat{p}\nabla\cdot\widehat{\nu}\rangle\right].$$

Written in terms of $\widehat{\nu}^{(m)}$ and $k_m$ we have

$$\begin{aligned}\mathcal{L} \;=\; & \frac{\lambda^2}{4(\lambda-1)}\langle(\phi' + Re)^2\rangle + Re^2 \\ & -\frac{1}{\lambda-1}\sum_{m=1}^{M}\left[\langle|\widehat{\nu}^{(m)\prime}|^2 + k_m^2|\widehat{\nu}^{(m)}|^2 + \lambda\widehat{\nu}_1^{(m)}\widehat{\nu}_3^{(m)}\phi' + \widehat{p}^{(m)}(k_m\widehat{\nu}_2^{(m)} + \widehat{\nu}_3^{(m)\prime})\rangle\right],\end{aligned}$$

where $\widehat{\nu}^{(m)} = [\widehat{\nu}_1^{(m)}, \widehat{\nu}_2^{(m)}, \widehat{\nu}_3^{(m)}]$, from which we can readily derive the $k_m$ variation

$$\frac{\delta\mathcal{L}}{\delta k_m} := k_m\langle|\widehat{\nu}^{(m)}|^2\rangle + \tfrac{1}{2}\langle\widehat{p}^{(m)}\widehat{\nu}_2^{(m)}\rangle = 0. \tag{2.26}$$

The only mixed mode terms in the solution of the optimal equations occur on the right hand sides of equations (2.16–2.17). These equations are now

$$\lambda = 2 - \frac{\sum_{m=1}^{M}\langle|\widehat{\nu}^{(m)\prime}|^2 + k_m^2|\widehat{\nu}^{(m)}|^2\rangle}{Re\sum_{m=1}^{M}\langle\widehat{\nu}_1^{(m)}\widehat{\nu}_3^{(m)}\rangle}, \tag{2.27}$$

$$\lambda(\phi' + Re) = \sum_{m=1}^{M}\left[\widehat{\nu}_1^{(m)}\widehat{\nu}_3^{(m)} - \langle\widehat{\nu}_1^{(m)}\widehat{\nu}_3^{(m)}\rangle\right]. \tag{2.28}$$

(The $\frac{1}{2}$ multiplying the left hand side of equation (2.17) has cancelled with one coming from integrating $\cos^2(k_m y)$.) The fact that $\phi'$ is even in $z$ means that solutions to (2.25a) and (2.25b) can be sought with the pair $(\widehat{v}_1^{(m)}, \widehat{v}_3^{(m)})$ even in $z$ and $(\widehat{v}_2^{(m)}, \widehat{p}^{(m)})$ odd in $z$, and vice versa. Our numerical solution of the CDH problem proceeds in two parts.

(i) Continuation calculation from the Energy Stability point

We employ a numerical continuation program called PITCON (Rheinboldt & Burkardt, 1983*a*,*b*) to continue the solution of the Euler–Lagrange equations in $Re$ from the Energy Stability point $Re = Re_{ES}$, when the laminar flow state ceases to be the global attractor for the Navier–Stokes equation (see Joseph, 1976), through successive spanwise wavenumber bifurcations, up to asymptotically high Reynolds number. One can show that up to $Re_{ES}$ the optimal solution of the CDH problem is the laminar solution $\phi(z) = -Re\, z$. First this $\phi$, arbitrary $a$ and $\widehat{\boldsymbol{v}} = \mathbf{0}$ trivially solve the Euler–Lagrange equations. Second the spectral constraint for laminar $\phi$ and $a = \infty$ (or equivalently $\lambda = 1$) is

$$\mathcal{H}_{\{-Re\, z, \lambda=1\}}(\widehat{\boldsymbol{v}}) = \langle |\nabla \widehat{\boldsymbol{v}}|^2 \rangle - Re\langle \widehat{v}_1 \widehat{v}_3 \rangle \geq 0 \qquad \forall \widehat{\boldsymbol{v}} \in V \tag{2.29}$$

which is the condition that the laminar flow is globally asymptotically stable and holds for $Re \leq Re_{ES}$. At $Re_{ES} = 82.65$, the inequality in (2.29) is made marginal by an eigenfunction $\widehat{\boldsymbol{v}} = \widehat{\boldsymbol{v}}_{ES}(z)$ with the critical horizontal wavenumber $k_{ES} = 3.117$. The continuation procedure starts by setting $k_1 = k_{ES}$ and $\widehat{\boldsymbol{v}}^{(1)} = A\widehat{\boldsymbol{v}}_{ES}$, and adjusting either the amplitude $A$ or the stepsize in $Re$ until convergence occurs to a non-trivial solution.

(ii) The spectral constraint and incoming wavenumbers

The second part of the calculation consists of enforcing $\mathcal{H}$ to be positive-semidefinite. This so-called spectral constraint can be shown to be equivalent to solving the linear eigenvalue problem

$$2(\boldsymbol{v}'' - k^2\boldsymbol{v}) - \lambda\phi' \begin{bmatrix} v_3 \\ 0 \\ v_1 \end{bmatrix} + \begin{bmatrix} 0 \\ -kp \\ p' \end{bmatrix} = \mu\boldsymbol{v} \tag{2.30}$$

over the space of functions $\mathcal{V}$

$$\mathcal{V} = \{ \boldsymbol{v} \,|\, kv_2 + v_3' = 0, \quad \overline{\boldsymbol{v}} = \boldsymbol{0}, \quad \boldsymbol{v}(z = \pm\tfrac{1}{2}) = \boldsymbol{0} \}, \tag{2.31}$$

and verifying that $\mu \leq 0$ for real values of $k$. Here the implicit assumption is made that only streamwise-independent velocity fields are important which is unproven but appears true (Busse, 1969*a*, 1970; Nicodemus *et al.*, 1998*a*). Letting $\overline{\mu}(k)$ be the maximum eigenvalue of this linear eigenvalue system at a given $k$, it is important to realise that the zeros of $\overline{\mu}$ correspond to fields which satisfy (2.25a-*b*). At $Re = Re_{ES}$, $\overline{\mu}$ has a unique maximum at $k = k_{ES}$ (i.e. $\overline{\mu}(k_{ES}) = 0$). However, as the continuation calculation proceeds by increasing $Re$, $\overline{\mu}(k)$ develops another maximum which if unchecked bursts through the $\mu = 0$ axis (see figure 2.1). Just before this occurs, that is when $\overline{\mu} \leq 0$ over $k$ and $\overline{\mu}(k_1) = \overline{\mu}(k_2) = 0$ for $k_1 \neq k_2$, the continuation procedure must be stopped and the solution extended to include an extra fluctuation field $\widehat{\boldsymbol{\nu}}^{(2)}$ to take account of this new marginal wavenumber. The calculation is restarted by shooting the solution off into the new fluctuation field 'direction', i.e.

$$\widehat{\boldsymbol{\nu}}_{new} = \widehat{\boldsymbol{\nu}}_{old} + A \begin{bmatrix} \widehat{\nu}_1^{(2)} \cos(k_2 y) \\ \widehat{\nu}_2^{(2)} \sin(k_2 y) \\ \widehat{\nu}_3^{(2)} \cos(k_2 y) \end{bmatrix}. \tag{2.32}$$

The two points $\overline{\mu}(k_1)$ and $\overline{\mu}(k_2)$ are now pinned to zero through equation (2.25a) although the wavenumbers $k_1$ and $k_2$ change with $Re$. The graph of $\overline{\mu}(k)$ is again monitored to check if a third new maximum has emerged. In this way successive bifurcations are found and the number of fluctuation fields in the optimal solution gradually increases. See Doering & Hyman (1997) for an earlier numerical study in which they see evidence of the first wavenumber bifurcation in the spectral constraint.

Supplementary to finding and incorporating incoming modes, the spectral constraint eigenvalue calculation was also used as an additional test that $N$, the $z$-direction truncation, was sufficient, by checking that the $M$ modes in the fluctuation field decomposition correspond to accurate zeros and maxima of the $\overline{\mu}(k)$ graph. The spectral calculation is independent of the optimal fluctuation field depending only on $\phi$ and $a$. So this subsidiary check of resolution is as important as checking

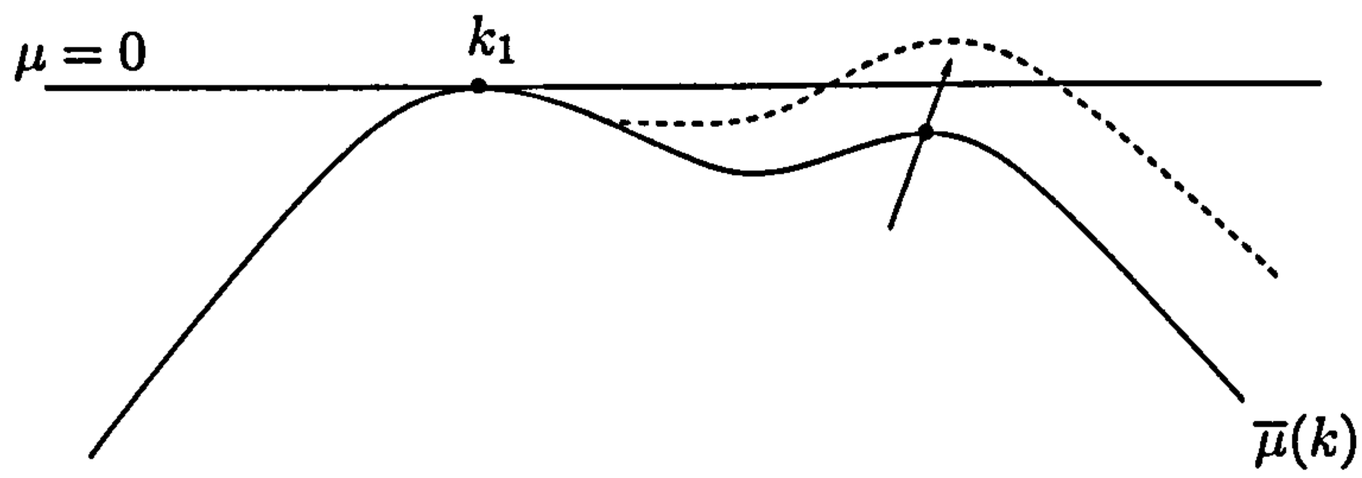


Figure 2.1: Diagram showing a new wavenumber maximum passing through the $\mu = 0$ axis.

that a higher resolution in $z$ produces the same global properties of the optimal solution such as the dissipation rate. The background field develops a boundary layer structure near the wall which is $\mathcal{O}(1/Re)$. As a result the truncation $N$ required scales like $Re^{1/2}$ since the Chebyshev collocation points have an $\mathcal{O}(1/N^2)$ spacing at the walls.

## 2.4 Results and comparison with asymptotic expressions

The main result of this work is presented in figure 2.2 which shows how the full-solution upper bound behaves as a function of $Re$. Also included for comparison are the results from the trail-function approach of Nicodemus *et al.* (1998*a*) and Busse's (1970) original asymptotics. The first observation is that the exact upper bound is indeed *lower* than Busse's asymptotic estimate. Furthermore, the full solution clearly does not possess the local minimum found by Nicodemus *et al.* but rather monotonically decreases to an asymptotic value of $\epsilon_{bound} = 0.008553$. This plot also shows that the wavenumber bifurcation points are close to being evenly spaced in $\log(Re)$. This is a first indication that there is a self-similar structure to the spanwise wavenumbers which emerge as part of the solution. This is also clearly seen in figure 2.3. Incoming wavenumbers always emerge low down in the wavenumber spectrum, between $k_1$ and $k_2$ or $k_2$ and $k_3$. This property was also observed in a study by

| $M$ | $Re_m$ | $N$ |
|---|---|---|
| 1 | 82.7 | 8 |
| 2 | 407.9 | 12 |
| 3 | 1418.4 | 25 |
| 4 | 4247.5 | 50 |
| 5 | 11660.1 | 100 |
| 6 | 30004.0 | 200 |
| 7 | 73300.1 | 250 |

Table 2.1: The Reynolds numbers, $Re_m$, at which new wavenumbers emerge and are built into the fluctuation field, versus the total number of modes, $M$, and the truncation number in the $z$-direction, $N$, required to calculate the optimal solution.

Vitanov & Busse (1997).

Unfortunately, it was only possible to find the solution up until the seventh wavenumber bifurcation ($Re = 7.33 \times 10^4$) in double precision arithmetic due to the sensitivity of the spectral constraint. The graph of $\overline{\mu}(k)$ at $Re = 7.33 \times 10^4$ (figure 2.4) shows a plateauing close to the 3rd lowest wavenumber in $\widehat{\nu}$ which is where the seventh wavenumber is emerging. In this region, $\overline{\mu} = \mathcal{O}(10^{-5})$ and $\widehat{\nu}_i = \mathcal{O}(10)$ so that the right hand side of (2.30) is $\mathcal{O}(10^{-4})$ whereas terms on the left hand side of (2.30) are typically $\mathcal{O}(Re^2 \sim 10^9)$ near the walls. This wide disparity in scales means that the emerging zero of the spectral eigenvalue problem gets swamped and so the narrow region of convergence for a seventh wavenumber solution is unattainable. Also at this stage the numerical effort is beginning to become an issue. At $Re = 7.32 \times 10^4$ with $N = 230$ and six wavenumbers, there were 5758 equations to be solved and every Newton–Raphson convergence took an hour on a 667MHz EV6 processor requiring 300MB of storage. An interesting feature of the continuation procedure was that PITCON automatically took smaller and smaller steps near a wavenumber bifurcation, that is, the code could sense the presence of an emerging wavenumber. Fortunately, the asymptotic behaviour of the upper bound is already clear by the seventh wavenumber bifurcation.

Further aspects of the optimising solution are shown in figures 2.5 to 2.8. Figure 2.5 shows how the parameter $\lambda$ starts with the value 1 when $Re = Re_{ES}$ and then converges exponentially to $\frac{3}{2}$ as $Re \to \infty$. The curve $\lambda(Re)$ is only $C^0$ being punctuated by discontinuities in the gradient as successive wavenumbers enter the optimal

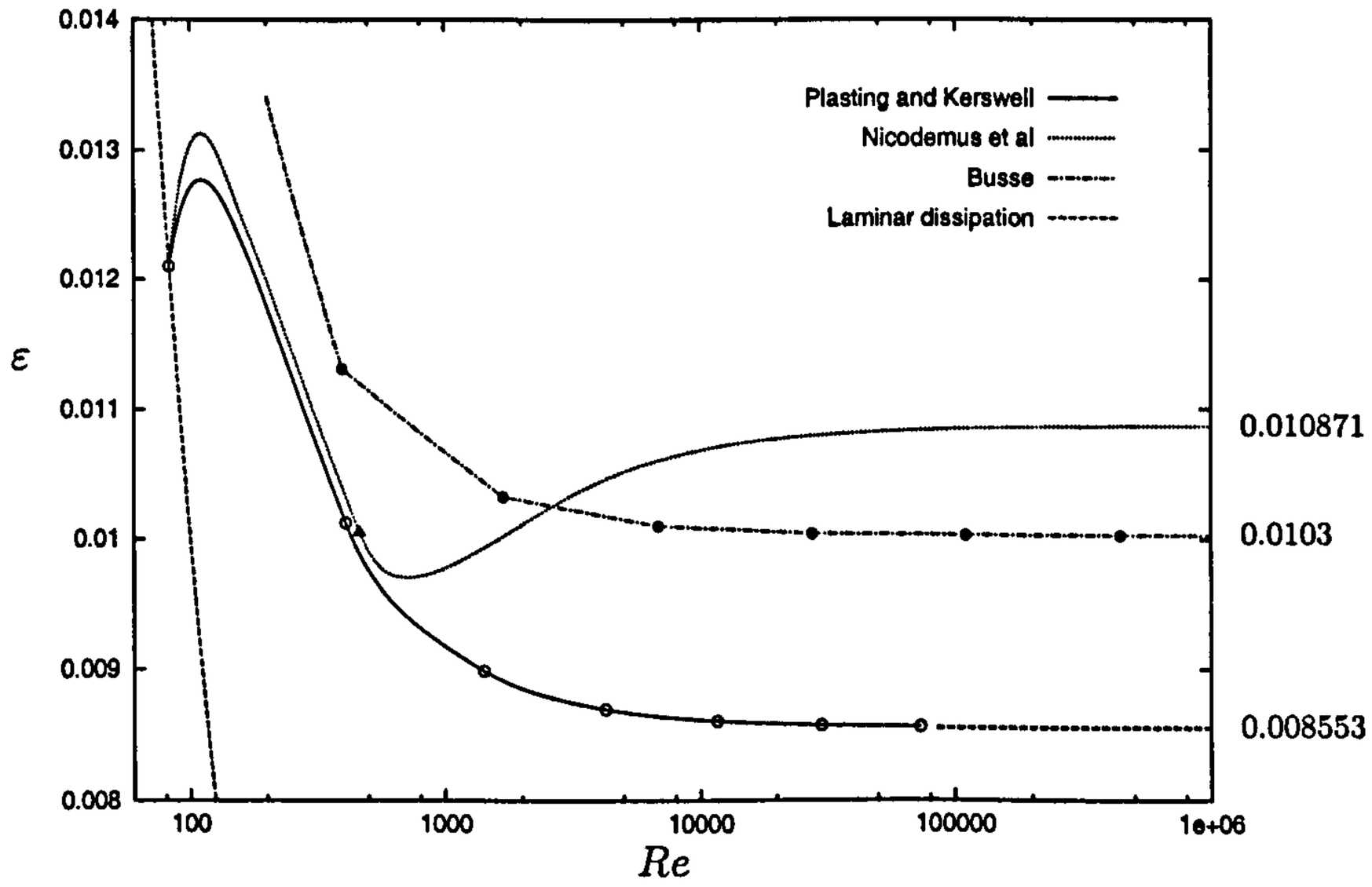


Figure 2.2: Comparison of bounds on the long time dissipation rate $\varepsilon$. The dashed line shows the dissipation rate for the laminar flow state which is a theoretical minimum for $\varepsilon$. The dotted line is the previous best bound calculated by Nicodemus *et al.* (1998*a*). The dash-dotted line is the asymptotic $Re$ bound of Busse (1970) extrapolated to finite Reynolds number. The solid line is the improved bound calculated here, with its extension to an asymptotic limit of 0.008553 depicted by the thick dashed line. Points represent the position of incoming modes. The open circles correspond to the wavenumber bifurcation points $Re_m$ from this calculation, as recorded in table 2.1. The open triangle is the point at which Nicodemus *et al.* find a wavenumber degeneracy in their spectral constraint calculation, and the solid circles are the points of incoming wavenumbers in the multi-$\alpha$ solutions.

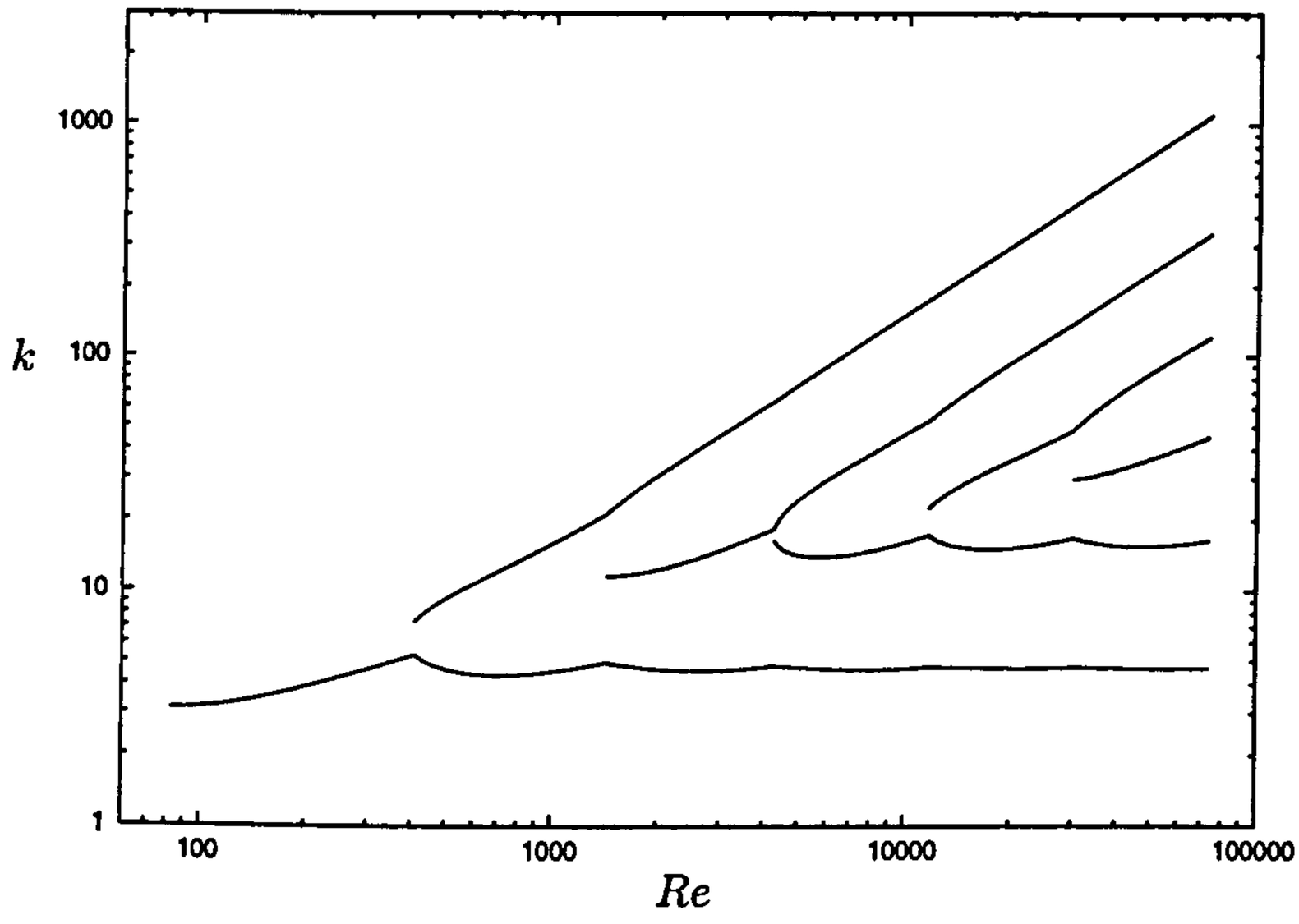


Figure 2.3: Bifurcation diagram for the spanwise wavenumber of the fluctuation field.

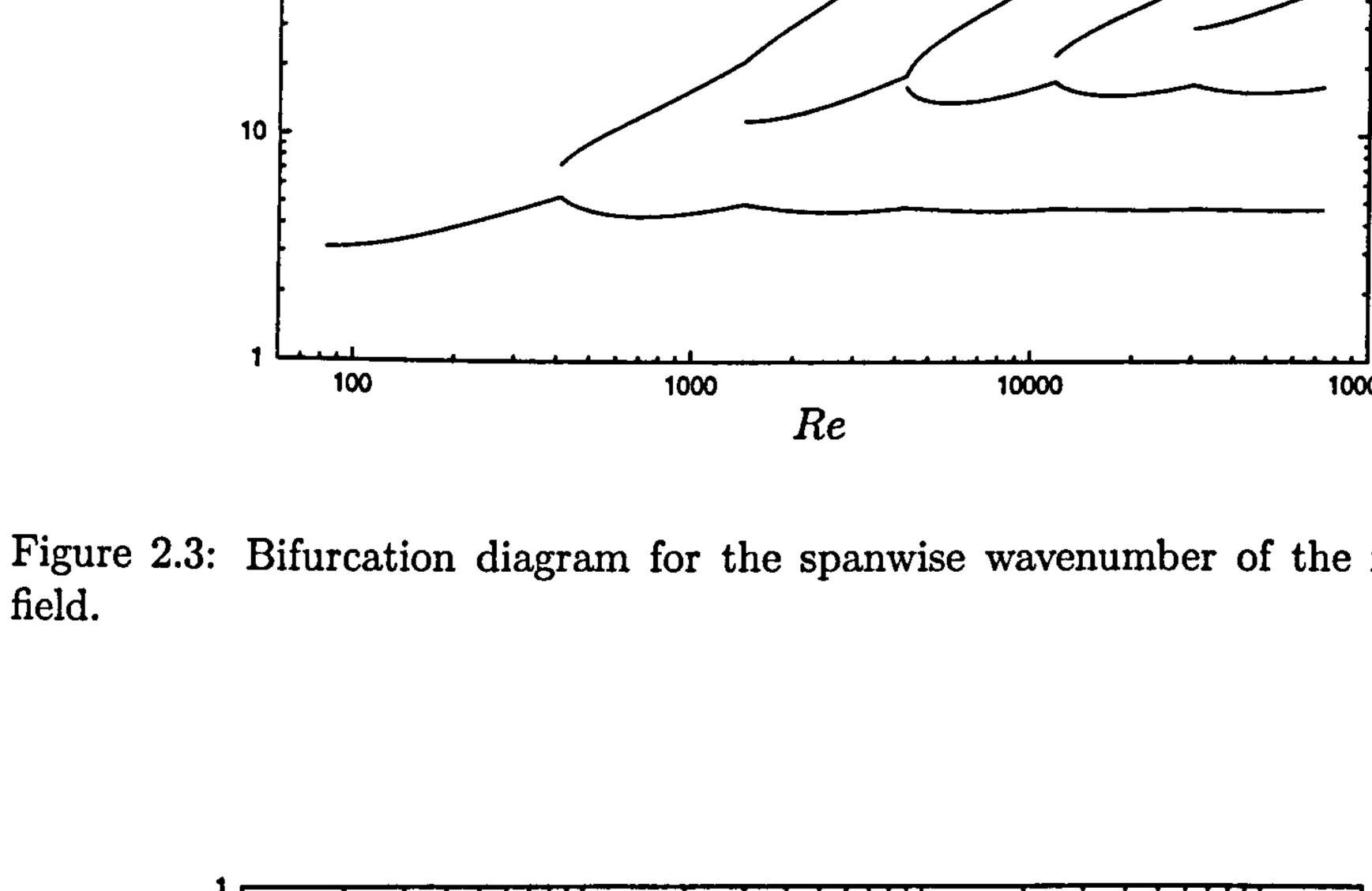


Figure 2.4: A plot of $\overline{\mu}(k)$ at $Re = 7.33 \times 10^4$ on a shifted logarithmic scale.

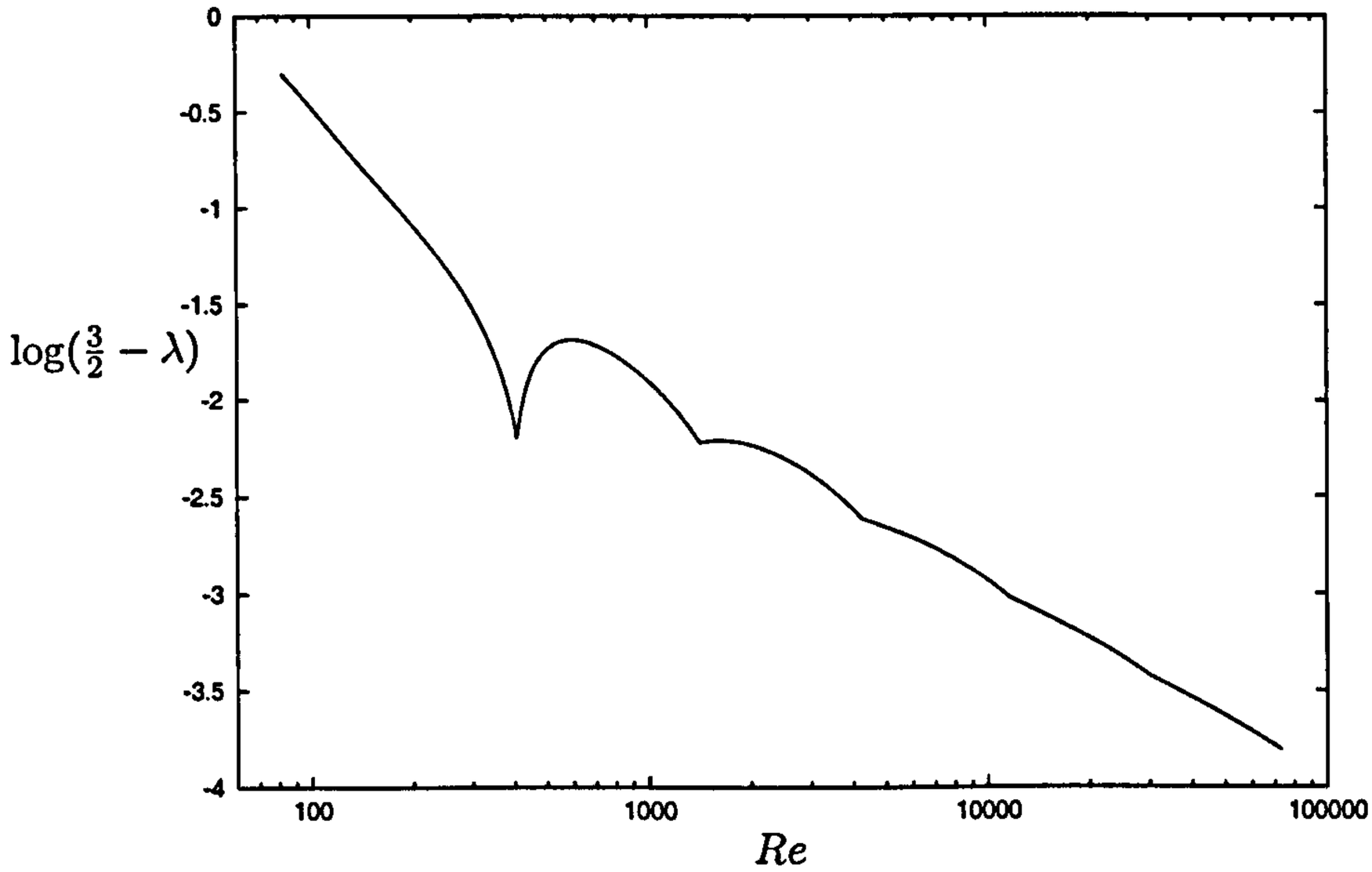


Figure 2.5: Logarithmic plot of the difference between the optimisation parameter $\lambda$ and its asymptotic limit $\frac{3}{2}$.

solution (see Table 1). The asymptotic limit $\lambda(\infty) = \frac{3}{2}$, or equivalently $a = 3$, is predicted by Busse's (1970) asymptotics and also emerges from the numerics of Nicodemus *et al.* (1998a). Figures 2.6 and 2.7 show the structure of the optimal mean profile (equation 2.15). The near-wall behaviour is emphasized in figure 2.6 by using traditional friction units. This clearly shows that the optimal mean profile does not have any logarithmic region outside the viscous sublayer as observed experimentally. The boundary layer is tighter than for real flows and the region outside this is flat rather than following a logarithmic increase. Figure 2.7 shows the characteristic $\frac{1}{4}$-shear through the interior (i.e. the shear is a $\frac{1}{4}$ of the laminar value) which is predicted by Busse's asymptotics and found also by Nicodemus *et al.* (1998*a*). Figure 2.8 illustrates the self-similarity of the various velocity fields associated with the wavenumbers which is consistent with Busse's asymptotics. These fields all have the parity of $(\widehat{\nu}_1^{(m)}, \widehat{\nu}_3^{(m)})$ both even and $(\widehat{\nu}_2^{(m)}, \widehat{p}^{(m)})$ both odd because this parity of solution turned out to be the most critical in the spectral constraint.

Further comparisons can be made with Busse's multiple boundary layer analysis which identifies the asymptotic behaviour of $N$ boundary layer trial-function

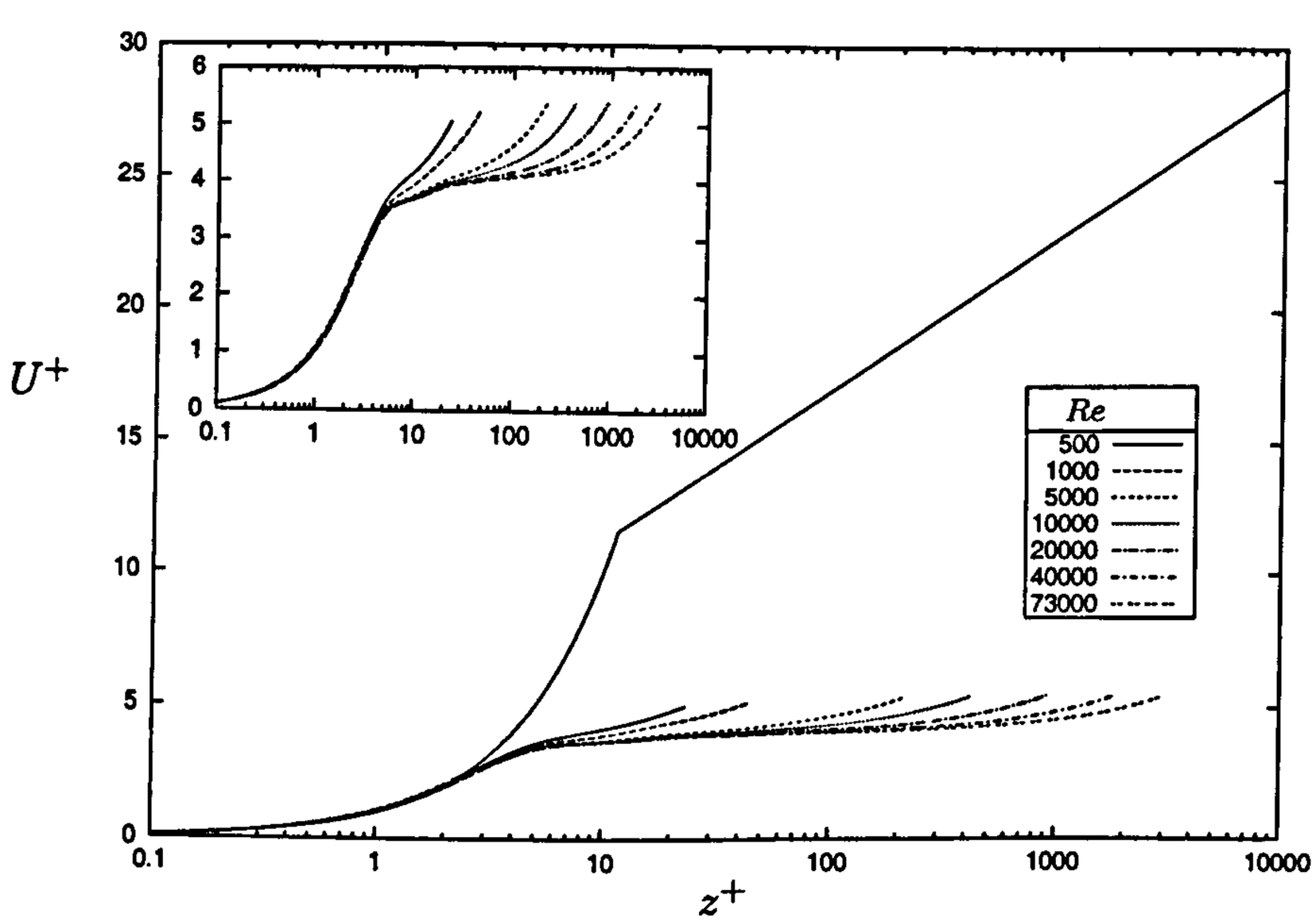


Figure 2.6: Plots of the optimal solutions mean velocity in friction units for various values of $Re$. Inset we plot a comparison of the mean velocity graphs only. On the main axes we plot the same optimal velocity graphs against the empirically observed mean velocity for turbulent plane Couette flow. This is defined by a viscous sublayer $U^+ = z^+$ and a logarithmic region $U^+ = 2.5 \ln z^+ + 5.5$. Our variables are $z^+ = Re_\tau(z + \frac{1}{2})$ where the friction Reynolds number $Re_\tau = \sqrt{\mathcal{E}/Re}$, and $U^+ = U/U_\tau$ where $U$ is the change in mean velocity away from the wall $U = \frac{Re}{2} - \overline{u} \cdot \widehat{x}$, and $U_\tau = \sqrt{\mathcal{E}/Re}$ is the friction velocity length scale .

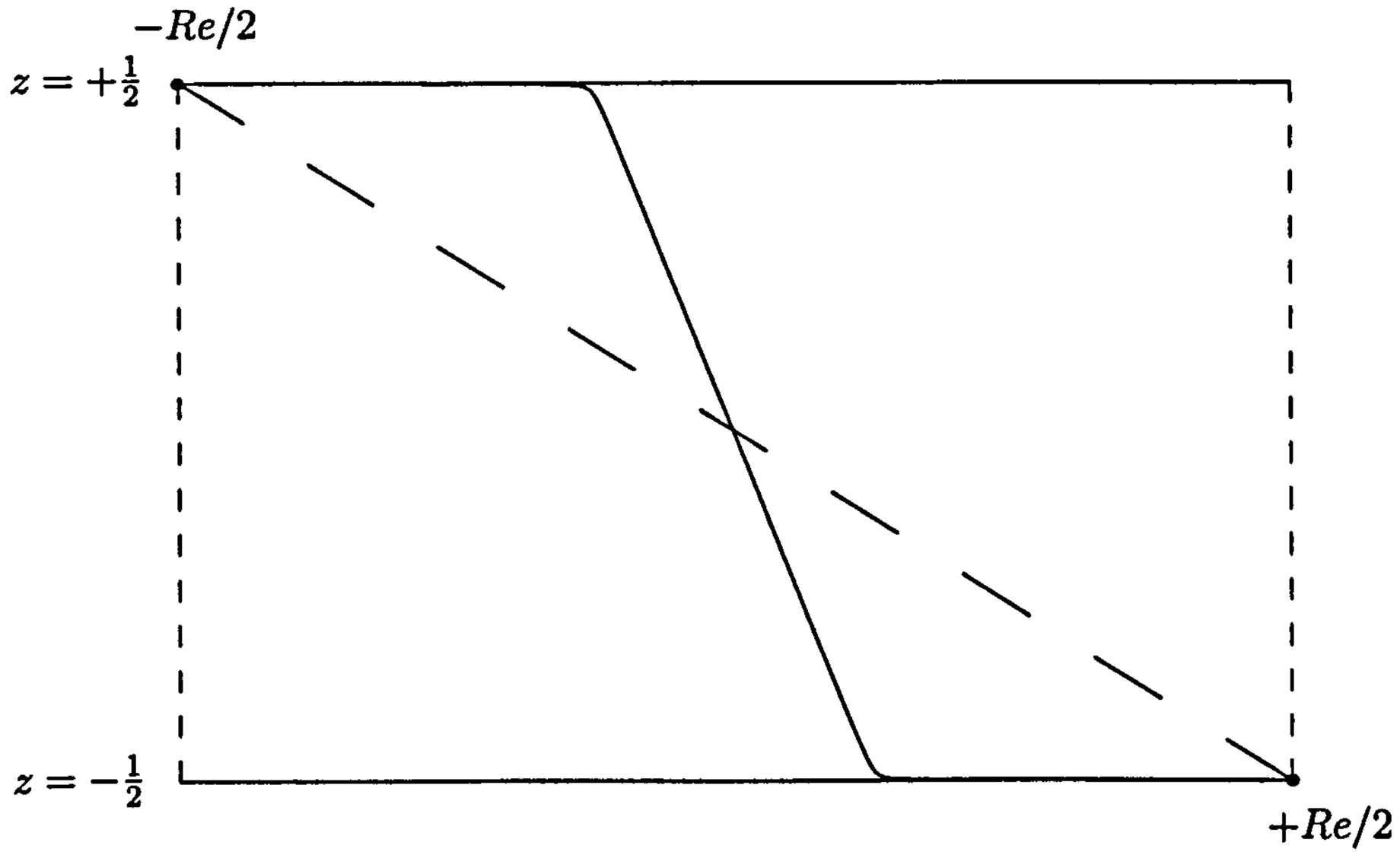


Figure 2.7: A plot of the mean velocity profile at $Re = 7.33 \times 10^4$ which clearly shows a channel interior gradient of $Re/4$, which in inviscid units is 1/4. The long dashed line is the laminar flow profile. This means that the mean velocity profile has an unphysical 1/4-shear in common with Busse's multi-$\alpha$ solutions.

solutions and their corresponding upper bounds $\varepsilon_N(Re)$ for $N \in \mathbb{N}$. Theoretically, each provides a lower estimate of the correct upper bound so that the highest such (as a function of $Re$) is of most interest. Figure 2.2 shows the bound corresponding to this estimate as $Re$ varies and since $\varepsilon_N$ scales as $Re^{-4-N}$, the curve is piecewise linear [1]. Figure 2.9 presents a comparison of the wavenumber bifurcation structure revealed here with that predicted by Busse. There is generally good agreement with the asymptotics capturing the largest wavenumber (corresponding to the innermost boundary layer structure) well. On the other hand, the asymptotics fails to reproduce the lowest wavenumber which is almost constant and $\mathcal{O}(1)$. Also by the largest $Re$ reached here, the asymptotics only predict five wavenumbers in the solution whereas, in fact, in the true solution the seventh is just about to appear.

[1] Technically, of course, Busse's results are only asymptotic but it is difficult to resist plotting their predictions down to finite $Re$ nevertheless.

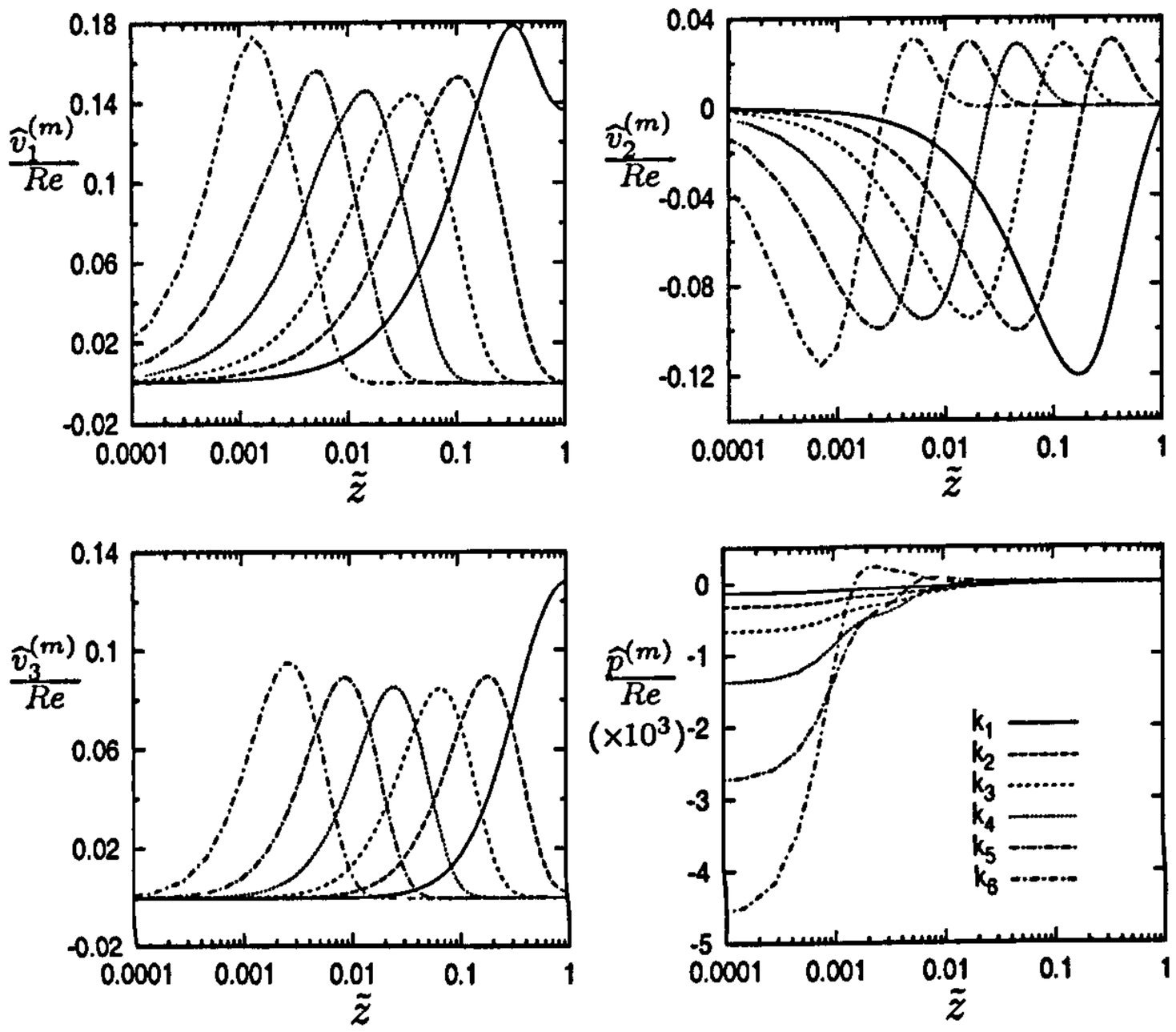


Figure 2.8: Plots of the $z$-dependent subfields of the fluctuation field at $Re = 7.33 \times 10^4$ where $\tilde{z} = 2z + 1$. The key for all of the plots is given in the pressure plot.

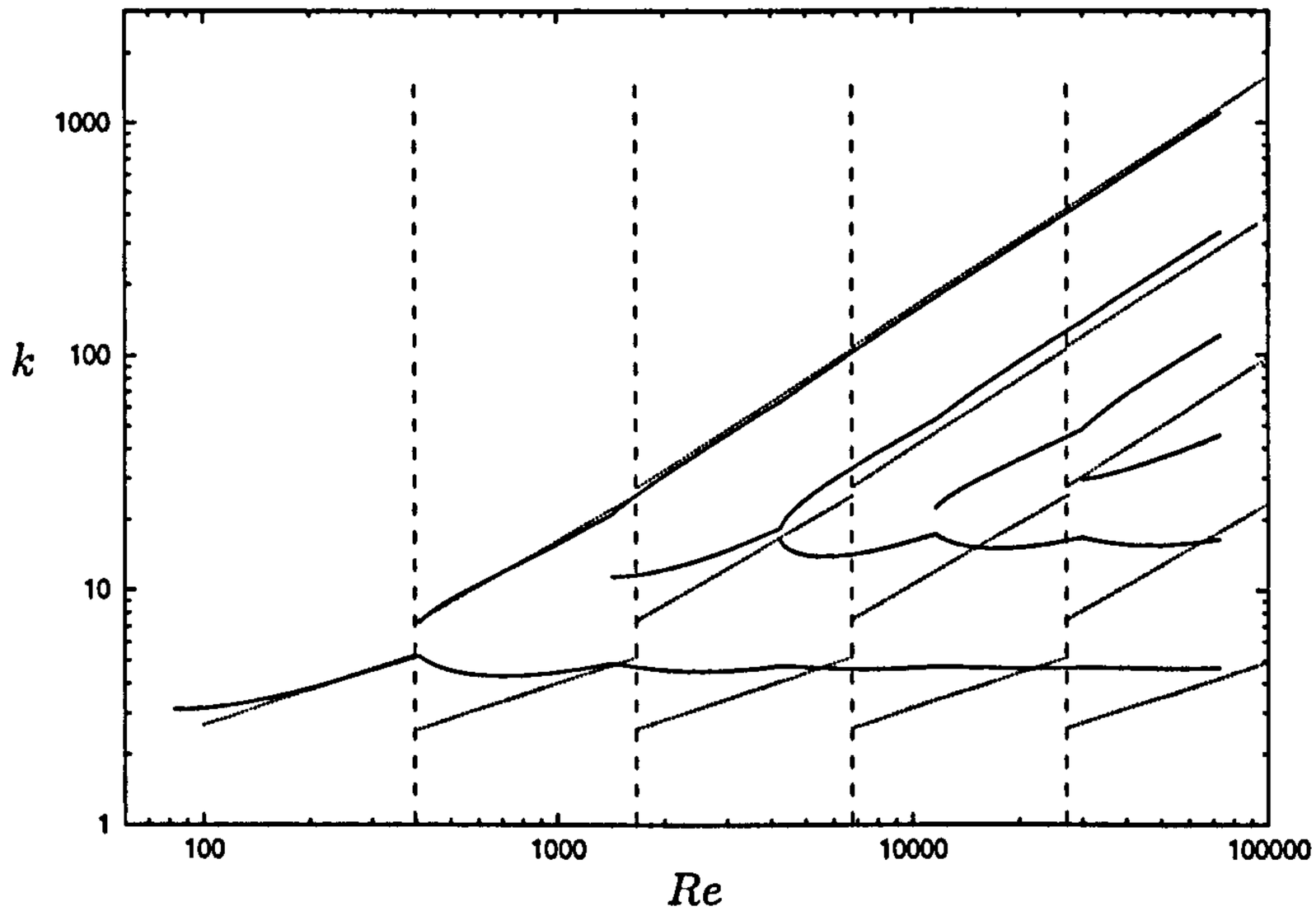


Figure 2.9: A comparison between the wavenumbers of the optimal solution and those in Busse's multi-$\alpha$ solutions. The dashed vertical lines indicate the points of incoming modes in the multi-$\alpha$ solution which are seen to occur later than the corresponding points for the optimal solution.

## 2.5 Discussion

This paper presents a complete solution to the CDH problem up until the seventh wavenumber bifurcation occurs at $Re = 73,300$. By this point, the asymptotic value of the upper bound can be predicted to be $\varepsilon_{bound} = 0.008553$ thereby improving the previous best bound found by Nicodemus *et al.* (1998*a*) by 21%. It is also clear that their use of a restricted form for the background field does give rise to anomalous behaviour in their results. Specifically, the global minimum that they find at $Re \approx 740$ is not a true feature of the exact bound. We also confirm that Busse's multiple-boundary-layer estimate is 17% too high. This discrepancy can be attributed to the neglect of supposedly 'higher order' terms in the derivation of the multiple-boundary layer solutions. In a little known technical report Busse (1968*b*), Busse estimated that there was a possible 20% margin of error in his upper bound result published in 1970, that is

$$0.8\,\varepsilon_{Busse} \approx \frac{1}{124.6} \leq \varepsilon_{bound} \leq \varepsilon_{Busse} \approx \frac{1}{99.7} \quad \text{as } Re \to \infty. \tag{2.33}$$

Since we have found $\varepsilon_{bound} = 0.008553 \approx 1/116.9$, this estimate now looks spot on.

More generally, we have confirmed that Busse's multiple-boundary technique for attacking the CDH variational problem does appear to capture the main features of the exact solution. These features include the fact that the solution develops an increasing number of nestled boundary layers corresponding to successive wavenumber bifurcations, that the velocity structures associated with each is self-similar and that the optimal mean flow assumes a $\frac{1}{4}$-shear profile. This success bodes well for other applications of this technique in different variational problems (Kerswell, 2002). We have also confirmed that the optimal mean profile does not exhibit a logarithmic layer beyond the viscous sublayer. Given the consensus view that there is vanishing interior shear at asymptotically large $Re$ (although see Busse 1996 for a counter-view), this means that the CDH variational problem only manages to capture the first (fairly trivial) essence of experimentally observed turbulent mean profiles — a viscous sublayer — albeit perhaps a factor of 3 thinner than it should be. The conclusion, if any has to be drawn, is that there is no evidence to support the hypothesis that a real turbulent flow tries to optimise the momentum transport (or equivalently the energy dissipation rate) between the plates.

The upper bound presented here is of the Kolmogorov form — the dissipation is independent of $\nu$ as $\nu \to 0$ — while experimental data and heuristic scaling methods imply a logarithmic dependence for the limiting dissipation rate. In the paper Doering, Spiegel & Worthing (2000) a dissipation bound for the problem of plane Couette flow with suction is found which is also independent of $Re$ in the limit of large $Re$. For that problem an exact steady solution has dissipation scaling exactly like the upper bound and, while there is no proof that this state is a lower bound on the dissipation, it is conjectured that the turbulent dissipation should be sandwiched between those two values and hence could not exhibit a logarithmic dependence on $Re$ in the limit of large $Re$.

We make the remark that the CDH variational problem is now exhausted. The best asymptotic bound calculated here ($\varepsilon < 0.008553$) represents just over a factor of 10 improvement on the original estimate by Doering & Constantin (1992) ($\varepsilon < 1/8\sqrt{2} \approx 0.08839$) found 10 years ago. New constraints will have to be added if this result is to be improved further.

Finally, it is worth remarking that the new upper bound derived in this paper can be converted in to an upper bound for arbitrary Prandtl number Boussinesq convection in the same geometry using techniques described in Section IV of Kerswell (2001). The upper bound result reported here $\varepsilon \leq 0.008553$ as $Re \to \infty$ is formally equivalent to the upper bound on the Nusselt number $Nu - 1 \leq 0.02634 Ra^{1/2}$ as $Ra \to \infty$.

We are grateful to F. H. Busse for bringing his 1968*b* report to our attention and along with C. Caulfield and C. Doering for many helpful comments on this manuscript. Thanks also to M. Holthaus for providing the numerical data from figure 8 of Nicodemus *et al.* (1998*a*) which is presented in our figure 2 for comparison purposes. We both gratefully acknowledge the support of the EPSRC.

## 2.A Appendix

We show here how to deduce expression (2.16) starting from the variational derivative for $a$ (equation 2.9). In what follows, we will use the formula for the mean of $\boldsymbol{\nu}$ (equation 2.14), the product $\langle \widehat{\boldsymbol{\nu}} \cdot \delta\mathcal{L}/\delta\widehat{\boldsymbol{\nu}} \rangle = 0$

$$\langle |\boldsymbol{\nabla}\widehat{\boldsymbol{\nu}}|^2 \rangle = -\lambda \langle \phi' \widehat{\nu}_1 \widehat{\nu}_3 \rangle, \tag{2.34}$$

and the equation for the background field (equation 2.17). Substituting $\boldsymbol{\nu} = \widehat{\boldsymbol{\nu}} + \overline{\nu_1}\widehat{\boldsymbol{x}}$ into equation (2.9) and using equation (2.14) we find that

$$\langle |\boldsymbol{\nabla}\widehat{\boldsymbol{\nu}}|^2 + \frac{(\lambda-2)^2}{4}(\phi' + Re)^2 + \phi'\widehat{\nu}_1\widehat{\nu}_3 + \frac{\lambda-2}{2}\phi'(\phi' + Re) \rangle = 0.$$

Now by separating the product $(\phi' + Re)^2$ by using equation (2.17) once only

$$(\phi' + Re)^2 = \frac{2}{\lambda}(\phi' + Re)(\overline{\widehat{\nu}_1\widehat{\nu}_3} - \langle \widehat{\nu}_1\widehat{\nu}_3 \rangle)$$

we are lead to the following

$$\left\langle |\boldsymbol{\nabla}\widehat{\boldsymbol{\nu}}|^2 + \frac{1}{2\lambda}\left[(\lambda-2)^2\phi'(\overline{\widehat{\nu}_1\widehat{\nu}_3} - \langle \widehat{\nu}_1\widehat{\nu}_3 \rangle) + 2\lambda\phi'\overline{\widehat{\nu}_1\widehat{\nu}_3} + 2(\lambda-2)\phi'(\overline{\widehat{\nu}_1\widehat{\nu}_3} - \langle \widehat{\nu}_1\widehat{\nu}_3 \rangle)\right] \right\rangle = 0$$

which simplifies to

$$\langle |\boldsymbol{\nabla}\widehat{\boldsymbol{\nu}}|^2 + \tfrac{1}{2}[(\lambda-2)\phi'(\overline{\widehat{\nu}_1\widehat{\nu}_3} - \langle \widehat{\nu}_1\widehat{\nu}_3 \rangle) + 2\phi'\overline{\widehat{\nu}_1\widehat{\nu}_3}] \rangle = 0.$$

Now exploiting $\langle\phi'\rangle = -Re$, which is a direct consequence of the boundary conditions on $\phi$, we may rewrite this as

$$\langle|\nabla\widehat{\nu}|^2\rangle + \tfrac{1}{2}[\lambda\langle\phi'\overline{\widehat{\nu}_1\widehat{\nu}_3}\rangle - (2-\lambda)Re\langle\widehat{\nu}_1\widehat{\nu}_3\rangle] = 0$$

and then use equation (2.34) to recover the result

$$\lambda = 2 - \frac{\langle|\nabla\widehat{\nu}|^2\rangle}{Re\langle\widehat{\nu}_1\widehat{\nu}_3\rangle}.$$

# Chapter 3

# Shear flow CDH problem: Additional constraints

## 3.1 Introduction

In this chapter we will present an algorithmic way of incorporating an additional constraint into the standard CDH problem for plane Couette flow, as solved in Chapter 2. There are two clear routes to including extra information in this bounding problem. First, one can extend the structure of the background field $\phi$, from a 1-D uni-directional function to being a function of more spatial and temporal variables or to being vector valued. This approach incorporates additional information directly from the governing equations; for instance with a steady two-dimensional background field[1] $\boldsymbol{\phi} = \phi_1(x,z)\widehat{\boldsymbol{x}} + \phi_2(x,z)\widehat{\boldsymbol{z}}$, the steady two-dimensional Navier–Stokes equations are the imposed constraints in that analysis. Constructing more general background fields clearly allows more information from the Navier-Stokes equations to be built into the variational problem as constraints (for further details see Kerswell, 1999, 2001). A systematic analysis of a class of extension based upon including extra moments of the governing equations, built upon the Howard-Busse method, can be found in Ierley & Worthing (2001).

The second route to adding extra information is to explicitly extend the Lagrangian (2.20) in the standard CDH problem, thereby remaining within the sphere

[1] With stream-function representation $\boldsymbol{\phi} = \boldsymbol{\nabla} \times \Psi(x,z)\widehat{\boldsymbol{y}}$.

of a single-valued uni-directional background field $\phi(z)$. Using Lagrange multipliers to enforce additional constraints is an easy way of extending the problem of Chapter 2, however, new constraints must be independent of existing constraints for the extension to make sense. If the full set of constraints are mutually congruent, then the necessary alterations to the previous optimal equations can be made in a transparent manner. In this Chapter, the additional constraint can not be derived from the governing equations, but is a constraint which is hypothetical and reflects a weak form of Malkus's second theory (see Malkus, 1954*a*, 1956). We will attempt to construct extremising solution of the standard CDH method for plane Couette flow with the added constraint that the optimal mean profile is marginally linear-stable. If the hypothesis that the turbulent means are only marginally stable to infinitesimal disturbances is true, then we would expect that our computed upper bound fit more closely with realised solutions and that the optimal fields should be quantitatively more like realised velocity fields. This project is, therefore, a test of a non-rigorous assumption and is not a 'rigorous' extension of the set of constraints.

The layout of this chapter will be as follows. We will begin by attempting to validate Busse's assumption (first made in Busse, 1969*a*, for the asymptotic multi-$\alpha$ calculation) that optimal solutions of the PCF variational problem are streamwise independent ($\partial_x = 0$); or equivalently that the critical eigenfunctions in the spectral constraint eigenvalue problem are streamwise rolls[2]. Given a positive result we can conclude that the solutions of Chapter 2 are indeed the true extremising solutions and no further improvements can be made to the solution of the standard upper bound problem. We will then turn to investigating the linear stability of the mean profiles computed in Chapter 2. This exercise then naturally leads on to formulating an extended bounding problem incorporating marginal linear-stability as a new hypothetical constraint. We will derive the full set of Euler–Lagrange equations, describe a possible solution strategy and present preliminary findings.

[2]This assumption meant that in Chapter 2 we studied optimal fluctuations of the form $\nu(x,y,z) = \widehat{\nu}(z)\mathrm{e}^{\mathrm{i}(\alpha x + ky)}$ where $\alpha = 0$.

## 3.2 Three-dimensional disturbance in the spectral constraint

The long standing hypothesis in bounding theory, with beginnings in the multi-$\alpha$ theory in Busse's shear flow variational problem (Busse, 1969*a*), is that the extremising solutions of the variational problem are streamwise independent — and therefore two-dimensional. This conjecture follows on from the absolute stability of plane Couette flow, for which the extremising fields have $\partial_x = 0$, because the spectral constraint is identical to absolute stability[3] except that the mean $U(z)$ is replaced by $\lambda\phi(z)$. However, no proof exists for the critical eigenfunctions of the spectral constraint for plane Couette flow being $x$-independent. Let us remind ourselves of the spectral constraint considered in Chapter 2: given a pair $(\phi, \lambda)$ the eigenvalues of the following problem are negative semi-definite

$$2\boldsymbol{\nabla}^2 \boldsymbol{v} - \lambda\phi' \begin{bmatrix} v_3 \\ 0 \\ v_1 \end{bmatrix} + \boldsymbol{\nabla} p = \mu \boldsymbol{v} \tag{3.1}$$

subject to $\boldsymbol{\nabla} \cdot \boldsymbol{v} = 0$ and the no-slip boundary conditions $\boldsymbol{v} = 0$ at $z = \pm\frac{1}{2}$. (This problem is self-adjoint, and therefore admits only real eigenvalues.) It has previously been taken for granted that the extremising vector fields are streamwise rolls with $\partial_x = 0$, which take this form:

$$\boldsymbol{v} = \boldsymbol{\nabla} \times [\Psi(z) \mathrm{e}^{\mathrm{i}ky} \widehat{\boldsymbol{x}}] + v_1(z) \widehat{\boldsymbol{x}}.$$

We will test this assumption for two optimal solutions calculated numerically in Chapter 2, one at $Re = 5017.1$ and another at $Re = 73300$, by computing a fine-grid $(\alpha, k)$ search for unstable three-dimensional perturbations.

### 3.2.1 General 3-D spectral constraint

The eigenvalue form of the spectral constraint (3.1) is equivalent to the functional

$$\mathcal{H}_{\phi,\lambda}(\boldsymbol{\nu}) = \langle |\boldsymbol{\nabla}\boldsymbol{\nu}|^2 \rangle + \lambda \langle v_1 v_3 \phi' \rangle \tag{3.2}$$

[3] We direct the reader to Drazin & Reid (1981) or Joseph (1976) for detailed studies of the stability properties of fluid flows.

being positive semi-definite for all admissible divergence-free vector fields satisfying Dirichlet boundary conditions. Now we are enlarging this field to include three-dimensional divergence free fields which take the general form:

$$\boldsymbol{v} = \boldsymbol{\nabla} \times (\boldsymbol{\nabla} \times \widehat{\varphi}(x,y,z)\widehat{\boldsymbol{z}}) + \boldsymbol{\nabla} \times \widehat{\psi}(x,y,z)\widehat{\boldsymbol{z}}.$$

If we allow the following abbreviations $\nabla_H^2 = \partial_x^2 + \partial_y^2$, and $\mathrm{D} \equiv (\,)' \equiv \mathrm{d}/\mathrm{d}z$, one can write a corresponding two equation eigenvalue set:

$$\begin{aligned} 2\nabla^2\nabla_H^2\widehat{\psi} + \lambda\phi'\nabla_H^2\partial_y\widehat{\varphi} &= \mu\nabla_H^2\widehat{\psi} \\ 2\nabla^4\nabla_H^2\widehat{\varphi} + \lambda\phi'\left(2\nabla_H^2\partial_{xz}\widehat{\varphi} + \nabla_H^2\partial_y\widehat{\psi}\right) + \lambda\phi''\nabla_H^2\partial_x\widehat{\varphi} &= \mu\nabla^2\nabla_H^2\widehat{\varphi} \end{aligned}$$

Using the decomposition

$$\widehat{\varphi}(x,y,z) = \mathrm{e}^{\mathrm{i}(\alpha x + ky)}\varphi(z)$$

and similarly for $\widehat{\psi}$ this system becomes

$$\begin{aligned} 2(\mathrm{D}^2 - \alpha^2 - k^2)\psi + \mathrm{i}k\lambda\phi'\varphi &= \mu\psi, \\ 2(\mathrm{D}^2 - \alpha^2 - k^2)^2\varphi + \mathrm{i}\lambda\phi'\left(2\alpha\mathrm{D}\varphi + k\psi\right) + \mathrm{i}\alpha\lambda\phi''\varphi &= \mu(\mathrm{D}^2 - \alpha^2 - k^2)\varphi, \end{aligned} \tag{3.3}$$

with the boundary conditions on the scalar functions being $\varphi = \mathrm{D}\varphi = \psi = 0$ at $z = \pm\frac{1}{2}$. We observe that transforming $k \to -k$ and $\psi \to -\psi$ leaves system (3.3) unchanged, which implies that the growth surface over the plane $(\alpha, k)$ has mirror symmetry in $k$. Also it is evident that plane Couette flow is invariant to a coordinate change of the form: $z \to -z$ and $x \to -x$. That is to say, the transformation $\alpha \to -\alpha$ and $z \to -z$ leave system (3.3) unchanged. Therefore, the growth surface also has mirror symmetry in $\alpha$.

### 3.2.2 Revisiting the CDH solutions

The highest order $z$-derivative of system (3.3) is fourth. Therefore, in a spectral methods solution of (3.3) the natural choice of orthogonal polynomials to expand $\psi$ and $\varphi$ are Jacobi polynomials for which the Galerkin projection of the $\mathrm{D}^4$ operator is sparse and unconditionally stable. The optimal solutions $\phi$ from Chapter 2 are converted from Chebyshev expansion to Jacobi expansion and an eigenvalue solver calculates the maximum eigenvalue for points in the $(\alpha, k)$ plane. Fine grid plots of

the growth surface at two different values of $Re$ are calculated. We find that the maximum growth rate is indeed attained at $\alpha = 0$ and figures 3.1 and 3.2 illustrate the degree of decay away from the $k$-axis with surface contours equi-spaced in log of the growth rate. The upshot of this is that the solutions of Chapter 2 are indeed optimal and that Busse's original assumption of two-dimensionality is correct.

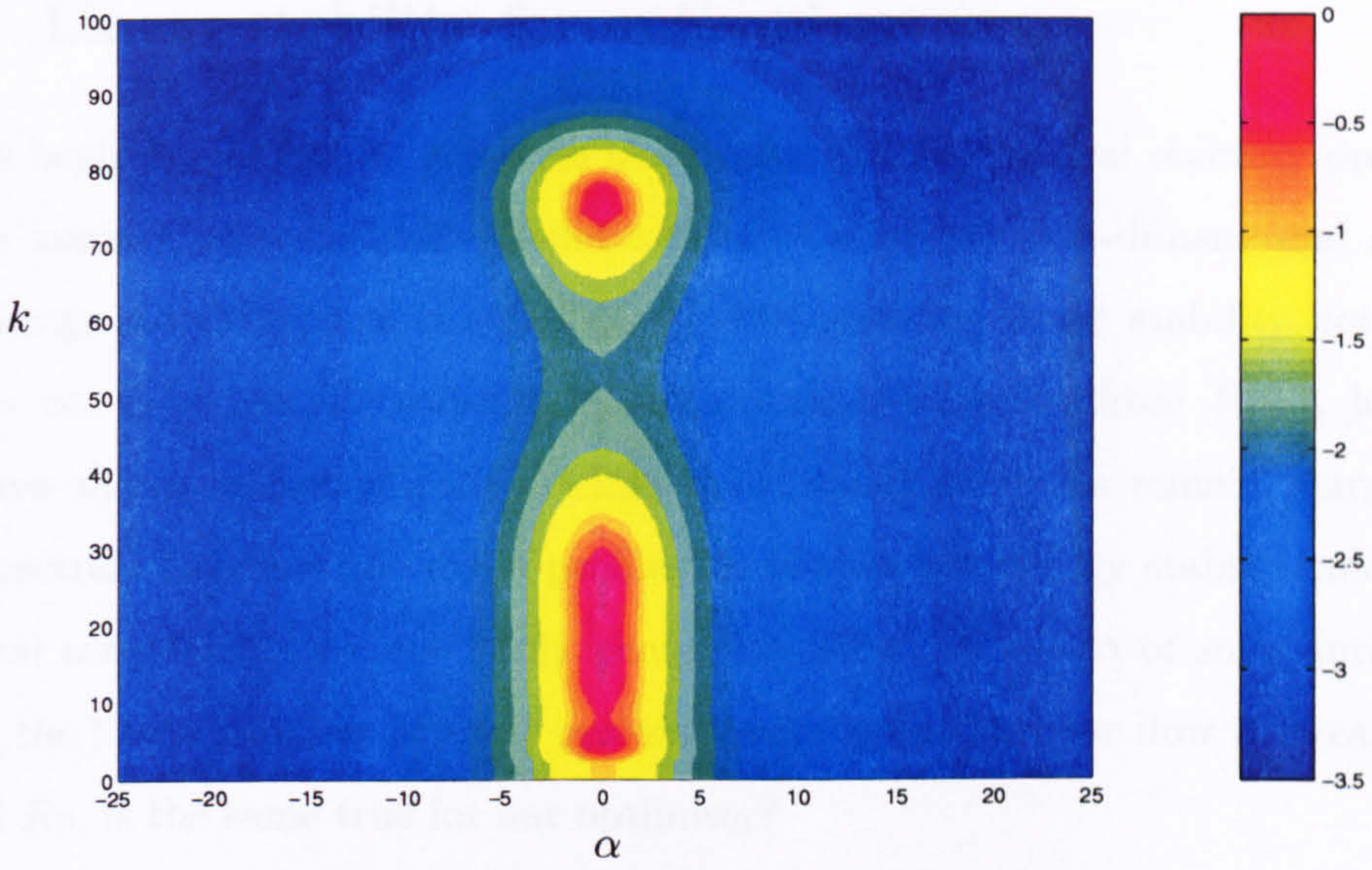


Figure 3.1: Plot of $-\log_{10}(1+|\mu|)$ for $\mu$ the maximum eigenvalue of (3.3) calculated for various pairs $(\alpha, k)$ for an optimal solution to the CDH problem with four fluctuation fields at $Re = 5017.1$.

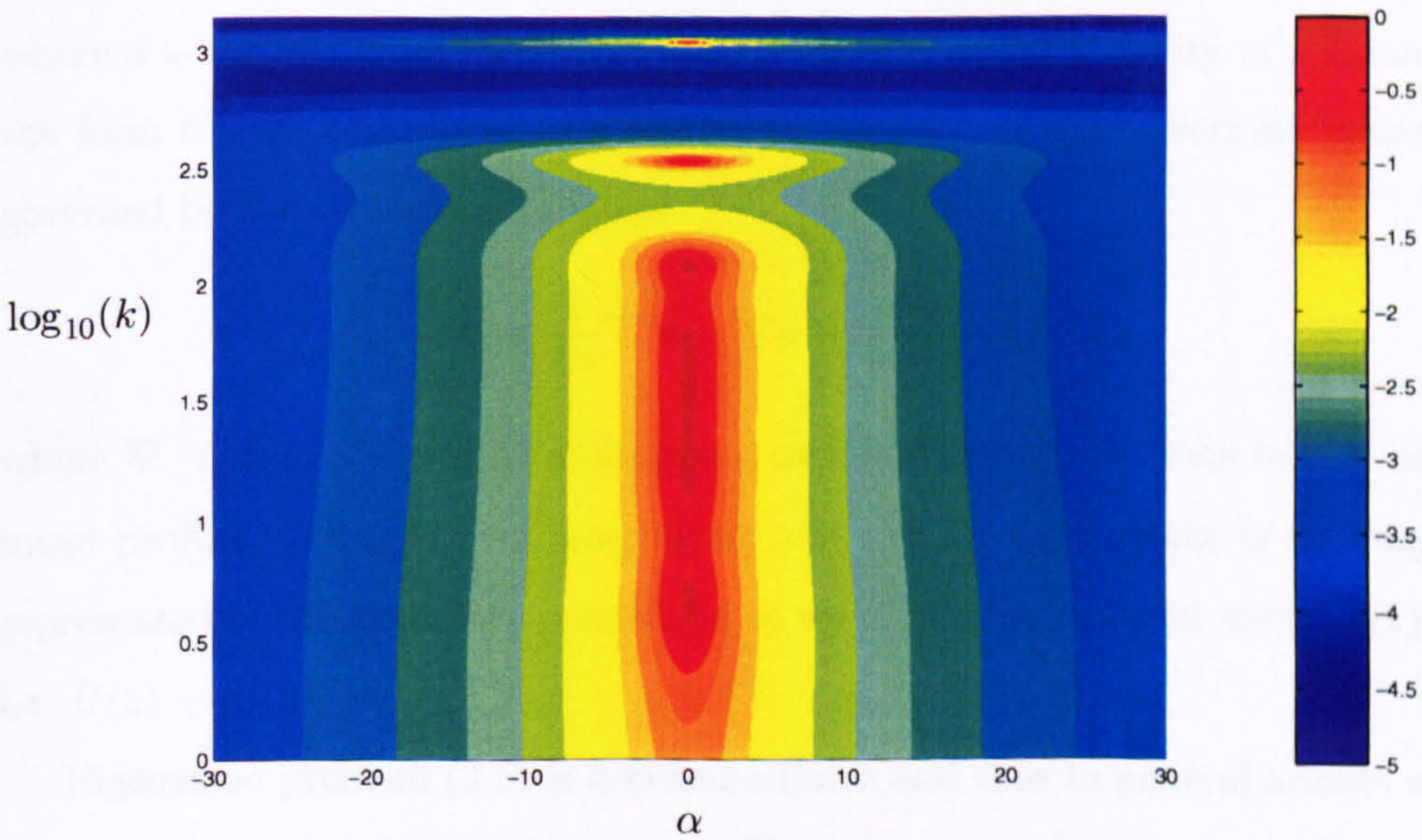


Figure 3.2: Plot of $-\log_{10}(1+|\mu|)$ for $\mu$ the maximum eigenvalue of (3.3) calculated for various pairs $(\alpha, k)$ for an optimal solution to the CDH problem with six fluctuation fields at $Re = 73300$.

## 3.3 Linear stability for optimal means

Let us begin by reminding ourselves about some of the classical stability properties of the laminar state in plane Couette flow. Under our non-dimensional scheme, the energy stability point is at $Re_{ES} = 82.66$ and the linear stability point is at $Re_c = \infty$. The optimal solution bifurcates super-critically from $Re_{ES}$, however, we have shown numerically that while the optimal solutions remain marginal to the spectral constraint the mean profiles do not remain energy stable. Indeed, the spectral constraint does not imply energy stability. It is also of some interest to study the linear stability of these optimal means. The laminar flow is linear stable for all $Re$, is the same true for our optimiser?

### 3.3.1 Primitive linear stability equations

The mean profile from Chapter 2 is just

$$U(z) = \frac{\lambda}{2}\left[\phi(z) + Re\, z\right] - Re\, z \tag{3.4}$$

where $\phi$ is the now familiar background field. The linear stability of a mean flow of the form $U(z)\widehat{\boldsymbol{x}}$, considered as a stationary solution of the governing equations, is governed by the eigenvalue problem

$$\mu\mathbf{q} = \frac{1}{Re}\nabla^2\mathbf{q} - \boldsymbol{\nabla} p - U\frac{\partial \mathbf{q}}{\partial x} - q_3 U'\widehat{\boldsymbol{x}}, \tag{3.5}$$

where $\boldsymbol{\nabla}\cdot\mathbf{q} = 0$. We will be looking not at a stationary solutions but at turbulent mean profiles, averaged over long times, and the $Re$ dependence is no longer only represented in the boundary conditions so we divide the optimal mean $U(z)$ by $Re$, i.e. $U(z) \to U(z)/Re$.

Eigenvalue problem (3.5) is non-self-adjoint and thus in general admits complex eigenvalue and eigenfunctions. Squire's Theorem states that the most excited eigenfunctions are spanwise rolls, for which $\partial_y = 0$, and have no $y$-component, $q_2 = 0$. Therefore, one only need consider fields of the form

$$\mathbf{q} = \mathbf{q}(z)\mathrm{e}^{\mathrm{i}\alpha x}$$

with $\mathbf{q}(z) = (q_1(z), 0, q_3(z))$. Under these simplifications we are left with the follow-

ing $z$-dependent eigensystem

$$\mu\mathbf{q} = \frac{1}{Re}(\mathrm{D}^2 - \alpha^2)\mathbf{q} - \begin{bmatrix} \mathrm{i}\alpha \\ 0 \\ \mathrm{D} \end{bmatrix} p - \mathrm{i}\alpha U\mathbf{q} - q_3 U'\widehat{\boldsymbol{x}}, \tag{3.6}$$

where $\mathrm{i}\alpha q_1 + \mathrm{D}q_3 = 0$.

The corresponding adjoint system to (3.6) with respect to the inner product $(\mathbf{a}, \mathbf{b}) = \langle \mathbf{a}^* \cdot \mathbf{b} \rangle$, is

$$\mu^*\mathbf{q}^\dagger = \frac{1}{Re}(\mathrm{D}^2 - \alpha^2)\mathbf{q}^\dagger - \begin{bmatrix} \mathrm{i}\alpha \\ 0 \\ \mathrm{D} \end{bmatrix} p^\dagger + \mathrm{i}\alpha U\mathbf{q}^\dagger - q_1^\dagger U'\widehat{\boldsymbol{z}}, \tag{3.7}$$

for divergence-free $\mathbf{q}^\dagger$: $\mathrm{i}\alpha q_1^\dagger + \mathrm{D}q_3^\dagger = 0$.

### 3.3.2 The Orr–Sommerfeld equation

The streamfunction form of this eigenvalue set is known as the Orr–Sommerfeld equation. Because $\mathbf{q}$ is a two-dimensional divergence-free field we can express it in terms of a streamfunction $\psi(z)$ by setting $q_1 = \mathrm{D}\psi$ and $q_3 = -\mathrm{i}\alpha\psi$. Then the system of primitive equations (3.6) is reduced to only $(\boldsymbol{\nabla} \times \mathrm{Eqn}(3.6)) \cdot \widehat{\boldsymbol{y}}$, which is simply

$$\frac{1}{Re}\nabla^4\psi - \mathrm{i}\alpha[(\nabla^2\psi)U - \psi U''] = \mu\nabla^2\psi \tag{3.8}$$

with corresponding boundary conditions $\psi = \psi' = 0$ at $z = \pm\frac{1}{2}$ and in this context $\nabla^2 = (\mathrm{D}^2 - \alpha^2)$. The adjoint problem with equivalent boundary conditions is:

$$\frac{1}{Re}\nabla^4\psi^\dagger + \mathrm{i}\alpha[(\nabla^2\psi^\dagger)U + 2(\mathrm{D}\psi^\dagger)U'] = \mu^*\nabla^2\psi^\dagger. \tag{3.9}$$

### 3.3.3 Over-stable optimal means

Selecting an optimal background profile at some point $Re$ from Chapter 2, one constructs the mean profile $U(z)$ by (3.4) and scale out $Re$ so that $U = \mp\frac{1}{2}$ at $z = \pm\frac{1}{2}$. The growth curve can be calculated at Reynolds numbers other than the flow Reynolds number $Re$. We may suppose that at some Reynolds number, say

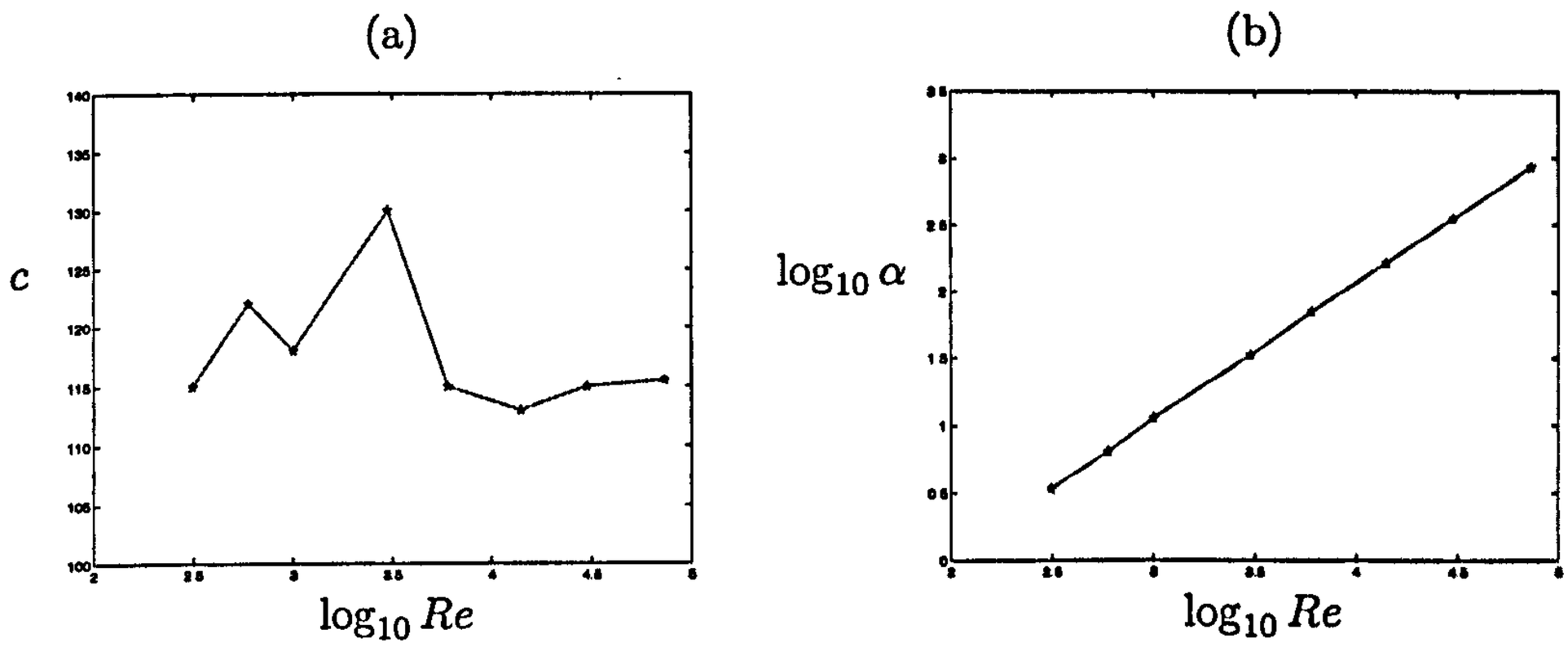


Figure 3.3: (a) Plot of the factor $c = Re_s/Re$ for optimal mean profiles of the standard CDH problem, (b) Plot of the critical streamwise wavenumber

$Re_s$, the mean profile $U$ is only marginally stable. Then let us define the factor $c := Re_s/Re$. If the mean profile is linearly stable at the flow Reynolds number then this factor quantifies the degree of *over-stability*, i.e. $c > 1$. Our numerical analysis of the optimal solutions from Chapter 2 shows that the mean profiles are in fact over-stable and the trend with increasing $Re$ is for the degree of over-stability to level off to around $c = 115$, as illustrated in figure 3.3.

## 3.4 Extending the CDH problem

We now turn to imposing a linear stability constraint on the mean profile of the standard CDH problem by extending the Lagrangian in (2.20) with a constraint which is only a function of the mean profile $U(z)$. We note that the mean was decomposed in the following way: $U(z) = \phi(z) + \overline{\nu_1}(z)$, where in the standard problem $\overline{\nu_1}(z)$ was found in terms of $\phi(z)$ to yield the mean profile in equation (3.4). A linear stability constraint will only alter the optimal equations for $\phi$ and $\overline{\nu_1}$ and, moreover, does not change the velocity decomposition $u = (\phi + \overline{\nu_1})\widehat{x} + \widehat{\nu}$, where $\overline{\widehat{\nu}} = 0$, or the form of the spectral constraint. However, the expression for the mean velocity (3.4) will no longer be valid.

With $\gamma$ denoting the Lagrange multiplier imposing the constraint of marginal linear stability for some $Re_s$; i.e. $\mathcal{R}e(\mu) = 0$ where $\mu$ is intended to represent the highest eigenvalue of equation (3.6) over all streamwise wavenumbers $\alpha$. Therefore

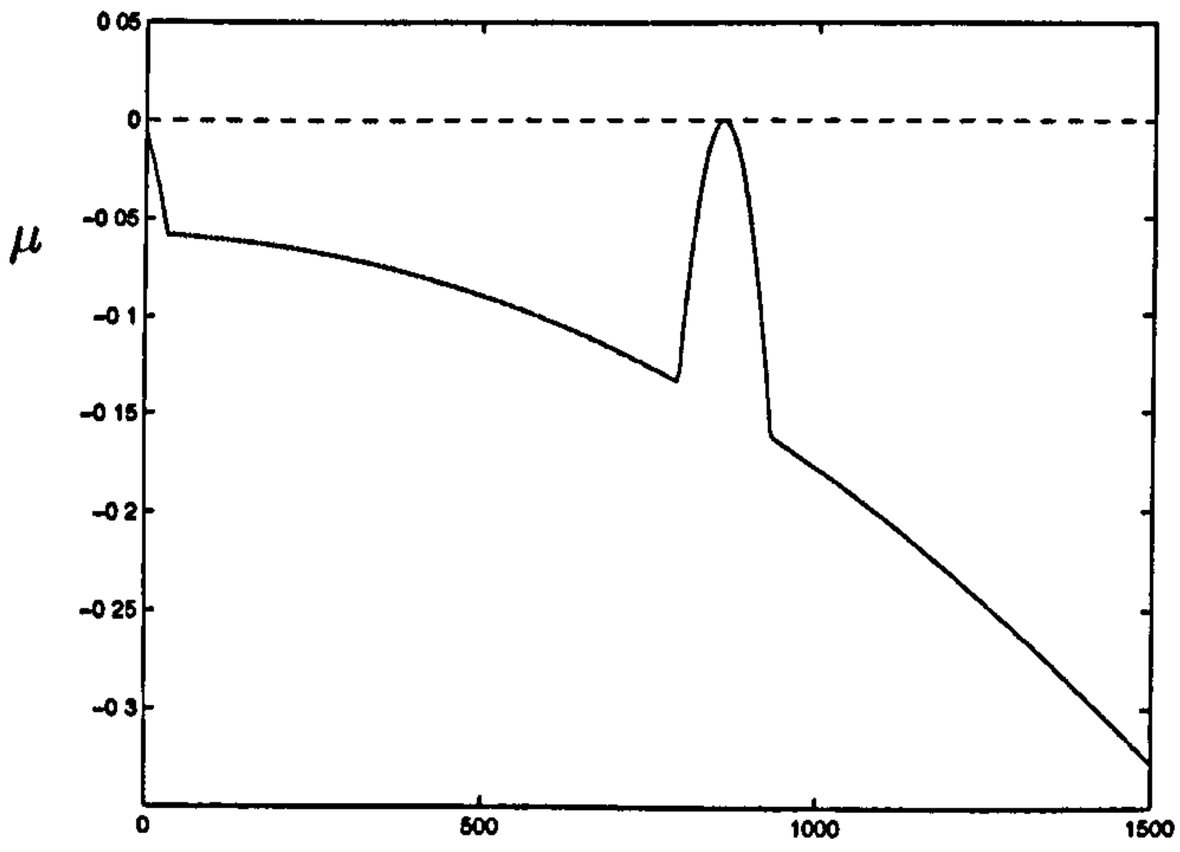


Figure 3.4: The growth rate curve for the optimal CDH mean profile at $Re = 73300$ with $c_{opt} = 115.51$

$\gamma$ is a function of the ratio $c$ and the extended Lagrangian functional is

$$\mathcal{L} = \langle(\phi' + \overline{\nu_1}')(\phi' + (1-a)\overline{\nu_1}')\rangle - \mathcal{H}_{\phi,a}(\widehat{\nu}) - \gamma\,\mathfrak{Re}(\mu) \tag{3.10}$$

after some manipulation of the terms in equation (2.20). The spectral constraint $\mathcal{H}_{\phi,a}(\widehat{\nu}) = (a-1)\langle|\nabla\widehat{\nu}|^2\rangle + a\langle\phi\widehat{\nu}_1\widehat{\nu}_3\rangle \geq 0$ is unchanged. The maximum eigenvalue of (3.6) $\mu$, is a function of the factor $c$, and we seek to control $c$ using Lagrange multiplier $\gamma$ with the objective of bringing $c$ to 1; at which point marginal linear stability is achieved at the flow Reynolds number. If we denote $c$ pictured in figure 3.3 for the standard CDH profile as $c_{opt}$, then we have a convenient starting point for a continuation study, at $c_{opt}$ the constraint is mute and $\gamma = 0$, and away from $c_{opt}$, we assume $\gamma$ is a continuous function of $c$, $\gamma$ will measure the degree of feedback of the eigenfunctions of (3.6) on $\phi$ and $\overline{\nu_1}$.

The spectral constraint (SC) and the linear stability (LS) constraint are independent constraints . Although SC is an energy stability (ES) type constraint we have verified previously that the extremal fields are spanwise rolls but that SC does not imply ES. SC is purely a constraint on $\phi$ and as such does not limit LS which is a constraint on the total mean $U$. LS has extremal fields which are streamwise rolls and it is best to understand this constraint as controlling $\overline{\nu_1}$, while independently SC controls $\phi$. In this scenario, we consider the fluctuation subfields to be attached to $\phi$ and the LS eigenfunctions attached to $\overline{\nu_1}$. Moreover, the optimal mean fields

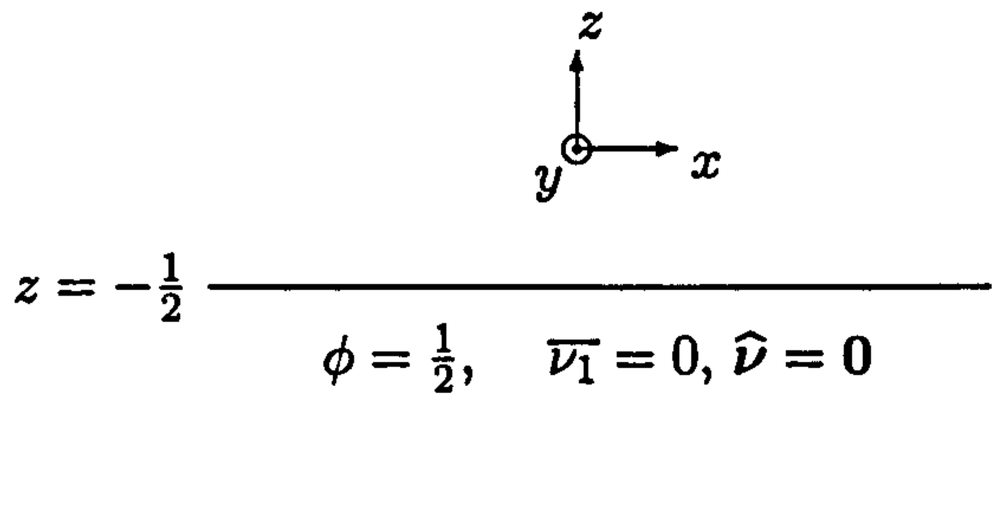


Figure 3.5: Re-scaled boundary conditions for linear stability problem

can simultaneously satisfy the spectral constraint and also be marginally linearly stable at $Re_s = cRe$ for any $c \geq 1$. The constraints are therefore independent.

### 3.4.1 Formulation

To begin developing a self-contained definition of the new problem let us scale out $Re$ from the boundary conditions. Let $\phi \rightarrow \phi/Re$ and $\overline{\nu_1} \rightarrow \overline{\nu_1}/Re$ then figure 3.5 describes the new boundary conditions.

Given that $Re_s = c\,Re$ and $U(z) = \phi(z) + \overline{\nu_1}(z)$, we can now restate the bounding problem as follows:

Minimise the following functional over the fields $\phi$ and $\overline{\nu_1}$ subject to the boundary conditions in figure (3.5)

$$\mathcal{L} = Re^2\langle(\phi' + \overline{\nu_1}')(\phi' + (1-a)\overline{\nu_1}')\rangle - \mathcal{H}_{\phi,a}(\widehat{\nu}) - \gamma\,\Re e(\mu(\overline{\nu_1};\phi,c)) \tag{3.11}$$

where

$$\mathcal{H}_{\phi,a}(\widehat{\nu}) = (a-1)\langle|\nabla\widehat{\nu}|^2\rangle + a\,Re\langle\phi\widehat{\nu}_1\widehat{\nu}_3\rangle$$

and $\mu$ is the largest eigenvalue, over all $\alpha$, of

$$\frac{1}{Re_s}\nabla^2\mathbf{q} - \nabla p - U'q_3\widehat{x} - i\alpha U\mathbf{q} = \mu\mathbf{q}$$

for divergence-free $\widehat{\nu}$ and $\mathbf{q}$ satisfying Dirichlet boundary conditions.

### 3.4.2 Euler–Lagrange equation

In the rest of this section we will present all of the details required to extend the optimal equations from the standard CDH problem. Lastly, we will discuss our

experiences with trying to implement this extended problem numerically. We begin with restating the equations which are unchanged under this extension and then consider the changes to the $\phi$ and $\overline{\nu_1}$ equation and beyond.

### 3.4.3 Preserved equations

Note that in the old $\lambda$-equation (2.16), $\overline{\nu_1}$ did not appear because it was expressed in terms of $\phi$. Now, however, we see from $\delta\mathcal{L}/\delta a$ that $\lambda = a/(a-1)$ is indeed a function of both of these fields:

$$\frac{\delta\mathcal{L}}{\delta a} := -\langle|\nabla\widehat{\nu}^{(m)}|^2 + Re\phi'\widehat{\nu}_1^{(m)}\widehat{\nu}_3^{(m)}\rangle - \langle\overline{\nu_1}'(\phi' + \overline{\nu_1}')\rangle = 0.$$

Using $\langle|\nabla\widehat{\nu}|^2\rangle = -\lambda Re\langle\phi'\widehat{\nu}_1\widehat{\nu}_3\rangle$ we can rewrite this as

$$\frac{\delta\mathcal{L}}{\delta a} = \langle\left[(\lambda-1)\phi' - \overline{\nu_1}'\right]\widehat{\nu}_1^{(m)}\widehat{\nu}_3^{(m)}\rangle.$$

Thus the four equations which go unchanged are

$$\frac{2}{Re}\nabla^2\widehat{\nu} - \lambda\phi'\begin{bmatrix}\widehat{\nu}_3\\0\\\widehat{\nu}_1\end{bmatrix} + \nabla\widehat{p} = 0, \tag{3.12}$$

$$\nabla\cdot\widehat{\nu} = 0, \tag{3.13}$$

$$\frac{k}{Re}\langle|\widehat{\nu}|^2\rangle + \tfrac{1}{2}\langle\widehat{p}\widehat{\nu}_2\rangle = 0, \tag{3.14}$$

$$\lambda = 1 + \frac{\langle\overline{\nu_1}'\widehat{\nu}_1^{(m)}\widehat{\nu}_3^{(m)}\rangle}{\langle\phi'\widehat{\nu}_1^{(m)}\widehat{\nu}_3^{(m)}\rangle}. \tag{3.15}$$

It is worth being pedantic here and explicitly defining the integrals which are summed over all fluctuations (denoted using superscript $(m)$). All other equations without superscripts are satisfied by each of the fluctuation subfields individually.

### 3.4.4 Changes to optimal equations

We now turn our attention to the extra terms in equations (2.10) and (2.13) that will come from the two identical variations

$$\frac{\delta\mu}{\delta\phi} = \frac{\delta\mu}{\delta\overline{\nu_1}},$$

which appear in the $\phi$ and $\overline{\nu_1}$ equations in the following manner:

$$\frac{\delta\mathcal{L}}{\delta\phi} := -2\phi'' + \frac{a}{Re}\widehat{\overline{\nu_1}\widehat{\nu_3}}' + (a-2)\overline{\nu_1}'' - \gamma\,\mathfrak{Re}\left(\frac{\delta\mu}{\delta\phi}\right) = 0, \tag{3.16}$$

$$\frac{\delta\mathcal{L}}{\delta\overline{\nu_1}} := 2(a-1)\overline{\nu_1}'' + (a-2)\phi'' - \gamma\,\mathfrak{Re}\left(\frac{\delta\mu}{\delta\overline{\nu_1}}\right) = 0. \tag{3.17}$$

Grounding our analysis within the space of odd $z$-functions for the mean fields, which seems most natural for this vertically symmetric problem, let $\delta\phi$ be an arbitrary odd perturbation on $\phi$. Then if system (3.6) is denoted in the operator form $\mu\mathbf{q} = \mathcal{M}\mathbf{q}$ the perturbed system is

$$\delta\mu\,\mathbf{q} + \mu\,\delta\mathbf{q} = (\delta\mathcal{M})\,\mathbf{q} + \mathcal{M}\,\delta\mathbf{q}. \tag{3.18}$$

where $\delta\mathbf{q}$ is the attributed change in $\mathbf{q}$ which is evidently also divergence-free because the incompressibility condition is invariant under a variation in $\phi$.

Multiplying equation (3.18) by the corresponding adjoint eigenvector $\mathbf{q}^\dagger$ and rearranging we have

$$\delta\mu(\mathbf{q}^\dagger,\mathbf{q}) + (\mathbf{q}^\dagger,(\mu-\mathcal{M})\delta\mathbf{q}) = (\mathbf{q}^\dagger,(\delta\mathcal{M})\mathbf{q}) \tag{3.19}$$

where the second term on the left hand side drops since

$$(\mathbf{q}^\dagger,(\mu-\mathcal{M})\delta\mathbf{q}) = ((\mu^*-\mathcal{M}^\dagger)\mathbf{q}^\dagger,\delta\mathbf{q}) = 0.$$

We can now see that to calculate $\mu$-variations we need both the eigenfunction and its adjoint. The variation of the operator $\mathcal{M}$ with $\phi$ is

$$(\delta\mathcal{M})\mathbf{q} = -i\alpha(\delta\phi)\mathbf{q} - q_3(\delta\phi)'\widehat{\boldsymbol{x}},$$

and therefore equation (3.19) can be rewritten as

$$\delta\mu(\mathbf{q}^\dagger,\mathbf{q}) = \langle[-i\alpha\mathbf{q}^{\dagger *}\cdot\mathbf{q} + (q_1^{\dagger *}q_3)']\delta\phi\rangle.$$

The $\mu$-variation required to complete equations (3.16) and (3.17) is therefore

$$\frac{\delta\mu}{\delta\phi} = \frac{[-i\alpha\mathbf{q}^{\dagger *}\cdot\mathbf{q} + (q_1^{\dagger *}q_3)']}{(\mathbf{q}^\dagger,\mathbf{q})}. \tag{3.20}$$

### 3.4.5 Symmetry considerations

A crucial aspect of this analysis is the need to preserve symmetry in $z$ for the fields $\phi$ and $\overline{\nu_1}$ because on physical grounds we can expect only a symmetric mean profile to emerge from a problem posed with up-down symmetry. This means that the optimal equations for $\phi$ and $\overline{\nu_1}$ (3.16 and 3.17) must contain only odd terms. In the standard CDH problem this is true because of the symmetric preserving nature of the spectral constraint eigenproblem. Now we need to do some more work to show that the additional contributions from $\delta\mu/\delta\phi$ are quite naturally symmetric.

We first note that in general the eigenfunctions of the linear stability problem are not symmetric. A discussion of this property can be found in Drazin & Reid (1981). In general there are four solutions which have the same real part of their eigenvalue and these can be found by the operations of complex conjugation and the rotation $S_2 : (x, y, z) \to (-x, y, -z)$. Consider the Orr–Sommerfeld equation

$$\frac{1}{Re_s}\nabla^4\psi - i\alpha[(\nabla^2\psi)U - \psi U''] = \mu\nabla^2\psi.$$

If we write this in the operator form $\mathcal{M}(\mathrm{i}\alpha, U(z))\psi = \mu\mathcal{G}\psi$ then the following observation is trivial

$$\psi(z)\mathrm{e}^{\mathrm{i}\alpha x} \text{ solution with } \mu \implies \psi^*(z)\mathrm{e}^{-\mathrm{i}\alpha x} \text{ solution with } \mu^*.$$

If we now take $z \to -z$ we have

$$\mathcal{M}(\mathrm{i}\alpha, U(-z))\psi(-z) = \mu\mathcal{G}\psi(-z)$$

and since $U(z)$ is odd $\mathcal{M}(\mathrm{i}\alpha, U(-z)) = \mathcal{M}(\mathrm{i}\alpha, -U(z)) = \mathcal{M}(-\mathrm{i}\alpha, U(z))$ which reveals that

$$\mathcal{M}(-\mathrm{i}\alpha, U(z))\psi(-z) = \mu\mathcal{G}\psi(-z)$$

and therefore that the eigenfunction operated on by $S_2$ has the same eigenvalue

$$\psi(z)\mathrm{e}^{\mathrm{i}\alpha x} \text{ solution with } \mu \implies \psi(-z)\mathrm{e}^{-\mathrm{i}\alpha x} \text{ solution with } \mu.$$

The group can be closed as depicted in figure (3.6). This conjugacy will enable us to show that the $\mu$-variation in the mean equations is indeed odd. To do this consider the form of the term (3.20)

$$Q(z) := -\mathrm{i}\alpha\mathbf{q}^{\dagger *} \cdot \mathbf{q} + (q_1^{\dagger *} q_3)'.$$

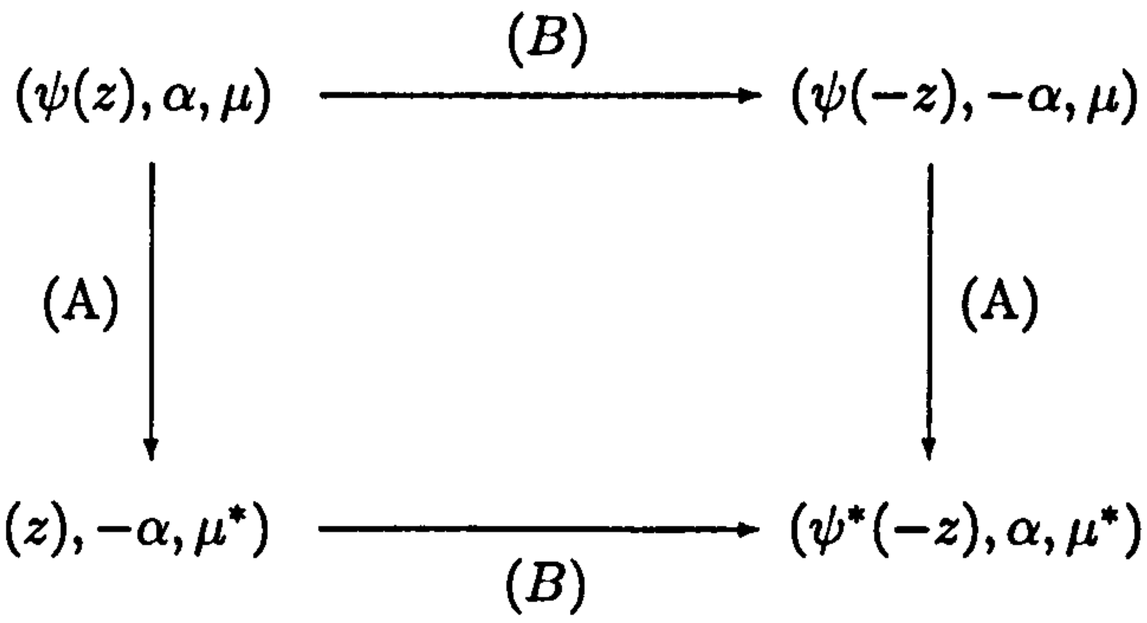


Figure 3.6: Eigenfunctions of the Orr–Sommerfeld operator which share the same real part of $\mu$. The arrows are intended to denote (A) complex conjugation and (B) the transformations $z \to -z$ and $x \to -x$. The triple $(\psi(z), \alpha, \mu)$ indicates that $\psi(z)\mathrm{e}^{\mathrm{i}\alpha}$ is an eigenfunction of equation (3.5) with corresponding eigenvalue $\mu$.

Can we show that this term has odd symmetry? If we take $\overline{\psi}(z) = \psi(z)\mathrm{e}^{\mathrm{i}\alpha x} + \psi(-z)\mathrm{e}^{-\mathrm{i}\alpha x}$ for the solution of the optimal equations, in other words if there are multiple points with neutral eigenvalues all with different values of the pair $(\alpha, \gamma)$

$$\mathcal{L} = (\dots) - \sum_{i=1}^{N} \gamma_i \, \mathfrak{Re}(\mu_i)$$

we let $\gamma_1 = \gamma_2$ for $\psi$ and its $S_2$ transform. Then $Q(z)$ is manifestly odd as illustrated here

$$\begin{aligned} Q(z) &= -\mathrm{i}\alpha \mathbf{q}^{\dagger *}(z) \cdot \mathbf{q}(z) + (q_1^{\dagger *}(z) q_3(z))' \\ &\quad - (-\mathrm{i}\alpha)\mathbf{q}^{\dagger *}(-z) \cdot \mathbf{q}(-z) + (q_1^{\dagger *}(-z) q_3(-z))' \\ &= -\mathrm{i}\alpha \left[ \mathbf{q}^{\dagger *}(z) \cdot \mathbf{q}(z) - \mathbf{q}^{\dagger *}(-z) \cdot \mathbf{q}(-z) \right] \\ &\quad + \left[ q_1^{\dagger *}(z) q_3(z) + q_1^{\dagger *}(-z) q_3(-z) \right]' . \end{aligned} \tag{3.21}$$

### 3.4.6 An $\alpha$-derivative

To complete the system of equations we require a condition to imply that the neutral streamwise wavenumbers are maxima of the linear stability growth curve. We are therefore interested in setting the total derivative $\mathrm{d}\mu/\mathrm{d}\alpha = 0$. Let $\mathcal{M}\mathbf{q} = \nabla^2\mathbf{q}/Re_s - U' q_3 \widehat{\boldsymbol{x}} - i\alpha U \mathbf{q}$ then

$$\mathcal{M}\mathbf{q} - \nabla p = \mu \mathbf{q} \quad \text{and} \quad \nabla \cdot \mathbf{q} = 0.$$

A small variation in $\alpha$ produces a change in both of these equations as follows

$$\delta\mathcal{M}\,\mathbf{q} - \mathrm{i}(\delta\alpha)p\widehat{\boldsymbol{x}} + (\mathcal{M}-\mu)\delta\mathbf{q} - \boldsymbol{\nabla}\delta p = \delta\mu\,\mathbf{q}, \tag{3.22}$$

$$\mathrm{i}(\delta\alpha)q_1 + \boldsymbol{\nabla}\cdot\delta\mathbf{q} = 0. \tag{3.23}$$

Now multiply (3.22) by the adjoint eigenfunction and integrate, taking incompressibility of $\mathbf{q}^\dagger$ into account, yields

$$(\mathbf{q}^\dagger, \delta\mathcal{M}\,\mathbf{q}) - \mathrm{i}(\delta\alpha)\langle q_1^{\dagger *} p\rangle + (\mathbf{q}^\dagger, (\mathcal{M}-\mu)\delta\mathbf{q}) = \delta\mu(\mathbf{q}^\dagger, \mathbf{q}). \tag{3.24}$$

The first term in this expression is just

$$\delta\mathcal{M}\,\mathbf{q} = \delta\alpha\left[-\frac{2\alpha}{Re_s}\mathbf{q} - \mathrm{i}U\mathbf{q}\right],$$

and the third term comes after integration by parts

$$(\mathbf{q}^\dagger, (\mathcal{M}-\mu)\delta\mathbf{q}) = ((\mathcal{M}^\dagger - \mu^*)\mathbf{q}^\dagger, \delta\mathbf{q}) = (\boldsymbol{\nabla}p^\dagger, \delta\mathbf{q}) = -(p^\dagger, \boldsymbol{\nabla}\cdot\delta\mathbf{q}),$$

using equation (3.23) this implies that $(\mathbf{q}^\dagger, (\mathcal{M}-\mu)\delta\mathbf{q}) = \mathrm{i}(\delta\alpha)\langle p^{\dagger *} q_1\rangle$. Putting all this together equation (3.24) becomes

$$\frac{\mathrm{d}\mu}{\mathrm{d}\alpha} = -\frac{2\alpha}{Re_s} - \mathfrak{Re}\left(\mathrm{i}\frac{\langle U\mathbf{q}^{\dagger *}\cdot\mathbf{q}\rangle + \langle q_1^* p^\dagger\rangle + \langle q_1^{\dagger *} p\rangle}{\langle \mathbf{q}^{\dagger *}\cdot\mathbf{q}\rangle}\right). \tag{3.25}$$

We have checked this expression against the numerical gradient calculated from the graph of $\mu(\alpha)$ for some random mean profiles and found perfect agreement.

### 3.4.7 Normalising q

Now that we have a complete set of optimal equations for this extended bounding problem we are in a position to apply some simplifications to the expressions already derived by setting the complex phases and amplitudes of $\mathbf{q}$ and $\mathbf{q}^\dagger$. We are free to do this because of the linear and homogeneous nature of the linear stability problem. We normalise the eigenfunctions such that their $L_2$ norm is unity

$$\|\mathbf{q}^\dagger\|^2 = \|\mathbf{q}\|^2 = 1.$$

Setting the phases allows for simplification to equation (3.25)

$$\mathfrak{Im}\,q_1(1/\sqrt{2}) = \mathfrak{Im}(\mathbf{q}^\dagger, \mathbf{q}) = 0.$$

Now, we can do some cross substitution in equations (3.16) and (3.17), and integration to write an equation for the mean flow

$$(\phi' + 1) + \overline{\nu_1}' - \frac{1}{Re}(\overline{\widehat{\nu}_1\widehat{\nu}_3} - \langle\widehat{\nu}_1\widehat{\nu}_3\rangle) = 0, \tag{3.26}$$

and an equation for $\overline{\nu_1}$, where the operation of taking the odd part of the $\mathbf{q}$ contribution is implied,

$$\overline{\nu_1}'' - \frac{1}{Re}\left(\frac{\lambda-2}{\lambda}\right)\overline{\widehat{\nu}_1\widehat{\nu}_3}' - \frac{\gamma}{(\mathbf{q}^\dagger,\mathbf{q})}\mathfrak{Re}\left(-i\alpha\mathbf{q}^{\dagger *}\cdot\mathbf{q} + (q_1^{\dagger *}q_3)'\right) = 0. \tag{3.27}$$

The simplification to equation (3.25) is as follows:

$$-\frac{2\alpha}{Re_s} + \frac{\mathfrak{Im}\left(\langle U\mathbf{q}^{\dagger *}\cdot\mathbf{q}\rangle + \langle q_1^* p^\dagger\rangle + \langle q_1^{\dagger *} p\rangle\right)}{\langle\mathbf{q}^{\dagger *}\cdot\mathbf{q}\rangle} = 0. \tag{3.28}$$

### 3.4.8 Complete system of Euler–Lagrange equations

The complete set of equations for the optimal solution are equations (3.12)-(3.15), (3.6), (3.7), (3.26), (3.27), (3.28), and the divergence-free condition on $\mathbf{q}$ and $\mathbf{q}^\dagger$. The complete set of boundary conditions are

$$\phi = \mp\tfrac{1}{2} \text{ at } z = \pm\tfrac{1}{2},$$

and

$$\overline{\nu_1} = 0,\ \widehat{\nu} = \mathbf{q} = \mathbf{q}^\dagger = \mathbf{0} \text{ at } z = \pm\tfrac{1}{2}.$$

For this extended variational problem the upper bound on the energy dissipation rate, in inviscid units of $V^3/d$, is therefore

$$\varepsilon = \frac{1}{Re}\left\langle(\phi' + \overline{\nu_1}')\left(\phi' + \frac{\overline{\nu_1}'}{1-\lambda}\right)\right\rangle. \tag{3.29}$$

### 3.4.9 Solution technique

We have considered two possible prescriptions for computing the optimal solution of this extended variational problem with the objective of seeking the $c = 1$ solution branch. The first is to take a Chapter 2 solution; fix $Re$; find the marginally stable

$Re_s$ and calculate $c_{opt}$, at which $\gamma = 0$; and use the critical LS eigenvectors to enable continuation in the direction of lesser $c$. Hopefully, the continuation will advance monotonically toward $c = 1$. The second alternative is use the homotopy $U = \phi + \eta\overline{\nu_1}$: find a $\eta$ for which $U$ is marginally stable at the flow Reynolds number i.e. $c = 1$; then employ continuation to bring $\eta$ to 1.

We will describe the first prescription in more detail. After selecting an optimal solution from Chapter 2 the over-stability factor $c_{opt}$ is calculated. One can use an eigenvalue solver to find the most unstable eigenvector in terms of either the primitive variables in a Chebyshev basis, or the streamfunction variables in a Jacobi basis. The normalisation and rotations described in Section 3.4.7 can then be applied to these eigenfunction representations. Under the new boundary conditions we divide $\phi$ by $Re$, and at $\overline{\nu_1}$ initially takes the form

$$\overline{\nu}_1 = \left(\frac{\lambda}{2} - 1\right)(\phi + z).$$

With these ingredients we have a starting point, at $(Re, c_{opt})$ and $\gamma = 0$, for a continuation at fixed $Re$ in the direction of decreasing $c$. A generic black box iterator can be employed for the continuation in accord with Chapter 2.

It is worth noting that there is nothing special about the point $c_{opt}$, other than the obvious significance to Chapter 2, and we can either perform a continuation to take the solution in the direction of reduced or increased $c$. The Lagrange multiplier $\gamma$ depends only on $c$ and simply changes sign through the point $c = c_{opt}$.

## 3.5 Preliminary results

We have described in full the inclusion of a new constraint in the standard CDH method and the derivation of the Euler–Lagrange equations for the extended variational problem. The non-self-adjointness of the LS eigenvalue problem make it neccassary to compute both the LS eigenfunction and its adjoint. The numerical solution, much like Chapter 2, requires one to store and follow the evolution of neutral eigenfunction. Our preliminary calculations of the optimal solution of this extended problem for $c < c_{opt}$ (for three different points in $Ra$) proceeds smoothly until at $c \approx 11$ where there is a turning point in phase space and the solution branch loops

back on itself. Thus at the time of writing we have located a barrier to progressing toward $c = 1$ with the first continuation technique. In future work we intend to try the homotopy method to join the $c = c_{opt}$ branch to the $c = 1$ branch.

# Chapter 4

# Convection at infinite Prandtl number: (I) Optimal bounds and asymptotic analysis

## 4.1 Introduction

We now turn from the subject of shear flows, to the subject which will form the second half of this thesis: a study of a bounding problem in convection. The physics described here will be very different situation to the classical examples of shear flow; channel flow and Couette flow; in which fluid is either sheared by counter-propagating walls, or driven under a pressure gradient across no-slip boundaries. The velocity field will instead be forced by a scalar field — temperature — which itself is controlled by fixed-value boundary conditions. We will consider a de-stabilising temperature gradient; heating is applied from below; and the control parameter is proportional to the temperature difference between top and bottom plate — namely $\Delta T = T_{bot} - T_{top}$.

The established model of fluid convection is the Rayleigh–Bénard system of equations (henceforth referred to as the RB equations). Staying in the plane-parallel Cartesian geometry of the previous chapters: the velocity and temperature fields

are assumed horizontally-periodic; gravity perpendicular to the plates and downward pointing ($\mathbf{g} = -g\hat{\boldsymbol{z}}$); boundary conditions on $\boldsymbol{u}$ and $T$ are uniform in the horizontal coordinate. The fluid is assumed ideal: the velocity field is divergence-free; and thermal and viscous properties are constant, namely kinematic viscosity $\nu$, thermometric conductivity $\kappa$ and thermal expansion $\alpha$. The RB equations may be written in non-dimensional form as

$$\begin{aligned} \frac{1}{\sigma}\left(\frac{\partial \boldsymbol{u}}{\partial t} + \boldsymbol{u}\cdot\boldsymbol{\nabla}\boldsymbol{u}\right) + \boldsymbol{\nabla} p &= \nabla^2 \boldsymbol{u} + Ra\, T\hat{\boldsymbol{z}}, \\ \frac{\partial T}{\partial t} + \boldsymbol{u}\cdot\boldsymbol{\nabla} T &= \nabla^2 T, \\ \boldsymbol{\nabla}\cdot\boldsymbol{u} &= 0, \end{aligned} \tag{4.1}$$

where velocity is measured in units of $\kappa/d$; lengths by $d$; time by $d^2/\kappa$; pressure by $\rho(\nu\kappa/d^2)$, where $\rho$ is the constant mean density; and temperatures by $\Delta T$. The temperature boundary conditions are at the top boundary $T_{top} = T_0$ and at the bottom boundary $T_{bot} = T_0 + \Delta T$, where $\Delta T > 0$. The dimensionless parameters $\sigma$ and $Ra$ in (4.1) are respectively, the Prandtl number and the Rayleigh number:

$$\sigma = \frac{\nu}{\kappa}, \qquad Ra = \frac{\alpha g \Delta T d^3}{\kappa\nu}.$$

We shall study the case where the Prandtl number of the fluid is infinite ($\sigma = \infty$) for which the velocity equation is a linear equation with no explicit time-dependence

$$\nabla^2 \boldsymbol{u} + Ra\, T\hat{\boldsymbol{z}} = \boldsymbol{\nabla} p. \tag{4.2}$$

In the upper bound problem, equation (4.2) can be employed as a pointwise constraint in space. By including constraint (4.2) the upper bounding problem supersedes the arbitrary Prandtl number convection problem, and a lower scaling exponent is achievable.

To complete this description of the fluid model we need to impose velocity boundary conditions. In accordance with tradition we study two types of velocity conditions. The first, now familiar from Chapters 2 and 3, is *no-slip* which models a rigid boundary. The velocity is assumed continuous to the wall

$$\boldsymbol{u} = 0 \quad \text{at } z = 0 \text{ and } 1, \tag{4.3}$$

which, owing to incompressibility, implies that $w = w_z = 0$ at $z = 0$ and 1. The second is *stress-free* (or *slip*) which models an undisplaced free surface. Fluid is not

allowed to flow through the surface but may attain any velocity parallel to it while imposing no tangential stress on the surface

$$w = 0; \quad u_z = v_z = 0 \quad \text{at } z = 0 \text{ and } 1.$$

Incompressibility then implies that $w = w_{zz} = 0$ at $z = 0$ and 1. For a full discussion of the derivation of the RB equations and of the boundary conditions see Chandrasekhar (1961).

Upper bounds on the average heat transport in arbitrary Prandtl number convection have been calculated by both the Howard–Busse and the Constantin–Doering–Hopf methods. In this regime — when $\sigma < \infty$ — Kerswell (1997, 2001) has shown that the two methods are provably equivalent. The result of solving the optimal equations of the HB method are: Busse (1969*b*) uses his multi-$k$ asymptotic analysis to prove an asymptotic scaling of $Ra^{1/2}$ for no-slip; while a numerical solution of the stress-free problem in Vitanov & Busse (1997) also suggests an asymptotic $Ra^{1/2}$ scaling. On the other hand, in Doering & Constantin (1996), the CDH method was used to extract an analytic estimate of the upper bound which scaled as $Ra^{1/2}$ and holds true for either boundary condition; therefore, owing to the prove of Kerswell (2001) the optimal scaling for either boundary conditions is accepted to be $Ra^{1/2}$. The arbitrary Prandtl number result is an *umbrella* result for the infinite Prandtl number problem, and we can here conclude that the asymptotic scaling for the latter problem has a $Ra$-exponent certainly less than 1/2.

The problem of infinite Prandtl number convection also has a long history in the bounding literature. For no-slip boundaries the first stones were laid by Chan (1971) who applied the HB method and obtained a $Ra^{1/3}$ asymptotic scaling for the average heat transport; while some twenty-eight years later, with the new techniques of the CDH method revitalising the subject, Doering & Constantin (2001) and Otero (2002) produced rigorous estimates on the optimal scaling which took the asymptotic form $Ra^{2/5}$; and using extra PDE information — outside of the standard analysis — Constantin & Doering (1999) deduced a logarithmic bound of the form $Ra^{1/3}(\log Ra)^{2/3}$; the effect of adding rotation has also been studied in Constantin, Hallstrom & Putkaradze (2001). Recent interest in the the upper bounding problem with stress-free boundaries is covered in Vitanov (1998, 2000*c*,*a*,*b*); however, this

area of investigation is only in its infancy.

Our motivation for visiting this particular convection problem is that the HB method yields a $Ra^{1/3}$ scaling, while the CDH method without any *additional* information yields an estimate of the form $Ra^{2/5}$ : this does not present a contradiction, but this discrepancy does reveal an aspect of the relationship between the two methods not otherwise seen in bounding problems. In this Chapter we will prove that the two bounding techniques are dual variational problems; the CDH method estimates a saddle point from above and the HB method estimates the same saddle point from below. We will numerically calculate the optimal solutions for both boundary conditions and use the empirical evidence to justify the asymptotic analysis of Chan (1971) and to critique Vitanov (1998).

## 4.2 Formulation

Let us denote equation (4.2) as $\mathcal{N} := \nabla^2 \boldsymbol{u} + Ra\,T\widehat{\boldsymbol{z}} - \boldsymbol{\nabla} p = 0$ with components $\mathcal{N}_i$ for $i = 1, 2, 3$. Given that $u$ and $v$ depend only on the pressure and that $\boldsymbol{u}$ is divergence-free we can use $\boldsymbol{\nabla} \cdot (\mathcal{N})$ and $\nabla^2(\mathcal{N}_3)$, which are respectively:

$$\nabla^2 p = Ra T_z; \qquad \nabla^4 w + Ra \nabla^2 T = \nabla^2 p_z,$$

to form a dynamical constraint on $w$ in terms of only the temperature field $T$ and the Rayleigh number:

$$\nabla^4 w + Ra \nabla_H^2 T = 0, \tag{4.4}$$

where the horizontal Laplacian is $\nabla_H^2 = \partial_x^2 + \partial_y^2$. The problem of enforcing the linear momentum equation is now entirely down to satisfying (4.4) pointwise for fields satisfying the no-slip:

$$w = w_z = 0 \quad \text{at} \quad z = 0 \text{ and } 1, \tag{4.5}$$

or stress-free boundary conditions:

$$w = w_{zz} = 0 \quad \text{at} \quad z = 0 \text{ and } 1. \tag{4.6}$$

The associated dimensionless boundary conditions on $T$ are: $T(0) = 1$ and $T(1) = 0$. See figure 4.1 for a summary of the geometry and boundary conditions.

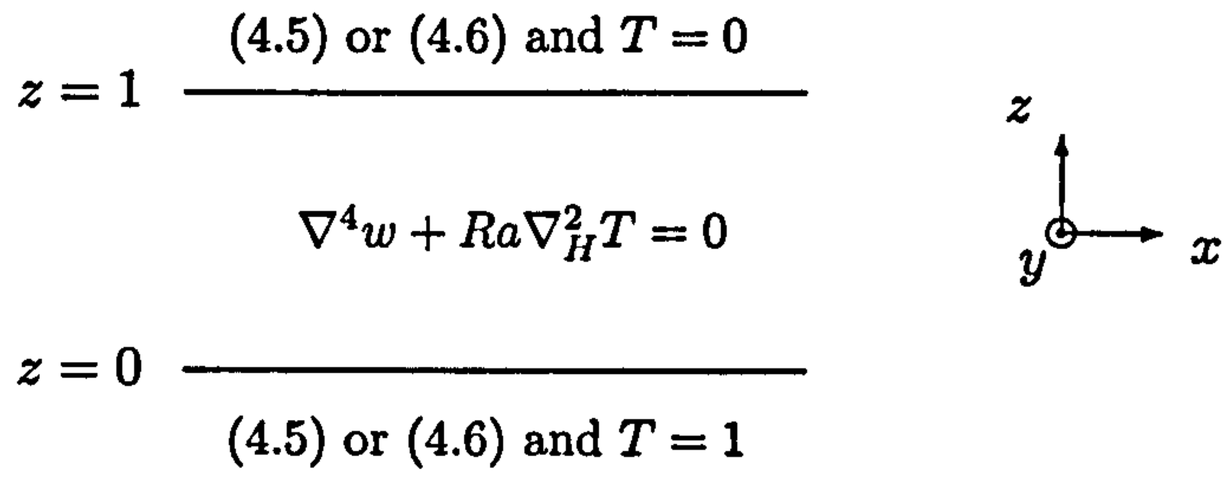


Figure 4.1: Momentum equation and boundary conditions for infinite Prandtl number convection

Now let us concentrate on the time-dependent heat equation from system (4.1), denoted $\mathcal{H}$:

$$\mathcal{H} := \frac{\partial T}{\partial t} + \boldsymbol{u} \cdot \boldsymbol{\nabla} T - \nabla^2 T. \tag{4.7}$$

Writing this in terms or the conductive heat flux ($\mathbf{j} := -\boldsymbol{\nabla} T$) and the convective heat flux ($\mathbf{J} := \boldsymbol{u}T$) we have:

$$\frac{\partial T}{\partial t} = -\boldsymbol{\nabla} \cdot (\mathbf{j} + \mathbf{J}) .$$

In a purely conductive state (with $\boldsymbol{u} = \mathbf{0}$) the transport of heat (or heat flux) across the parallel plates is just $\langle \widehat{\boldsymbol{z}} \cdot (-\boldsymbol{\nabla} T) \rangle = -T(1) + T(0) = 1$, while in general the heat transport between the plates is $\langle \widehat{\boldsymbol{z}} \cdot (\mathbf{j} + \mathbf{J}) \rangle = 1 + \langle wT \rangle$. Define the Nusselt number of the flow (hereafter denoted $Nu$) as the ratio of the long-time averaged total heat transport to the conductive heat transport between the plates:

$$Nu = 1 + \langle wT \rangle \tag{4.8}$$

Another expression for $Nu$ can be deduced from the global entropy flux balance $\langle T\mathcal{H} \rangle = 0$, which is:

$$\frac{1}{2}\frac{\mathrm{d}}{\mathrm{d}t}\|T\|^2 + \|\boldsymbol{\nabla} T\|^2 = 1 + \langle wT \rangle \tag{4.9}$$

and upon long-time averaging and an appeal to the temperature maximum principle yields:

$$Nu = \|\boldsymbol{\nabla} T\|^2. \tag{4.10}$$

In the following discussion equations (4.8), (4.10) and momentum constraint (4.4) are used to formulate two variational problems. First the CDH formulation will be

derived in common with the previous chapters and then the HB variational problem will be derived in accord with Chan (1971).

We note that owing to the geometry and to the homogeneity in the boundary conditions there will be no preferred horizontal direction in the optimal solution. In fact, the issue of a three-dimensional instability in the spectral constraint, studied in Chapter 3 for the shear flow problem, will not concern us here since horizontal derivatives only appear in the combination $\nabla_H^2$ in equation (4.4), (4.8), and (4.10).

### 4.2.1 CDH method

Decompose the temperature field into background and fluctuation part

$$T(x,t) = \tau(z) + \theta(x,t) \tag{4.11}$$

where the background field takes on the temperature boundary conditions: $\tau(0) = 1$ and $\tau(1) = 0$, and $\theta$ satisfies Dirichlet boundary conditions. Substituting (4.11) into (4.7) gives:

$$\frac{\partial\theta}{\partial t} + \boldsymbol{u}\cdot\boldsymbol{\nabla}\theta = \nabla^2\theta + \tau'' - w\tau'. \tag{4.12}$$

Multiplying this equation by $\theta$ and averaging produces

$$\frac{1}{2}\frac{\mathrm{d}}{\mathrm{d}t}\|\theta\|^2 = -\|\boldsymbol{\nabla}\theta\|^2 + \langle\theta\tau'' - w\theta\tau'\rangle, \tag{4.13}$$

while expanding out $\|\boldsymbol{\nabla}T\|^2$ leads to

$$\|\boldsymbol{\nabla}T\|^2 = \|\boldsymbol{\nabla}\theta\|^2 + \|\tau'\|^2 - 2\langle\theta\tau''\rangle. \tag{4.14}$$

Taking the sum $b\times$ (4.14) + (4.13) gives

$$\frac{b}{2}\frac{\mathrm{d}}{\mathrm{d}t}\|\theta\|^2 + \|\boldsymbol{\nabla}T\|^2 = \|\tau'\|^2 - \mathcal{G}_{\tau,b}(w,\theta) \tag{4.15}$$

where $\mathcal{G} = \langle(b-1)\|\boldsymbol{\nabla}\theta\|^2 - (b-2)\theta\tau'' + bw\theta\tau'\rangle$. Long-time averaging equation (4.15) and using expression (4.10) the following upper bound on $Nu$ emerges

$$Nu \le \|\tau'\|^2 - \inf_{w,\theta}\mathcal{G}_{\tau,b}(w,\theta) \tag{4.16}$$

where the infimum is attained by steady fields and hence no time average appears on the right hand side.

The task of calculating the upper bound on $Nu$ in equation (4.16) is greatly simplified by reducing the problem to one just involving $w$, $\theta$ with no horizontal-mean. This is achieved by considering the Lagrangian functional

$$L = \mathcal{G} - \langle q(\boldsymbol{x})(\nabla^4 w + Ra\nabla_H^2\theta)\rangle$$

where the Lagrange multiplier $q(\boldsymbol{x})$ is used to impose equation (4.4) and satisfies the natural boundary conditions for the problem, which are those satisfied by $w$. The minimum over $\theta$ is attained by setting the $\theta$ variation to zero:

$$\frac{\delta L}{\delta\theta} = -2(b-1)\nabla^2\theta - (b-2)\tau'' + bw\tau' - Ra\nabla_H^2 q = 0.$$

Taking a horizontal average of this equation, considering periodicity and boundary conditions, we find that the mean part of the optimal fluctuation field is given by

$$2(b-1)\overline{\theta}'' + (b-2)\tau'' = 0, \tag{4.17}$$

which can be integrated twice to reveal that:

$$\overline{\theta} = -\frac{(b-2)}{2(b-1)}[\tau + z - 1]. \tag{4.18}$$

Therefore by setting $\widehat{\theta} = \theta - \overline{\theta}$ we can restate problem (4.16) as an optimisation over meanless fields, namely

$$Nu - 1 \leq \frac{b^2}{4(b-1)}(\|\tau'\|^2 - 1). \tag{4.19}$$

subject to the spectral constraint $\tilde{\mathcal{G}}_{\tau,b}(w,\widehat{\theta}) = (b-1)\|\nabla\widehat{\theta}\|^2 + b\langle w\widehat{\theta}\tau'\rangle \geq 0$ for all meanless fields $(w,\widehat{\theta})$ which satisfy equation (4.4) (which is now $\nabla^4 w + Ra\nabla_H^2\widehat{\theta} = 0$) and the specific boundary conditions. The Lagrangian associated with this variational problem is

$$\tilde{L} = \frac{b^2}{4(b-1)}(\|\tau'\|^2 - 1) - \tilde{\mathcal{G}}_{\tau,b}(w,\widehat{\theta}) - \langle q(\boldsymbol{x})(\nabla^4 w + Ra\nabla_H^2\theta)\rangle. \tag{4.20}$$

The form of this variational problem appears very similar to the shear flow problem, however, the imposition of the momentum constraint and the variety of boundary conditions strongly impact upon the solution method and structure of the optimal solution.

### 4.2.2 HB method

Howard and Busse's Optimum Theory is based upon the assumption of statistical stationarity for all horizontal averages. So in particular we have $\frac{\mathrm{d}\overline{T}}{\mathrm{d}t} = 0$ and $\langle wT \rangle$ is time independent, and, moreover,

$$Nu - 1 = \langle wT \rangle.$$

The mean-fluctuation decomposition of the temperature field is made $T(\boldsymbol{x}, t) = \overline{T}(z) + \widehat{\theta}(\boldsymbol{x}, t)$ (note that periodicity and incompressibility imply that $\overline{w} = 0$ and hence $w = \widehat{w}$).

Under the mean-fluctuation decomposition the heat equation (4.7) becomes:

$$\mathcal{H} := \frac{\partial \theta}{\partial t} + w\overline{T}_z + \boldsymbol{u} \cdot \boldsymbol{\nabla}\widehat{\theta} - \overline{T}_{zz} - \boldsymbol{\nabla}^2\widehat{\theta} = 0. \tag{4.21}$$

Two pieces of information are used to derive the variational functional: $\overline{\mathcal{H}} = 0$ and $\langle T\mathcal{H} \rangle = 0$ which are respectively

$$\overline{T}_z = \overline{w\widehat{\theta}} - \langle w\widehat{\theta} \rangle - 1; \qquad \left\| \overline{T}_z \right\|^2 + \overline{T}_z \Big|_{z=0} = -\|\boldsymbol{\nabla}\widehat{\theta}\|^2 \tag{4.22}$$

and can be combined to deduce the so-called second power integral

$$\|\boldsymbol{\nabla}\widehat{\theta}\|^2 + \|w\widehat{\theta} - \langle w\widehat{\theta} \rangle\|^2 = \langle w\widehat{\theta} \rangle. \tag{4.23}$$

One can form unity by taking the ratio of terms in the previous balance

$$1 = \frac{\langle w\widehat{\theta} \rangle - \|\boldsymbol{\nabla}\widehat{\theta}\|^2}{\|w\widehat{\theta} - \langle w\widehat{\theta} \rangle\|^2},$$

which when multiplied by $\langle w\widehat{\theta} \rangle$ produces a homogeneous functional

$$F = \frac{\langle w\widehat{\theta} \rangle^2 - \langle w\widehat{\theta} \rangle \|\boldsymbol{\nabla}\widehat{\theta}\|^2}{\|w\widehat{\theta} - \langle w\widehat{\theta} \rangle\|^2} \tag{4.24}$$

the supremum of which is an upper bound on the Nusselt number, $Nu - 1 \leq \sup F$. The maximisation of $F$ is performed over the competitor fields (those which satisfy the momentum constraint (4.4) and the boundary conditions), while the power constraint in equation (4.23) is imposed *ex post facto* by normalising $\langle w\widehat{\theta} \rangle = F$. This is now exactly the homogeneous functional which Chan (1971) seeks to maximise.

In fact, Chan solved the Euler–Lagrange equations of the following Lagrangian functional:

$$G = F - \langle q(\boldsymbol{x})(\nabla^4 w + Ra\nabla_H^2\widehat{\theta}) \rangle \tag{4.25}$$

where $q(\boldsymbol{x})$ is a Lagrange multiplier imposing the pointwise momentum constraint in equation (4.4). This is exactly the functional in equation (25) of Chan (1971) without the normalisation $\langle w\widehat{\theta}\rangle = 1$. Taking variations of this functional with respect to $w$ and $\widehat{\theta}$ and substituting in $\|\boldsymbol{\nabla}\widehat{\theta}\|^2 = \langle w\widehat{\theta}\rangle - \|w\widehat{\theta} - \langle w\widehat{\theta}\rangle\|^2$ we deduce the following Euler–Lagrange equations:

$$\widehat{\theta}\big[\langle w\widehat{\theta}\rangle + \|w\widehat{\theta} - \langle w\widehat{\theta}\rangle\|^2\big] - 2F\widehat{\theta}\big[w\widehat{\theta} - \langle w\widehat{\theta}\rangle\big] - (\nabla^4 q)\,\|w\widehat{\theta} - \langle w\widehat{\theta}\rangle\|^2 = 0, \tag{4.26}$$

$$\begin{aligned} 2(\nabla^2\widehat{\theta})\langle w\widehat{\theta}\rangle + w\big[\langle w\widehat{\theta}\rangle + \|w\widehat{\theta} - \langle w\widehat{\theta}\rangle\|^2\big] \\ - 2Fw\big[w\widehat{\theta} - \langle w\widehat{\theta}\rangle\big] - Ra(\nabla_H^2 q)\|w\widehat{\theta} - \langle w\widehat{\theta}\rangle\|^2 = 0. \end{aligned} \tag{4.27}$$

If we normalise $w$ and $\widehat{\theta}$ as Chan does, namely $w \to \langle w\widehat{\theta}\rangle^{-1/2} Ra^{-1/2} w$ and $\widehat{\theta} \to \langle w\widehat{\theta}\rangle^{-1/2} Ra^{1/2}\widehat{\theta}$ so that $\langle w\widehat{\theta}\rangle \to 1$ then equations (4.27) and (4.26) become exactly the Euler–Lagrange equations (27) in Chan (1971).

## 4.3 Unification: CDH and HB methods

In the previous section the HB method was shown to be a variational method which seeks the supremum of a homogeneous functional (equation 4.24) while the CDH method seeks to minimise a functional (equation 4.19) subject to positivity of a quadratic form. The correspondence between these two techniques seems fascinatingly unclear, however, one can show that they both derived from one functional. Recall that Kerswell (2001) proved this duality in the case of arbitrary Prandtl number; this proof is for the specific case of $\sigma = \infty$.

**Claim:** The CDH method and the HB method are dual variational problems estimating the highest stationary point; that with highest associated heat transport; of the following functional:

$$N := \|\boldsymbol{\nabla} T\|^2 - b\langle\theta\mathcal{H}\rangle - \langle q(\boldsymbol{x})(\nabla^4 w + Ra\nabla_H^2 T)\rangle \tag{4.28}$$

where $T = \tau(z) + \theta(\boldsymbol{x}, t)$ and $\mathcal{H}$ is the heat equation:

$$\mathcal{H} := \frac{\partial\theta}{\partial t} + \boldsymbol{u}\cdot\boldsymbol{\nabla}\theta - \nabla^2\theta + w\tau' - \tau'' = 0.$$

**Proof:** Start by deriving all of the variational derivatives of $N$. Express the functional $N$ in terms of $\tau$ and $\theta$ so that

$$\begin{aligned} N(\tau, w, \theta, b, q) = \|\tau'\|^2 - \langle (b-1)|\nabla\theta|^2 - (b-2)\theta\tau'' + b\theta w\tau' \rangle \\ - \langle q(\boldsymbol{x})(\nabla^4 w + Ra\nabla_H^2\theta)\rangle. \end{aligned} \tag{4.29}$$

Variations equations for $\tau(z)$, $\theta(\boldsymbol{x})$, $w(\boldsymbol{x})$, $q(\boldsymbol{x})$ and the variational equation for the mean and fluctuating part of $\theta$ are deduced.

$$\frac{\delta N}{\delta \tau} = -2\tau'' + (b-2)\overline{\theta}'' + b(\overline{w\theta})' = 0 \tag{4.30}$$

$$\frac{\delta N}{\delta \theta} = 2(b-1)\nabla^2\theta + (b-2)\tau'' - bw\tau' - Ra\nabla_H^2 q = 0$$

$$\frac{\delta N}{\delta w} = -b\theta\tau' - \nabla^4 q = 0 \tag{4.31}$$

$$\frac{\delta N}{\delta q} = \nabla^4 w + Ra\nabla_H^2\theta = 0 \tag{4.32}$$

$$\frac{\delta N}{\delta \theta} = 0 \quad \begin{cases} \dfrac{\delta N}{\delta \overline{\theta}} = 2(b-1)\overline{\theta}'' + (b-2)\tau'' = 0 \\ \dfrac{\delta N}{\delta \widehat{\theta}} = 2(b-1)\nabla^2\widehat{\theta} - bw\tau' - Ra\nabla_H^2 q = 0 \end{cases} \tag{4.33}$$

In the following discussion the optimal variables (the solutions of the Euler–Lagrange equations) are denoted by a subscript *opt*. It will be shown that both of the techniques can be derived by solving different subsets of the variational equations and rewriting the remaining equations appropriately.

### Case 1: CDH method

Solving $\delta N/\delta\,\overline{\theta} = 0$ yields an expression for the mean of the optimal $\theta$

$$\overline{\theta}_{opt} = -\frac{b-2}{2(b-1)}\left[\tau + z - 1\right].$$

Substituting this into $N$ we have

$$\begin{aligned} \check{N}(\tau, w, \widehat{\theta}, b, q) - 1 &= N(\tau, w, \overline{\theta}_{opt} + \widehat{\theta}, b, q) - 1 \\ &= \frac{b^2}{4(b-1)}\left(\|\tau'\|^2 - 1\right) - \langle (b-1)|\nabla\widehat{\theta}|^2 + bw\widehat{\theta}\tau'\rangle - \langle q(\boldsymbol{x})(\nabla^4 w + Ra\nabla_H^2\widehat{\theta})\rangle. \end{aligned} \tag{4.34}$$

This is the Lagrangian functional constructed in Section 4.2.1. It is clear that the quadratic term in $(w, \widehat{\theta})$ has a minimum value only if $b > 1$.

**Case 2: HB method**

Solving $\delta N/\delta\,\overline{\theta} = 0$ and $\delta N/\delta\tau = 0$ simultaneously allows us to deduce equations for the optimal background field and the mean of the fluctuation field in terms of the mean-less fluctuation field $\widehat{\theta}$ and $w$, respectively

$$\tau'_{opt} = \frac{2(b-1)}{b}\left[\overline{w\widehat{\theta}} - \langle w\widehat{\theta}\rangle\right] - 1; \qquad \overline{\theta}'_{opt} = -\frac{b-2}{b}\left[\overline{w\widehat{\theta}} - \langle w\widehat{\theta}\rangle\right]. \tag{4.35}$$

Substituting these expressions into $N$ and some algebra yields

$$\begin{aligned}\mathring{N}(w,\widehat{\theta},b,q) - 1 &= N(\tau_{opt}, w, \overline{\theta}_{opt} + \widehat{\theta}, b, q) - 1 \\ &= \langle w\widehat{\theta}\rangle + (b-1)\left\{\langle w\widehat{\theta}\rangle - \|w\widehat{\theta} - \langle w\widehat{\theta}\rangle\|^2 - \|\nabla\widehat{\theta}\|^2\right\} - \langle q(\boldsymbol{x})(\nabla^4 w + Ra\nabla_H^2\widehat{\theta})\rangle.\end{aligned} \tag{4.36}$$

In this context $(b-1)$ is a Lagrange multiplier imposing the second power integral balance (4.23) and $q(\boldsymbol{x})$ imposes the pointwise momentum constraint in (4.4). The remaining variational equations for $w$ and $\widehat{\theta}$ are

$$\frac{\delta N}{\delta\widehat{\theta}} = w + (b-1)\left\{w - 2w\left[\overline{w\widehat{\theta}} - \langle w\widehat{\theta}\rangle\right] + 2\nabla^2\widehat{\theta}\right\} - Ra\nabla_H^2 q = 0, \tag{4.37}$$

$$\frac{\delta N}{\delta w} = \widehat{\theta} + (b-1)\left\{\widehat{\theta} - 2\widehat{\theta}\left[\overline{w\widehat{\theta}} - \langle w\widehat{\theta}\rangle\right]\right\} - \nabla^4 q = 0. \tag{4.38}$$

In order to obtain a value for the optimal $b$ we calculate $\langle\widehat{\theta}(\delta N/\delta\widehat{\theta})\rangle = 0$ and $\langle w(\delta N/\delta w)\rangle = 0$, which are respectively:

$$(2-b)\langle w\widehat{\theta}\rangle - Ra\langle(\nabla_H^2 q)\widehat{\theta}\rangle = 0,$$

and

$$(2-b)\langle w\widehat{\theta}\rangle + 2(b-1)\|\nabla\widehat{\theta}\|^2 - \langle(\nabla^4 q)w\rangle = 0.$$

Given that $\langle(\nabla^4 q)w\rangle = \langle q(\nabla^4 w)\rangle = \langle q(-Ra\nabla_H^2\widehat{\theta}\rangle$ these equation can be added to give

$$b = \frac{\|\nabla\widehat{\theta}\|^2 - 2\langle w\widehat{\theta}\rangle}{\|\nabla\widehat{\theta}\|^2 - \langle w\widehat{\theta}\rangle}, \tag{4.39}$$

while the second power integral can be employed to deduce a simple expression for $(b-1)$, which may be easily inserted back into equations (4.37) and (4.38):

$$b-1=\frac{\langle w\widehat{\theta}\rangle}{\|w\widehat{\theta}-\langle w\widehat{\theta}\rangle\|^2} \tag{4.40}$$

After minor simplifications the $w$ and $\widehat{\theta}$ variations turn out to be

$$\widehat{\theta}[\langle w\widehat{\theta}\rangle+\|w\widehat{\theta}-\langle w\widehat{\theta}\rangle\|^2]-2\widehat{\theta}\langle w\widehat{\theta}\rangle[\overline{w\widehat{\theta}}-\langle w\widehat{\theta}\rangle]-(\nabla^4 q)\,\|w\widehat{\theta}-\langle w\widehat{\theta}\rangle\|^2=0 \tag{4.41}$$

$$\begin{aligned}2(\nabla^2\widehat{\theta})\langle w\widehat{\theta}\rangle+w[\langle w\widehat{\theta}\rangle+\|w\widehat{\theta}-\langle w\widehat{\theta}\rangle\|^2]-2w\langle w\widehat{\theta}\rangle[\overline{w\widehat{\theta}}-\langle w\widehat{\theta}\rangle]\\ -Ra(\nabla_H^2 q)\,\|w\widehat{\theta}-\langle w\widehat{\theta}\rangle\|^2=0\end{aligned} \tag{4.42}$$

which, if we replace each $\langle w\widehat{\theta}\rangle$ that multiplies $(\overline{w\widehat{\theta}}-\langle w\widehat{\theta}\rangle)$ with the functional $F$, are exactly the Euler–Lagrange equations which we derived from Chan's homogeneous ratio (equations 4.26-4.27).

As a final comment we note that for the problems to intersect the Optimum theory problem must also satisfy the spectral constraint to ensure that the top maximum is selected. Indeed, in general equations (4.41) and (4.42) will have multiple solutions, one of which will be a global maximum for $F$. Equation (4.40) implies that $(b-1)>0$, which is consistent with fulfilment of the spectral constraint.

This concludes the proof of duality. In the following sections the optimal solution for the CDH method will be calculated numerically and then comparison will be made with the asymptotic results of the optimum theory.

## 4.4 Solution technique

Following the CDH method, we now present the programme for solving the optimal problem. Starting with equation (4.34) and replacing $b$ in favour of the parameter $\lambda=b/(b-1)$ the functional may be written as

$$\check{N}-1=\frac{\lambda^2}{4(\lambda-1)}\left(\|\tau'\|^2-1\right)-\frac{1}{\lambda-1}\{\|\nabla\widehat{\theta}\|^2+\lambda\langle w\widehat{\theta}\tau'\rangle-\langle q(\boldsymbol{x})(\nabla^4 w+Ra\nabla_H^2\widehat{\theta})\rangle\}. \tag{4.43}$$

### 4.4.1 Euler–Lagrange equations

The system of Euler–Lagrange equations can be cosine-Fourier transformed owing to presence of only even horizontal derivatives in the $w$, $\widehat{\theta}$ and $q$ variations (respectively 4.31, 4.32 and 4.33). Therefore under the ansatz of the solution being single-moded

$$w = w(z)\cos(kx); \qquad q = q(z)\cos(kx); \qquad \widehat{\theta} = \widehat{\theta}(z)\cos(kx),$$

the variations (4.31-4.33) become

$$2(D^2 - k^2)\widehat{\theta} - \lambda w\tau' + Rak^2 q = 0 \tag{4.44}$$

$$(D^2 - k^2)^2 q + \lambda\widehat{\theta}\tau' = 0 \tag{4.45}$$

$$(D^2 - k^2)^2 w - Rak^2\widehat{\theta} = 0 \tag{4.46}$$

which are now supplemented by a $k$-derivative, owing to the Fourier expansion, which is easily derived from expression (4.43)

$$\langle\widehat{\theta}^2\rangle - 2\langle q(D^2 - k^2)w\rangle - Ra\langle q\widehat{\theta}\rangle = 0. \tag{4.47}$$

The non-linear and non-local equation for the optimal background field from equation (4.35) is

$$\lambda(\tau' + 1) = w\widehat{\theta} - \langle w\widehat{\theta}\rangle, \tag{4.48}$$

where a multiplicative $\frac{1}{2}$ on the left hand side has dropped due to horizontal averaging of $\cos^2$, while the optimal balance parameter from equation (4.40) is

$$\lambda = 2 - \frac{\langle(D\widehat{\theta})^2 + (k\widehat{\theta})^2\rangle}{\langle w\widehat{\theta}\rangle}. \tag{4.49}$$

### 4.4.2 Spectral constraint

A solution to the Euler–Lagrange equations can only translate to an upper bound on the heat transport if the background field is SC-stable. As we have seen before the spectral constraint regulates when a solution branch is upper bounding: at the point when a solution branch losing SC-stability an additional wavenumber enters into the solution, and a non-smooth branching in the optimal solution curve occurs. With the change of variable $b$ to $\lambda$ the spectral constraint becomes for $\lambda > 1$:

$$Q = \langle(D\widehat{\theta})^2 + (k\widehat{\theta})^2\rangle + \lambda\langle w\widehat{\theta}\tau'\rangle \geq 0 \tag{4.50}$$

which must be fulfilled on a wavenumber by wavenumber basis for single-mode $(w, \widehat{\theta})$ satisfying equation (4.46) and the specific boundary conditions. The discussion of why this condition must be satisfied for single-mode fields is deferred until the next chapter.

This condition can be posed as an eigenvalue problem: the background field $\tau$ and associated balance parameter $\lambda$ is SC-stable if the eigenvalues of the following system are non-positive ($\mu \leq 0$) for all wavenumbers $k \in \mathbb{R}$

$$\begin{aligned} 2(D^2 - k^2)\widehat{\theta} - \lambda w\tau' + Rak^2 q &= \mu\widehat{\theta}, \\ (D^2 - k^2)^2 q + \lambda\widehat{\theta}\tau' &= 0, \\ (D^2 - k^2)^2 w - Rak^2\widehat{\theta} &= 0, \end{aligned} \tag{4.51}$$

for; $w$, $q$, and $\widehat{\theta}$; eigenfunctions of $z$ only which satisfy the specific boundary conditions. Comparison with the optimal equations (4.44)-(4.46) therefore reveals that the optimal background field must in fact be SC-neutral.

### 4.4.3 Generic multi-$k$ solutions

The single-mode solution branch begins at the energy stability point $Ra_c$ at which the conduction state ($w = \widehat{\theta} = 0$ and $\tau = 1 - z$ for all $z \in [0, 1]$) is unstable to unimodal rolls. The critical Rayleigh number and wavenumber for no-slip boundary conditions are, respectively,

$$Ra_c = 1707.76; \qquad k_c = 3.117, \tag{4.52}$$

and for stress-free boundary conditions

$$Ra_c = \frac{27\pi^4}{4} \approx 657; \qquad k_c = \frac{\pi}{2}. \tag{4.53}$$

When $\lambda = 1$ the spectral constraint makes contact with the energy stability problem. Therefore, the optimal solution bifurcates from the conduction state onto the single-mode branch at $Ra = Ra_c$. Continuation in $Ra$ can be made along the single-mode branch while SC-neutrality is preserved. As is generally observed with these bounding problems (not least in Chapter 2), the single-mode solution gives way to a two-mode solution, which later (in $Ra$) loses stability to a three-mode solution and so on. We denote by $N_j$, for $j = 1, 2, \ldots$, the value of the functional for a

$j$-mode solution of the optimal equations. When $N_j = N_{j+1}$ the $j$-mode solution loses SC-stability to the $(j+1)$-mode branch of solution. The optimal upper bound on the Nusselt number will be denoted by

$$N = \max_{j \in \mathbb{Z}} N_j, \tag{4.54}$$

where the maximising subscript is a monotonic function of $Ra$.

Therefore at any particular $Ra$, the maximum will be achieved by the $M$-mode branch of solution, and the generic nature of the optimal fields is[1]

$$\widehat{\theta} = \sum_{m=1}^{M} \widehat{\theta}^{(m)}(z)\cos(k_m x); \quad w = \sum_{m=1}^{M} w^{(m)}(z)\cos(k_m x); \quad q = \sum_{m=1}^{M} q^{(m)}(z)\cos(k_m x). \tag{4.55}$$

Where each subfield $(k_m, w^{(m)}, q^{(m)}, \widehat{\theta}^{(m)})$ must individually satisfy the four equations (4.44)-(4.47), while they collectively force the background field and optimal balance parameter:

$$\lambda(\tau' - 1) = \sum_{m=1}^{M} (w^{(m)}\widehat{\theta}^{(m)} - \langle w^{(m)}\widehat{\theta}^{(m)} \rangle), \tag{4.56}$$

$$\lambda = 2 - \frac{\sum_{m=1}^{M} \langle (D\widehat{\theta}^{(m)})^2 + (k_m \widehat{\theta}^{(m)})^2 \rangle}{\sum_{m=1}^{M} \langle w^{(m)}\widehat{\theta}^{(m)} \rangle}. \tag{4.57}$$

### 4.4.4 Spectral decomposition for $z$-functions and numerics

Computation of the optimal solution closely follows Chapter 2 with the important exception that simple spectral collocation in Chebyshev polynomials is not appropriate owing to the fourth order derivatives in the optimal equations. The Chebyshev matrix representation of $D^4$ is found to be unstable at moderate values of $Ra$. A set of orthogonal polynomials which are tailor-made for such a problem are Jacobi polynomials for which the galerkin projection of $D^4$ is an unconditionally stable matrix for all $Ra$. The details of the Jacobi spectral-Galerkin method used will be given in Appendix A. The supplementary task of checking SC-stability was performed by an eigenvalue code solving system (4.51) for a broad sweep of wavenumbers.

[1] To be consistent with Chapter 2 superscript $m$ is used to index the individual fields.

## 4.5 Numerical results for 1-$k$

Owing to the fact that an asymptotic analysis of the multi-$k$ solution of the Euler–Lagrange equations necessarily begins and relies on an understanding of the asymptotics of the 1-$k$ solution we present first a complete description of the numerical solution of the Euler–Lagrange equations with only one horizontal mode. Even though the 1-$k$ solution branch will remain a valid upper bounding solution only while the spectral constraint is satisfied, the solution is calculated over many decades of $Ra$ in order to gain insight into the asymptotic behaviour of the solution. Subscript 1 will be used to denote the 1-$k$ solution, namely, $\lambda_1$, $k_1$ and $N_1$ are respectively the balance parameter, wavenumber and Nusselt number calculated according to expression (4.19).

### 4.5.1 No-slip 1-$k$ results

The asymptotic solution of the 1-$k$ problem presented in Chan (1971) can be compared directly to the numerical calculation of the 1-$k$ solution. The predictions to be studied are

$$k_1 = \left(\frac{R}{13}\right)^{1/4} \quad \text{as} \quad Ra \to \infty \tag{4.58}$$

(equation 54 in Chan, 1971) and the equation below (64) in Chan which implies that

$$\lambda_1 \to 23/13 \quad \text{as} \quad Ra \to \infty \tag{4.59}$$

[2]and that the interior slope of $\overline{T}$ remains $-1/13$ as $Ra \to \infty$ which incidentally implies that in the interior the slope of $\tau$ is positive, $\tau' = 1/23$. We will also study the overall prediction of the Nusselt number for the 1-$k$ branch (equation 118a of Chan)

$$N_1 = 0.1482 Ra^{3/10} (\log Ra)^{1/5} \quad \text{as} \quad Ra \to \infty. \tag{4.60}$$

[2]In Chapter 6 we give a formula for the limiting value of $\lambda$ which independently verifies 23/13 by assuming that $N_1 \sim Ra^{3/10}(\log Ra)^{\gamma_2}$ for any constant value of $\gamma_2$.

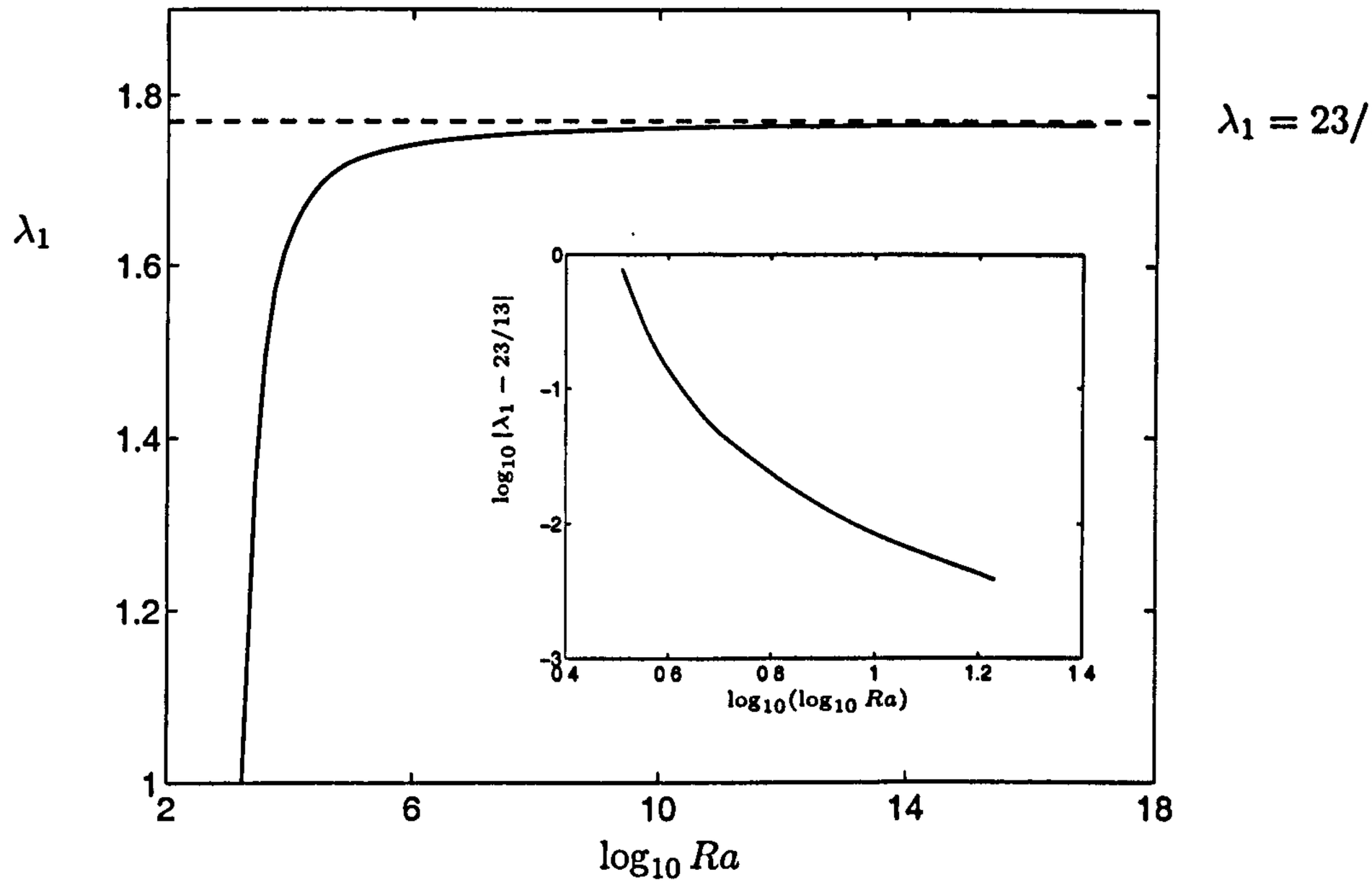


Figure 4.2: [No-slip] Plot of the balance parameter $\lambda_1$ with conjectured limiting value of 23/13. The inset plot shows that the residual of $\lambda_1$ and 23/13.

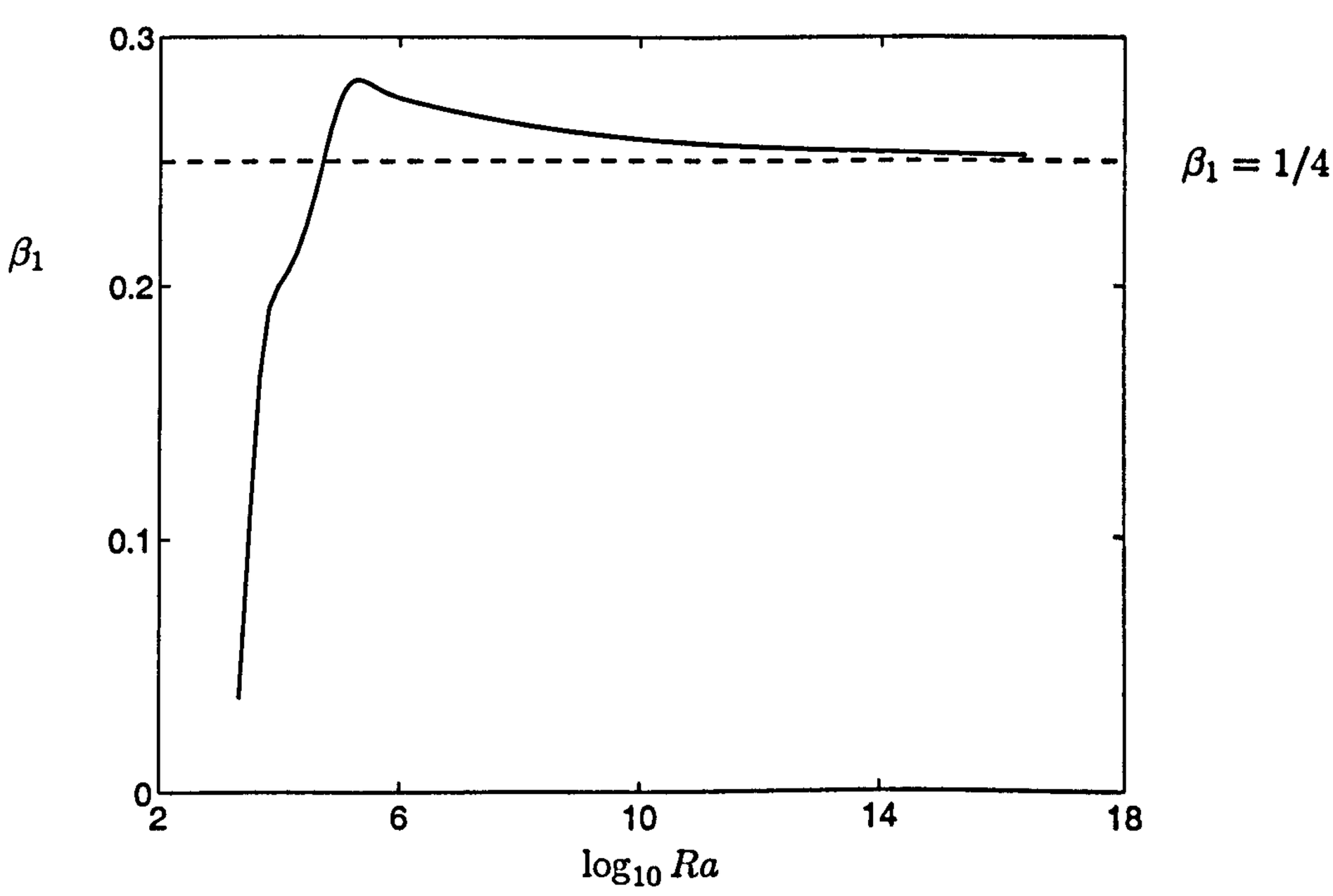


Figure 4.3: [No-slip] Plot of the exponent $\beta_1$ in the relation $k_1 = cRa^{\beta_1}$ calculated by taking the numerical derivative $\Delta \log k / \Delta \log Ra$ with the conjectured limiting value of 1/4.

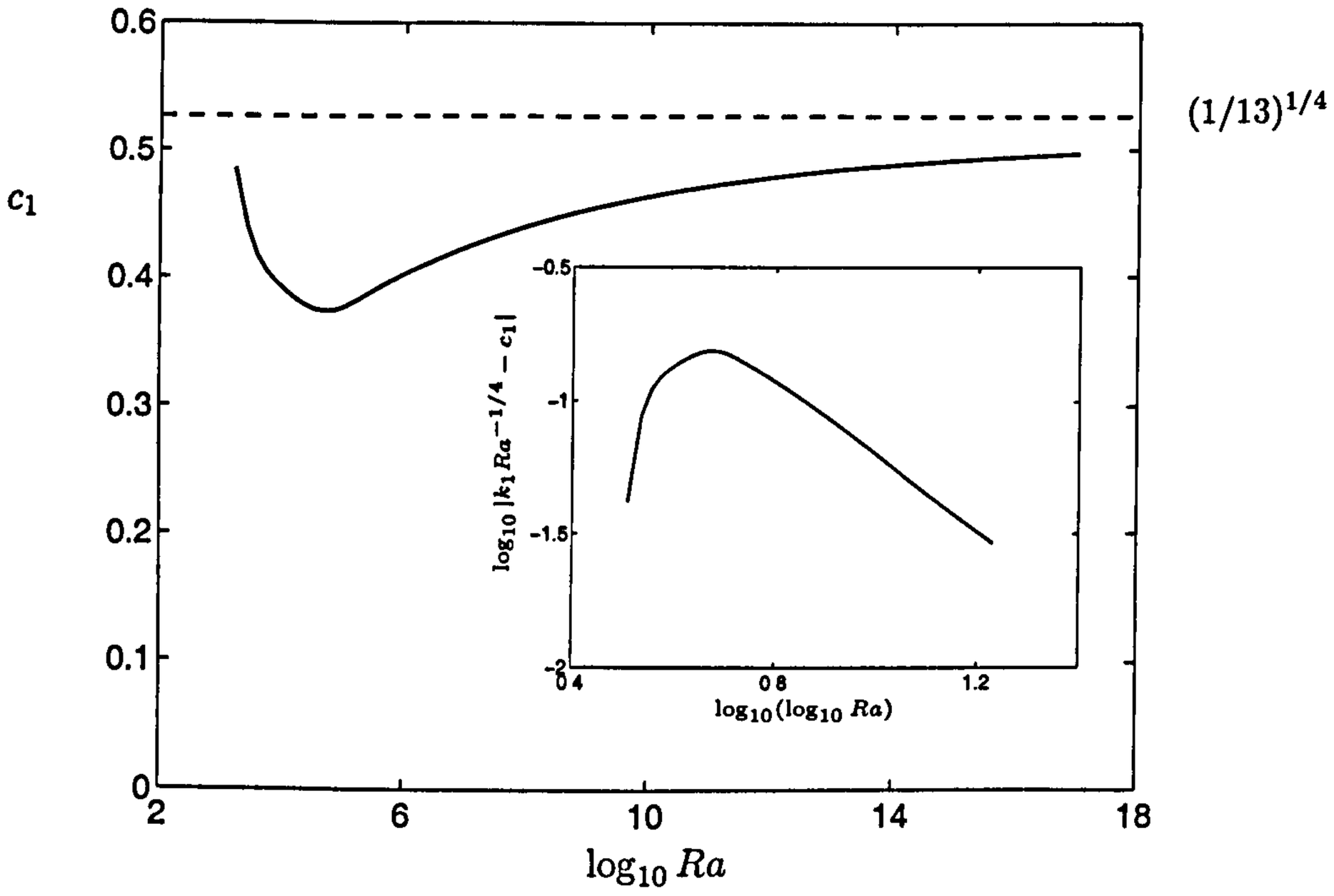


Figure 4.4: [No-slip] Comparison of the numerical data and the relation $k_1 = c_1 Ra^{1/4}$ where the conjectured prefactor is $c_1 = (1/13)^{1/4}$. The inset plot showing the residual of the prefactors is included to show the possible existence of a correction term algebraic in $(\log Ra)$.

Reliable data is computed over the range $\mathcal{O}(10^2)-\mathcal{O}(10^{16})$. In figure 4.2 the value of $\lambda_1$ is plotted and is found to converge convincingly to 23/13 while no algebraic dependence of the residual with $Ra$ or $(\log Ra)$ is found and only two and a half digits accuracy are achieved even at $Ra = 10^{17}$. In figures 4.3 and 4.4 we see that prediction (4.58) compare reasonably well with the data for the prefactor and exponent of $k_1$. The convergence rate is very slow and seems to be logarithmic from the inset in figure 4.4. In figure 4.5 we compare prefactors for relation (4.60) which supports a limiting value 0.1482. The exact nature of the local logarithmic dependence of $N_1$ on $Ra$ is tested in figure 4.6 which illustrates that even with fifteen decades of data one can not reliably conclude that the power of 1/5 in expression (4.60) is correct. However, the evidence in figures 4.2-4.6 together provides a convincing defence for the asymptotic predictions of the 1-$k$ problem reported in Chan (1971).

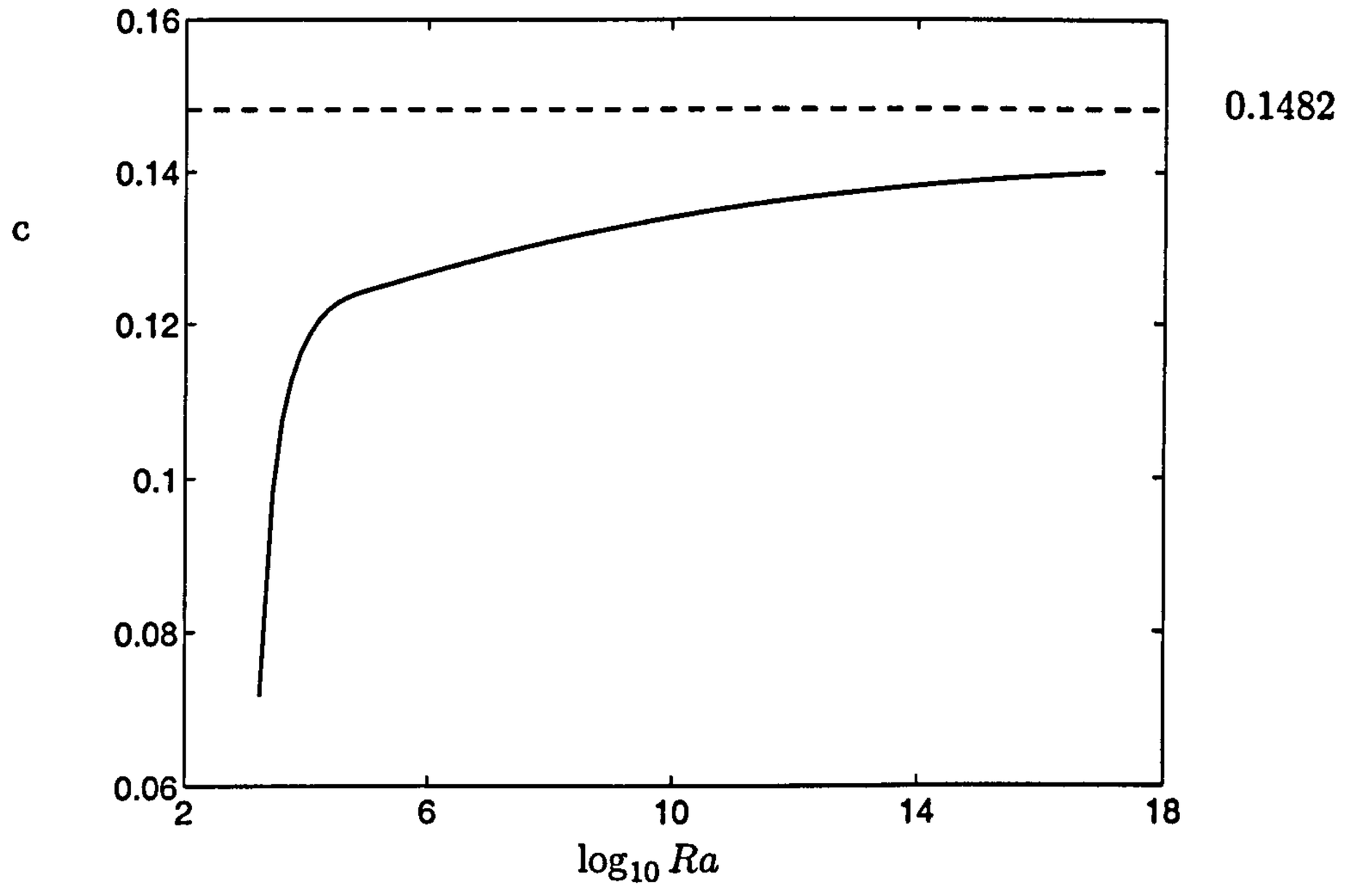


Figure 4.5: [No-slip] Plot of the prefactor in the relation $N_1 = cRa^{3/10}(\log Ra)^{1/5}$ with conjectured limiting value of $c$ shown as 0.1482.

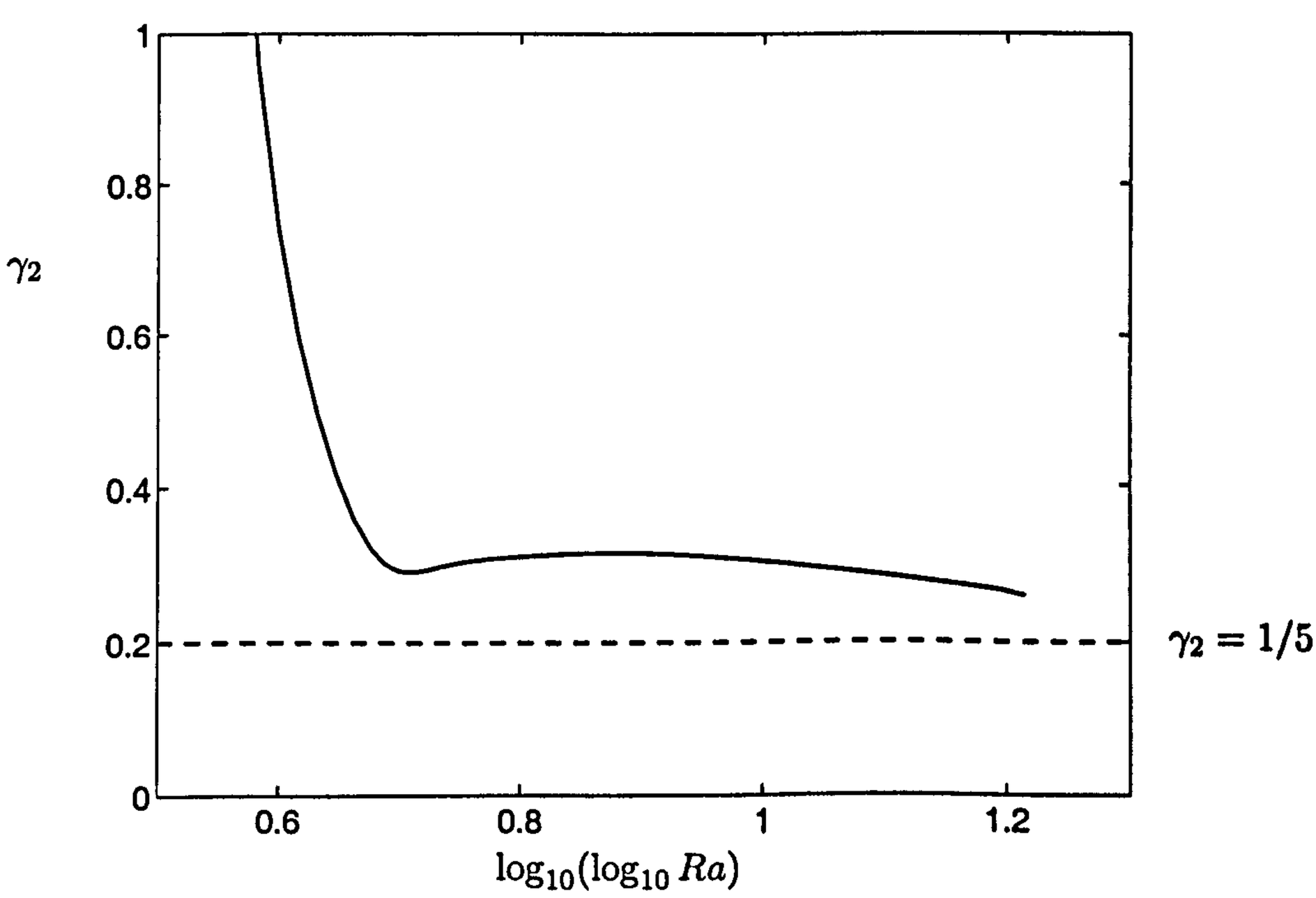


Figure 4.6: [No-slip] Under the assumption of a functional form $N_1 = cRa^{3/10}(\log Ra)^{\gamma_2}$, the power of $(\log Ra)$, $\gamma_2$, is evaluated locally by taking the numerical derivative $\Delta(\log N_1 - .3 \log Ra)/\Delta(\log(\log Ra))$.

### 4.5.2 Stress-free 1-$k$ results

Changing tack now, we consider the 1-$k$ solution branch for stress-free boundary conditions and critique the asymptotics study of this problem presented in Vitanov (1998). The contrast with the no-slip 1-$k$ solution is rather surprising. Equation (29) of Vitanov (1998) makes the following predictions:

$$N_1 = 0.3254 Ra^{1/3}, \quad k_1 = 0.2011 Ra^{1/6} \quad \text{as} \quad Ra \to \infty. \tag{4.61}$$

No prediction is made for the limiting value of $\lambda_1$. There are no logarithmic factors in this prediction and the numerical solution suggest that the next order correction are algebraic in $Ra$.

The limiting value of $\lambda_1$ is found to be 7/4 (see figure 4.7) and the residual scales as a power of $Ra$ convincingly over at least eight decades. In figure 4.8 we see Vitanov's assumption that $k_1$ scales as $Ra^{1/6}$ is invalid. In actuality, the limiting wavenumber is $\mathcal{O}(1)$, contrary to all other 1-$k$ analyses in Optimum theory in which the wavenumber scale with $Ra$. By luck, however, Vitanov's predicted Nusselt scaling is correct. In fact, in figure 4.9 we see that the predicted prefactor for $N_1$ in equation (4.61) is only slightly modified. An analysis of the inset plot in figure 4.9 demonstrates that the residual scales approximately like $Ra^{-1/3}$.

To summarise it has been shown that the boundary conditions alter the form of the solution and are capable of causing or suppressing the appearance of logarithmic factors in $N_1$. The asymptotic analysis of Chan (1971) is supported by the numerical solution of the no-slip problem although the fifteen decades of data is insufficient to present an irrefutable argument. For stress-free boundary conditions we have found an error with Vitanov (1998) and exposed a rather non-standard 1-$k$ solution. The evidence presented here has enabled R. Kerswell to fix the asymptotic analysis of the 1-$k$ solution. This work will be presented in a forthcoming joint publication.

The following section will deal with the continuation calculation of the upper bounding multi-$k$ solution of (4.54).

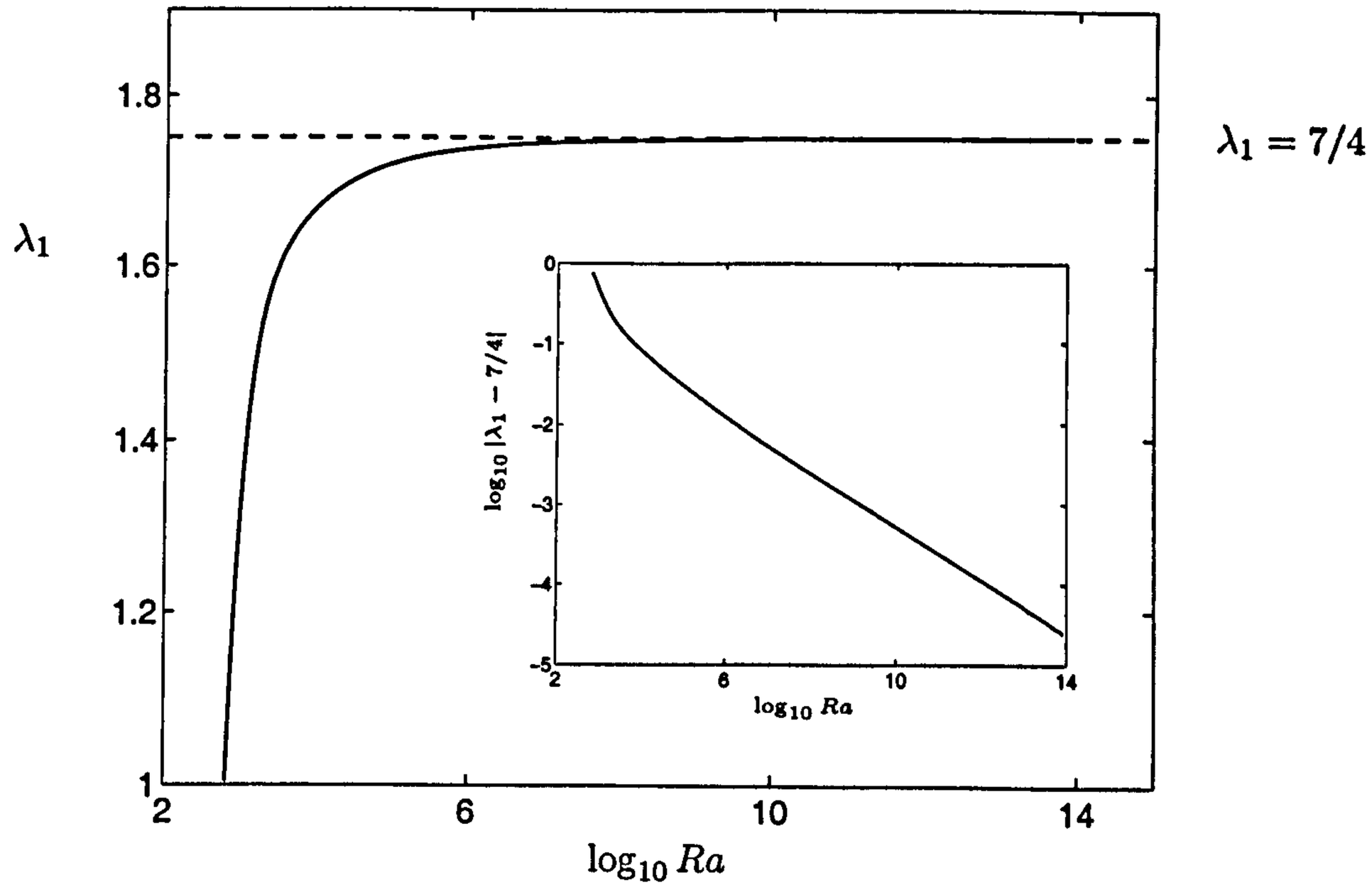


Figure 4.7: [Stress-free] Plot of the balance parameter $\lambda_1$ with limiting value of 7/4. The inset figure shows that the residual decays algebraically with $Ra$.

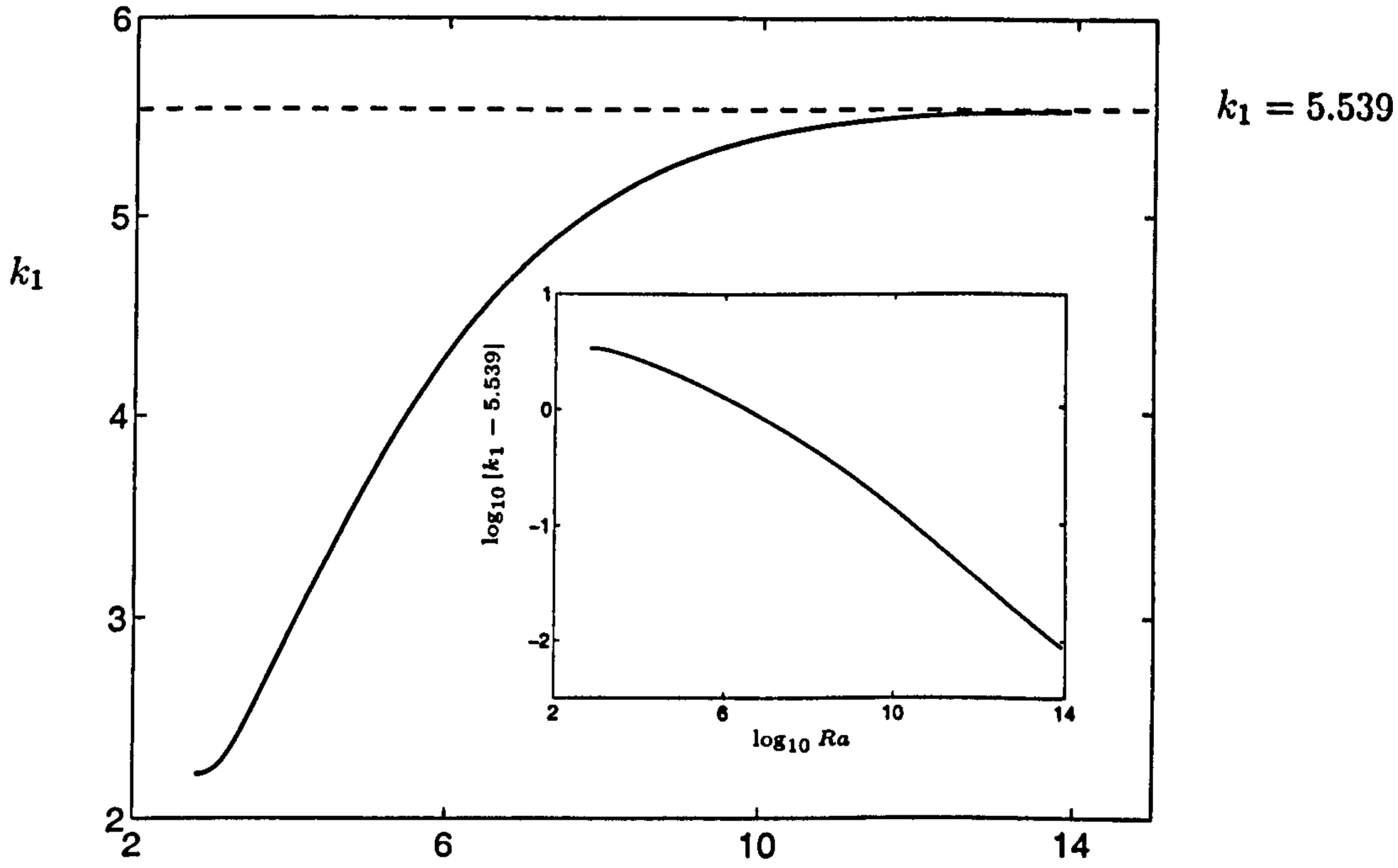


Figure 4.8: [Stress-free] Plot of $k_1$ showing convergence to an $\mathcal{O}(1)$ number with inset figure showing that the residual decays algebraically with $Ra$ after $Ra = 10^9$.

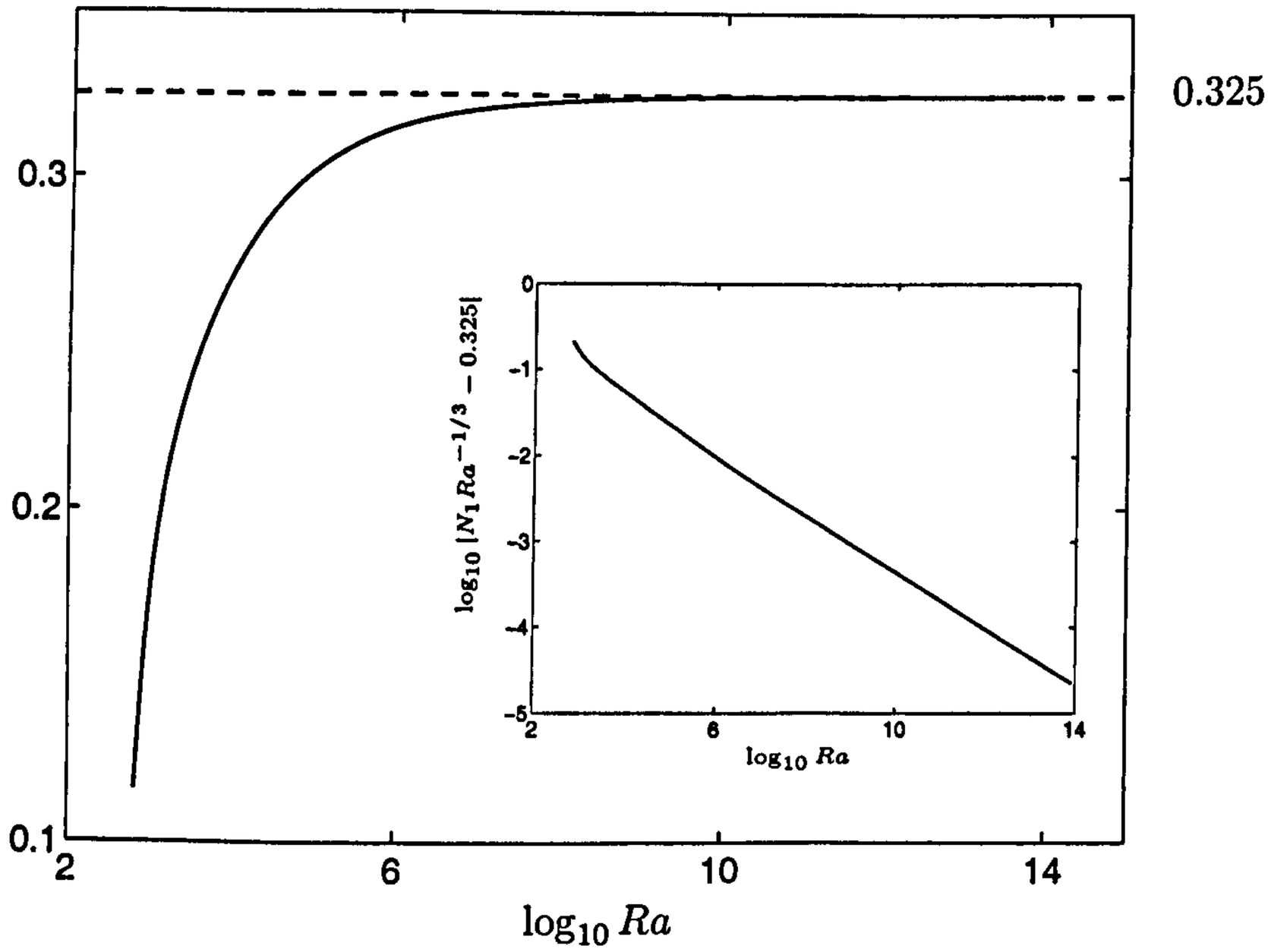


Figure 4.9: [Stress-free] Plot of the prefactor in the relation $N_1 = cRa^{1/3}$ with inset figure showing fast algebraic convergence to a value of 0.325.

## 4.6 Numerical results for multi-$k$

We have seen that the 1-$k$ solutions for stress-free and no-slip boundaries are fundamentally different. The stress-free solution for 1-$k$ is quick to converge to its asymptotic limit but has a non-standard $\mathcal{O}(1)$ wavenumber, while the no-slip 1-$k$ problem converges slowly due to logarithmic factors in the asymptotic series expansion of $N_1$ in $Ra$. What of the multi-$k$ solutions?

Ironically, the situation is reversed in the upper bounding multi-$k$ solutions. The no-slip solution quickly tends toward the asymptotic regime suggested by Chan (1971):

$$N = 0.152Ra^{1/3} \quad \text{as} \quad Ra \to \infty \tag{4.62}$$

while over the broad range of $Ra$ reported here the stress-free solution does not begin to have asymptotic characteristics. This pathological example of stress-free boundaries is, however, not restricted to infinite Prandtl number, in their arbitrary Prandtl number convection paper Vitanov & Busse (1997) commented that: "the [multi-k] method seems to fail in the case of stress-free boundaries".

### 4.6.1 No-slip multi-$k$ results

The optimal solution was calculated for up to four wavenumbers. The bifurcation to five wavenumbers was found to be at approximately $Ra = 9 \times 10^9$. In figure 4.10 the asymptotic $Ra^{1/3}$ nature is evident and we make the prediction that the prefactor is 0.139 which is about 9% lower than Chan's prediction in equation (4.62). Circles represent bifurcation between $j$-mode and $(j+1)$-mode solutions at which SC-neutrality switches to solutions with a greater number of nested boundary layers. Bifurcations in the horizontal wavenumbers of the optimal solution is shown in figure 4.11 which compares favourably to figure 2.3 in Chapter 2. Owing to the appearance of logarithms in Chan's asymptotic solution the point of bifurcations are severely under-estimated in Chan (1971). Chan states that the first bifurcation occurs at $Ra = 10^{10}$ and that asymptotically the number of wavenumbers in the solution grow as $(\log\log Ra)$. We find that, at least before $10^{10}$ the bifurcation point are approximately spaced evenly in $\log Ra$. The approach of $\lambda$ to the limiting value 7/4, which is calculated using a formula in Chapter 6 but is not reported in Chan (1971), is shown in figure 4.12.

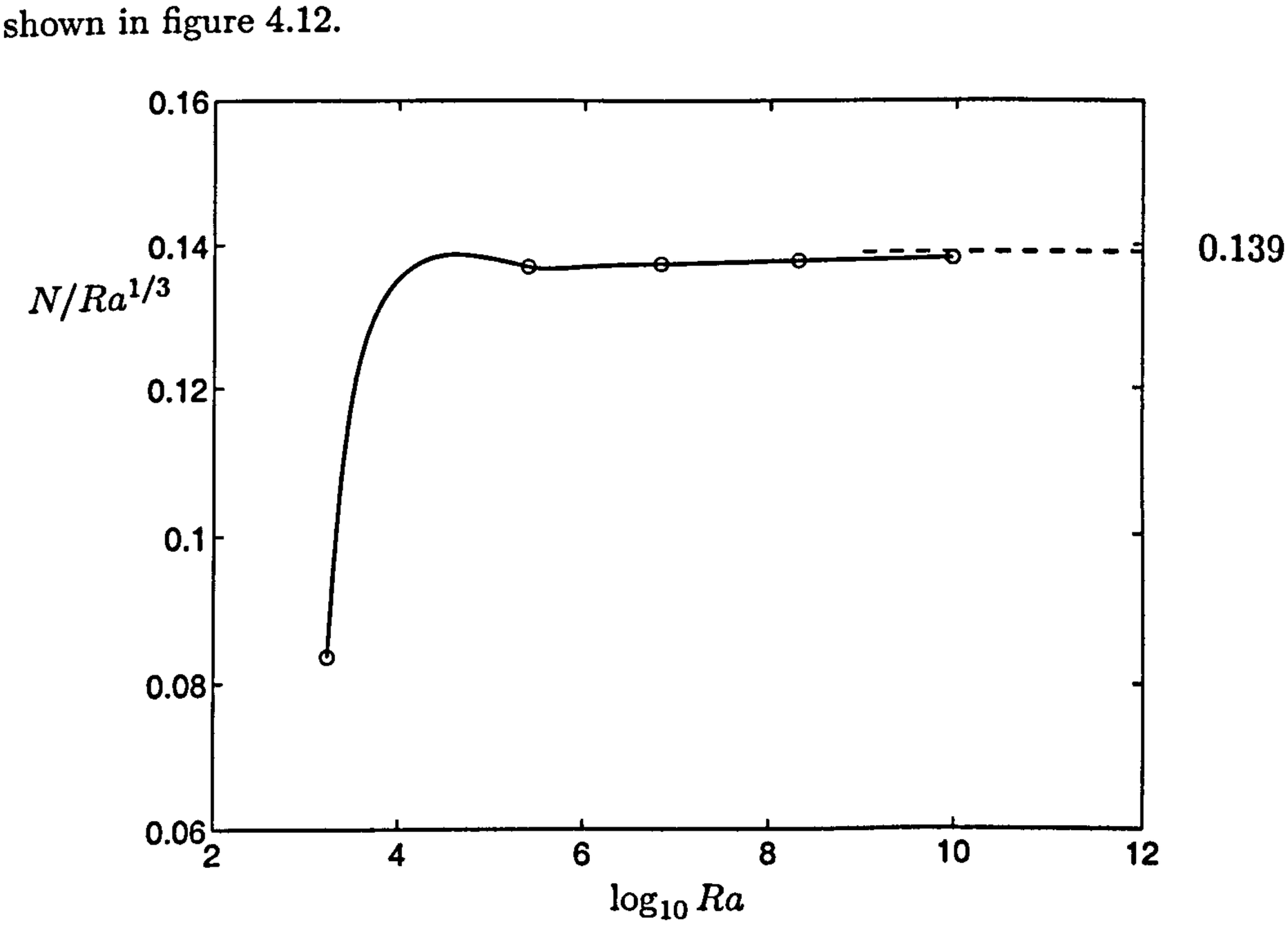


Figure 4.10: [No-slip] Plot of the Nusselt bound scaled by $Ra^{1/3}$. Here and henceforth circles indicates bifurcations from $(n)$-$k$ to $(n+1)$-$k$ solutions.

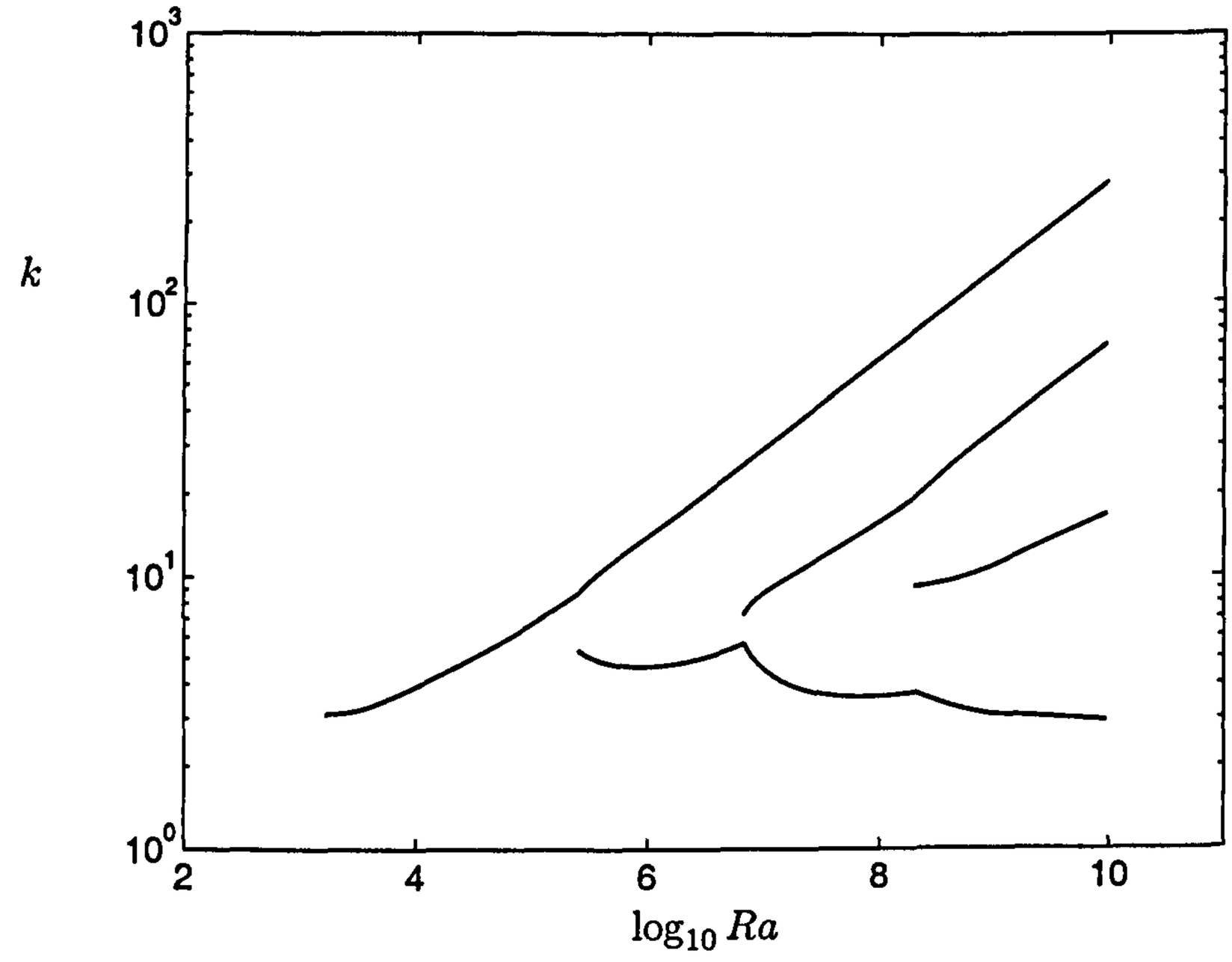


Figure 4.11: [No-slip] Bifurcation plot of the horizontal wavenumbers $k_m$ associated to the optimal solution.

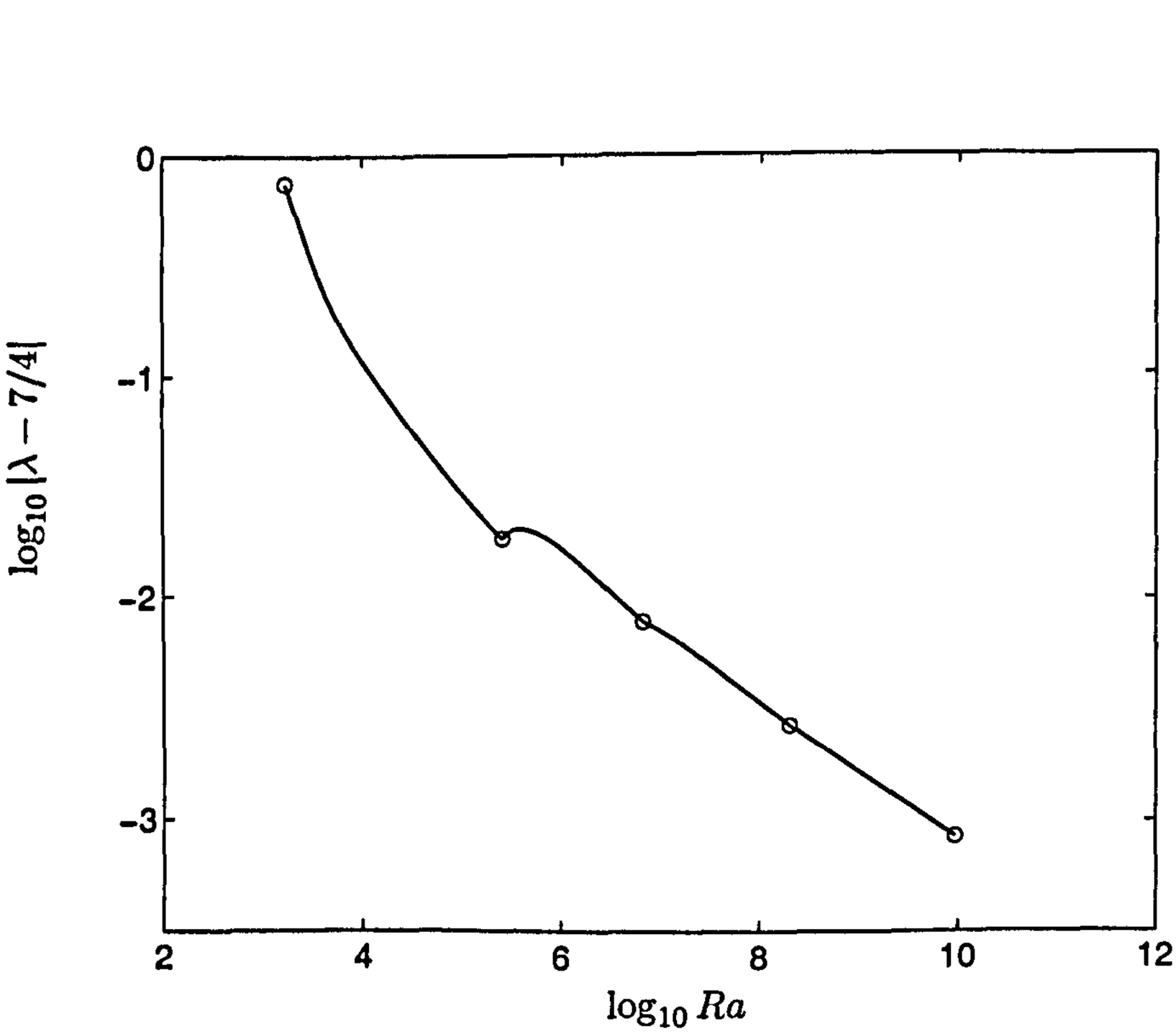


Figure 4.12: [No-slip] Plot of the residual of the optimal $\lambda$ with limiting value 7/4.

### 4.6.2 Stress-free multi-$k$ results

Thinking back to the solution of the shear problem in Chapter 2 the solution to the no-slip problem seems similar. The form of the $k$-bifurcation and the approach to limiting values look very familiar. Turning now to the stress-free multi-$k$ problem we find the solution is unorthodox in accord with a peculiarity inflicted by the boundary conditions alluded to by Vitanov & Busse (1997). In Section 4.3 we observed that the 1-$k$ Nusselt function $N_1$ scaled as $Ra^{1/3}$. Calculations of the asymptotics of the 2-$k$ function $N_2$ show a $Ra^{2/5}$ scaling which is supported by an asymptotic analysis by R. Kerswell. Progress on the 3-$k$ solution is, however, computationally very hard and the author cannot accurately comment on the exact scaling of $N_3$. The bifurcation to a 4-$k$ solution occurs at around $Ra = 7 \times 10^{11}$ but no points on the 4-$k$ branch have been calculated because of difficulties experienced getting onto that solution branch — no 4-$k$ guess solution was found to converge.

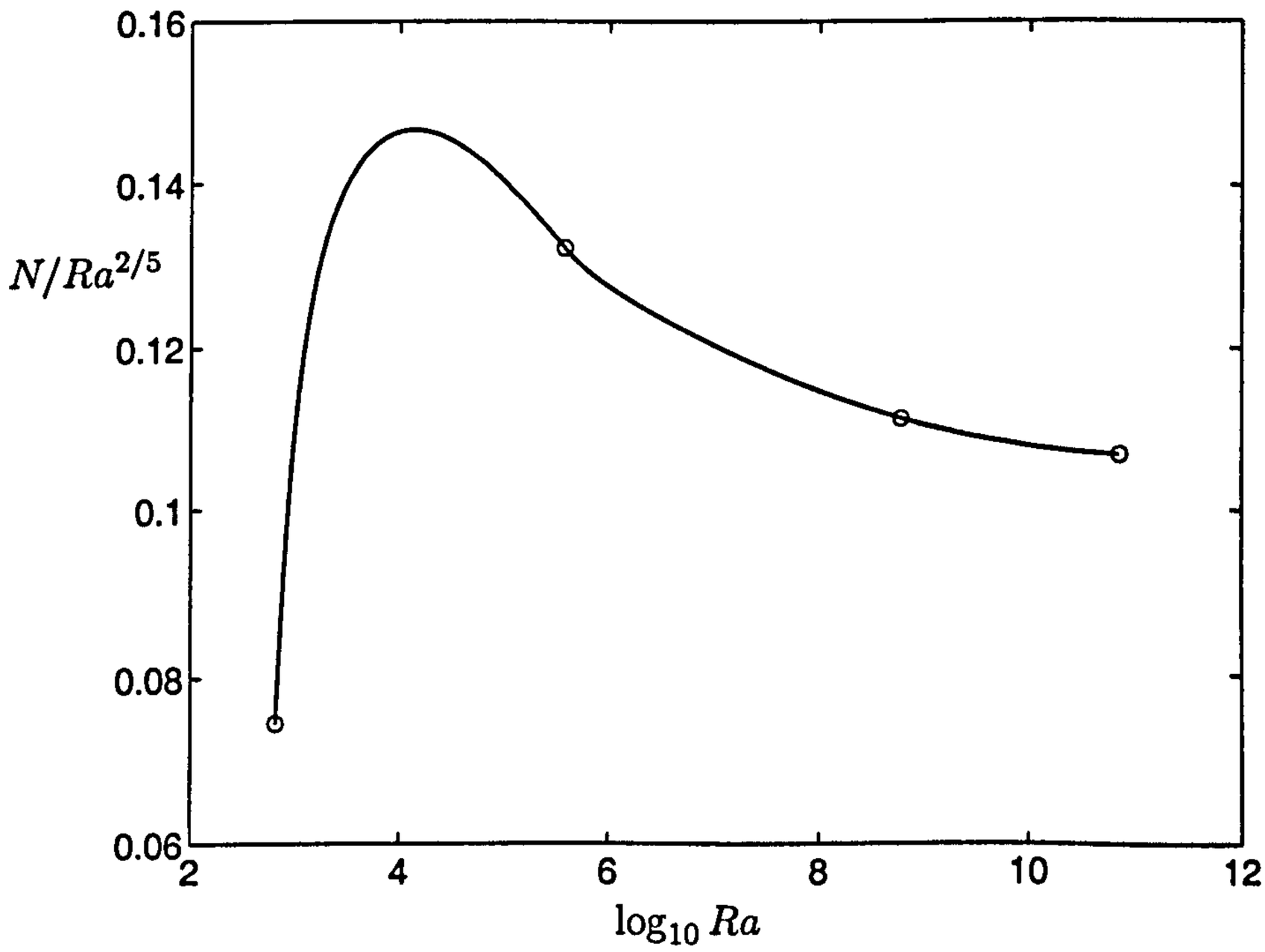


Figure 4.13: [Stress-free] Plot of the Nusselt bound scaled by $Ra^{2/5}$ (the asymptotic scaling of the 2-$k$ branch).

To give the reader an idea of the rate of approach to a limiting exponent we represent in figure 4.14 the local exponent as it varies with $Ra$ along the one-, two- and three-mode solution branches. If, in common with Busse's original multi-$k$ soltuion, the asymptotic exponent of the j-mode branch of solution follows a geometric series then the limiting exponent of the optimal solution may be 5/12 and hence we include it as a possible limiting value for $\beta_\infty$.[3] We would like to draw attention to the fact that 5/12 is also the same exponent which Otero (2002) finds for two-dimensional arbitrary Prandtl number convection for stress-free boundaries incorporating the enstrophy constraint. This means that for infinite Prandtl number convection with stress-free boundaries the linear velocity constraint is as potent a variational constraint as the enstropy constraint for 2-D convection. The similarity also suggests that the 3-D variational problem is insensitive to uniquely 3-D phenomena such as vortex stretching.

In the absence of a prediction for the asymptotic nature of the 3-$k$ solution, or for the upper bounding multi-$k$ solution, in figure 4.13 the Nusselt bound is depicted scaled by the 2-$k$ Nusselt function scaling of $Ra^{2/5}$. In figure 4.15 the $k$-bifurcation is depicted and in figure 4.16 the optimal $\lambda$ is shown although there is no obvious limiting value for $\lambda$ and a dash line at 1.7 has only been included to guide the eye. There are two features of the $k$-bifurcation diagram which set this solution apart from the no-slip solution. The first is that the distance from start point to first bifurcation and from first to second bifurcation point is almost the same (in fact the latter is a little longer). This is significant because it indicates that the 1-$k$ to 2-$k$ transition is as important as the 2-$k$ to 3-$k$ transition. In the canonical problem in Chapter 2 the 1-$k$ to 2-$k$ transition is most significant in changing the scaling properties of the upper bound on $Nu$ (compare with figure 4.10). On the contrary for stress-free boundaries the first two transition in the solution are equally significant to the scaling of the upper bound $N$. The second feature of the $k$-bifurcation which distinguishes the stress-free problem is that the lowest wavenumber decreasing monotonically after the 1-$k$ to 2-$k$ transition and is well separated from the other wavenumbers. This observation may be crucial to understanding the 3-$k$ asymptotics and could signal

[3] We postulate 5/12 as the asymptotic optimal exponent because it is the limit of a geometric series with first term 1/3 and second term 2/5 — and hence with absolute ratio 1/5.

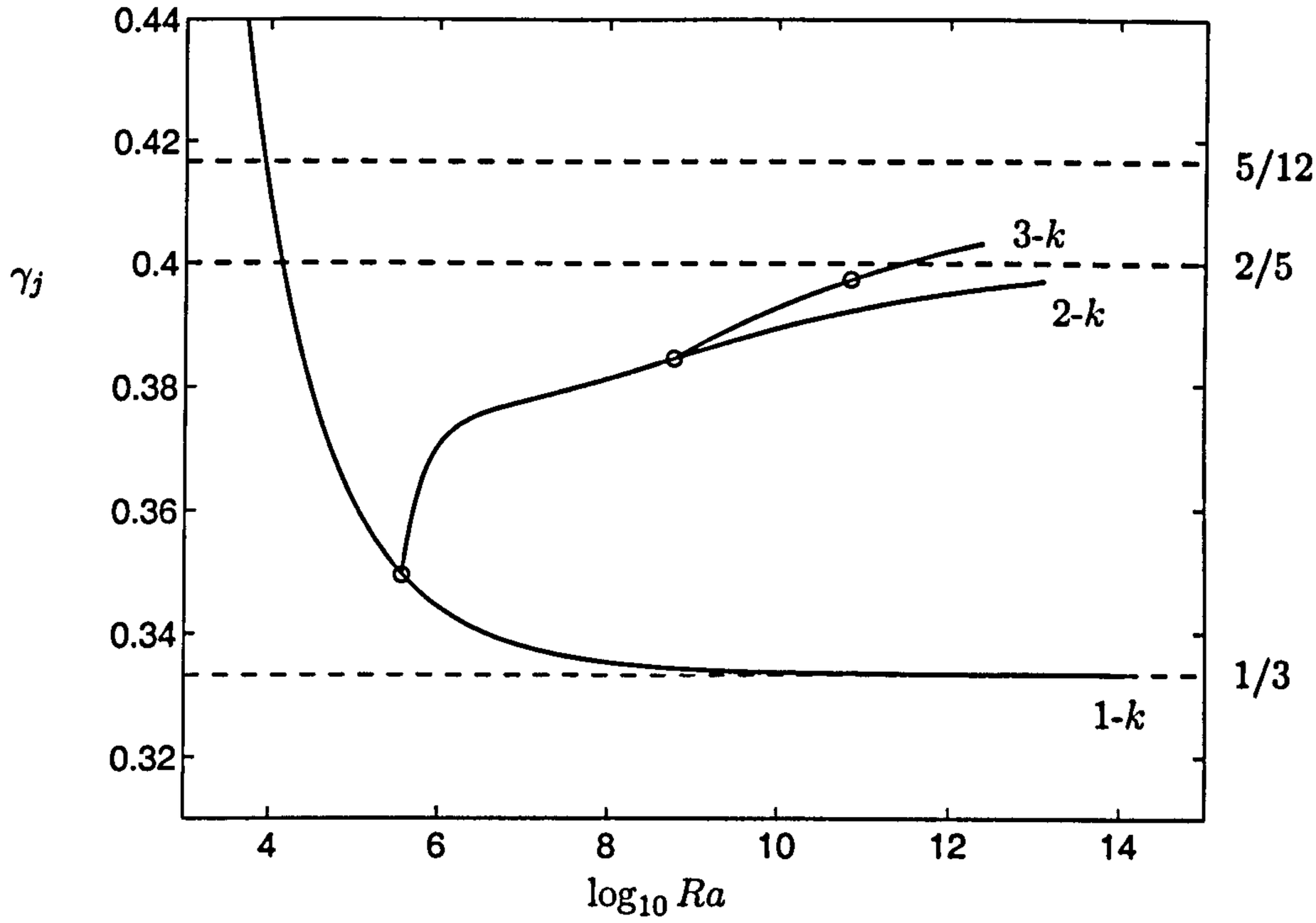


Figure 4.14: [Stress-free] Plot of the $Ra$-exponent of the function $N_j$ over the full range of $Ra$ calculated assuming the relation $N_j = cRa^{\gamma_j}$. Branches are labelled by their corresponding mode number $j$-$k$. Dashed lines are included for comparison at 1/3, the limiting expontent for 1-$k$, at 2/5, the limiting exponent for 2-$k$, and at 5/12 a possible exponent for the optimal solution. Circles represent the point of bifurcation from $j$-mode to $(j+1)$-mode solutions. No points have been calculated on the four-mode branch after the third circle.

difficulties in attempting a full multi-$k$ asymptotic analysis of the optimal solution. We therefore end this section with an incomplete picture of the optimal solution to the stress-free problem. More work will be needed to resolve the asymptotics of the 3-$k$ branch and to calculate perhaps three decades of the 4-$k$ branch. One could postulate from the evidence in figure 4.10 that the optimal asymptotic scaling of $N$ is $Ra^{2/5}$, but, it is certain that the scaling exponent must lie somewhere between 2/5 and 1/2. To narrow this range of uncertainty in the next Chapter we will perform a conservative bound estimate of the optimal solution or, to kidnap a phrase from Doering & Constantin (1998), we will be attempting to *bound the bounds* in order to estimate the optimal scaling. Before this we pause to analysis the optimal fields in order to gain some insight into what structure might play a role in deriving good conservative bounds.

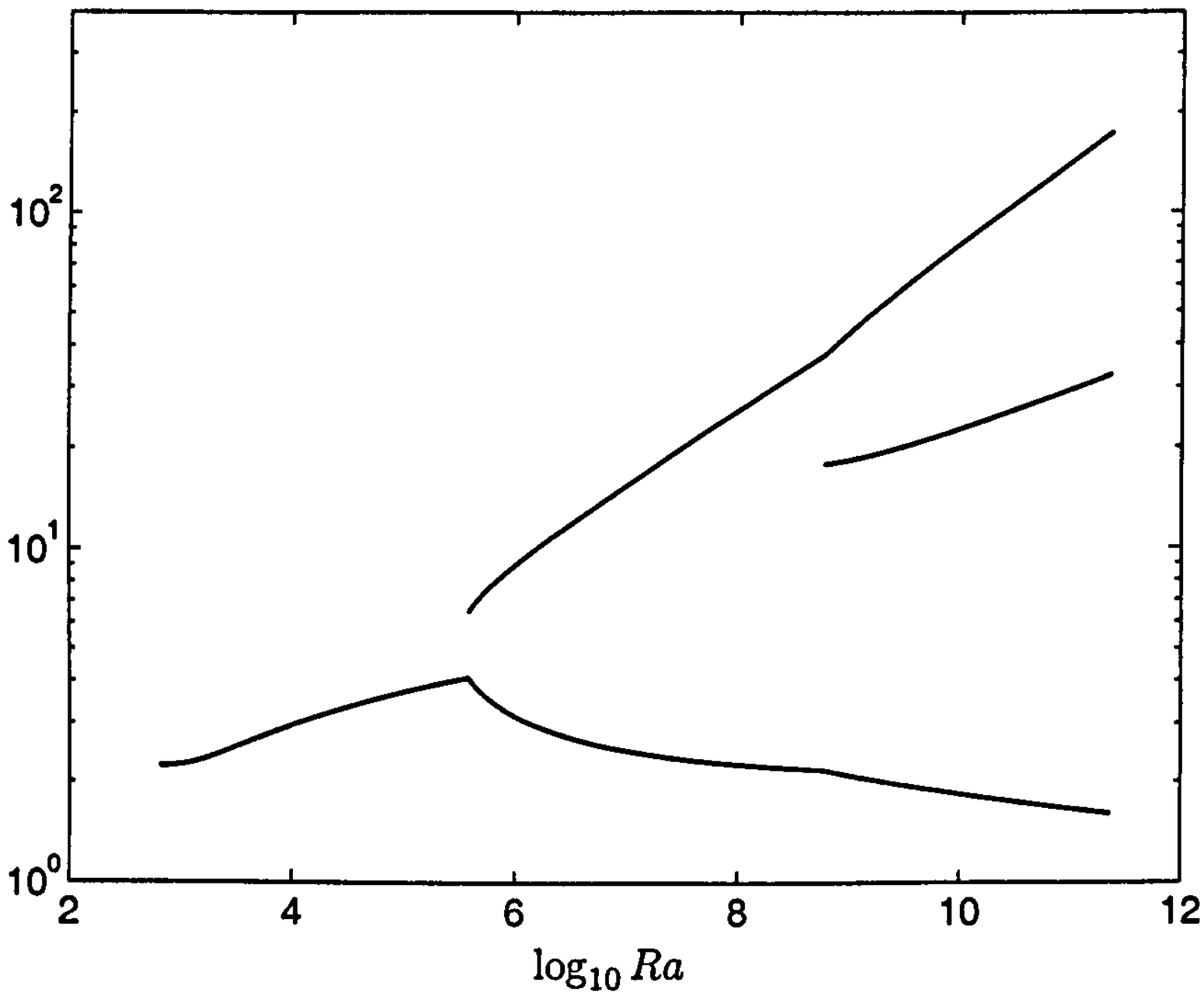


Figure 4.15: [Stress-free] Bifurcation plot of the horizontal wavenumbers $k$ associated to the optimal solution.

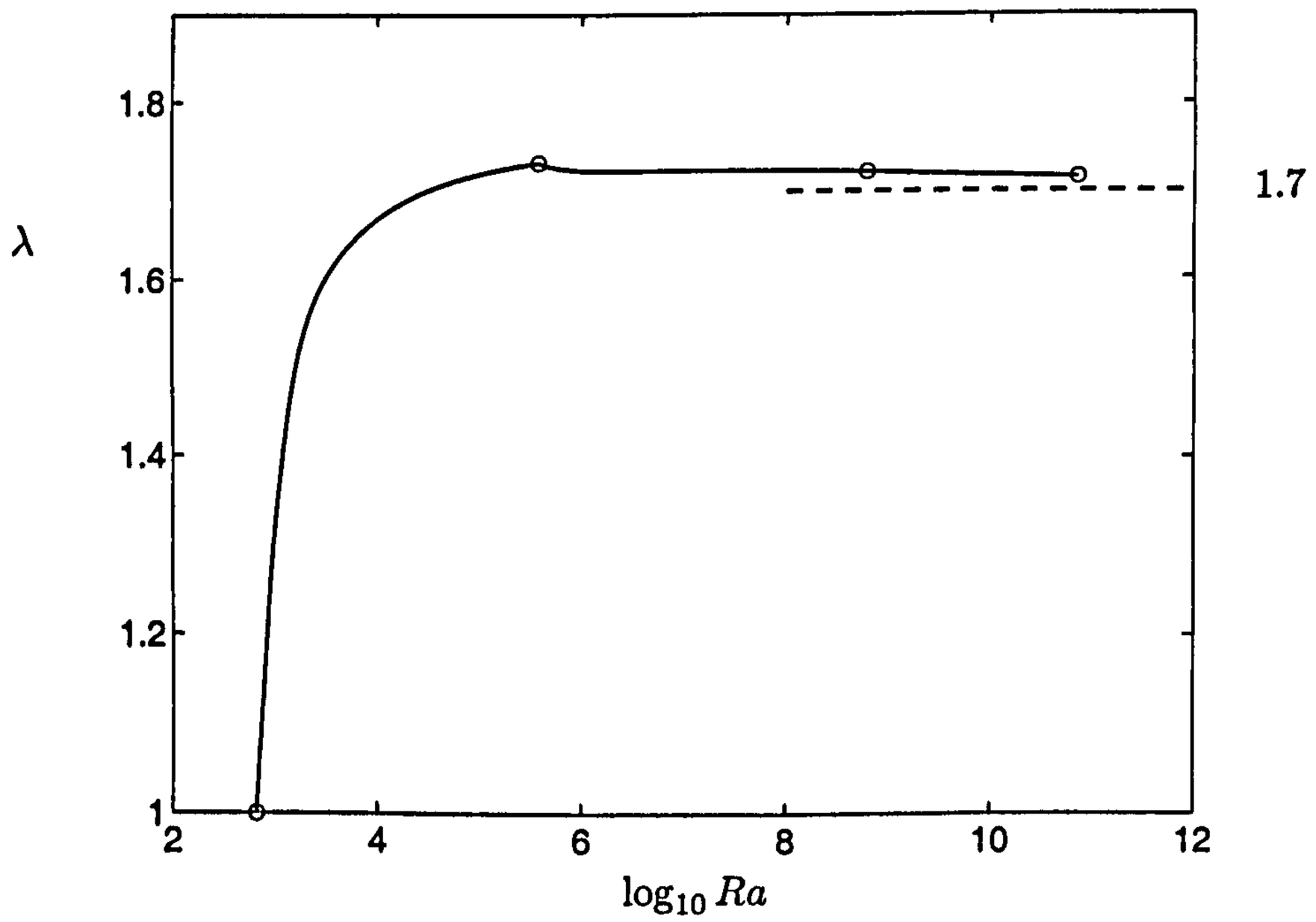


Figure 4.16: [Stress-free] Plot of the optimal $\lambda$ with the dashed line at 1.7 included to guide the eye.

## 4.7 Optimal means and future work

Recall that the mean gradient for the optimal solution (from 4.22) is computed according to

$$\overline{T}_z = \overline{w\widehat{\theta}} - \langle w\widehat{\theta} \rangle - 1, \tag{4.63}$$

while the optimal background is related to $\overline{T}$ by the equation

$$\overline{T}_z = \frac{\lambda}{2}(\tau' + 1) - 1. \tag{4.64}$$

Although we do not solve for the mean as part of the numerical programme, we can calculate the mean profile $\overline{T}$ directly from the fluctuation field by integrating (4.63) and invoking the boundary conditions:

$$\overline{T} = \int_{\tilde{z}=0}^{z} w(\tilde{z})\widehat{\theta}(\tilde{z})\mathrm{d}\tilde{z} - \langle w\widehat{\theta} \rangle z + 1 - z.$$

Therefore, in figure 4.17 we compare the optimal mean temperature profiles for

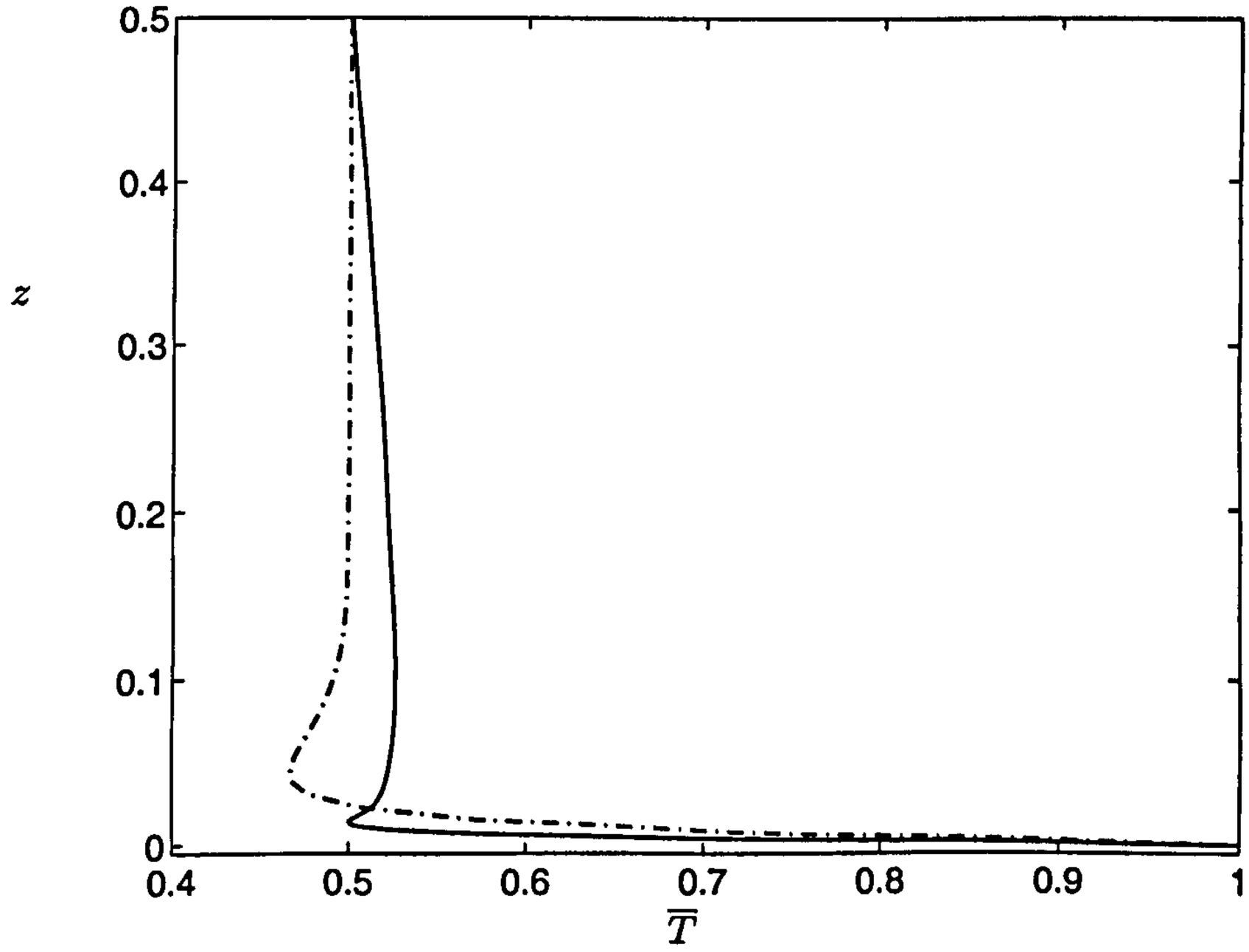


Figure 4.17: Comparison plot of the mean temperature profile for stress-free boundaries at $Ra = 10^7$ . The dot-dash curve is data from a 3D DNS experiment generously supplied by S. Labrosse.

stress-free problem (at $Ra = 10^7$) to 3D DNS data taken from figure 6 of Sotin & Labross (1999). The profiles are in qualitative agreement except for the non-zero interior gradient of the optimal mean. Each profile has an inversion in the sign of the gradient within the thermal boundary layer. For the optimal solution $\overline{T}_{zz}(0) = 0$ owing to optimal equation (4.44), however, this cannot be derived from the governing equation and is a feature of the bounding problem only. The data of Sotin & Labross (1999) does not exhibit this particular feature.

The value of $\tau'$ in the interior of the channel is actually positive for all $Ra$ in contrast to the shear flow problem in which the background field has no interior slope for high $Re$. In the following Chapter we will investigate the potency of this feature in the background field by calculating conservative estimates of $N$ using simplified test functions for $\tau$. The result of that study will also give us some insight into the asymptotic scaling rule for the optimal solution of the stress-free boundaries problem.

To round-up, we have established the validity of the asymptotic scaling of $Ra^{1/3}$ for the no-slip problem first stated by Chan (1971); good correspondence is found between the no-slip solution and the solution to the PCF problem in Chapter 2; and we found that the stress-free boundary condition strongly alters the nature of the solutions, delaying bifurcation to higher mode solutions and therefore slowing convergence to the asymptotic limit.

## 4.A Appendix

We consider here only the solution of the 1-$k$ optimal equations for simplicity of notation. The multi-$k$ is an easy extension of this programme once equations (4.56) and (4.57) are folded into the analysis.

If we denote by L the bi-Laplacian $(D^2 - k^2)^2$ then optimal equations (4.45) and (4.46) can be rewritten as

$$q = -\lambda \mathrm{L}^{-1}(\widehat{\theta}\tau') \quad \text{and} \quad w = Rak^2 \mathrm{L}^{-1}(\widehat{\theta}). \tag{4.65}$$

In this case, after some algebra, the non-scalar optimal equations (4.44, 4.45, 4.46 and 4.48) can be reduced to the following single equation:

$$2(D^2 - k^2)\widehat{\theta} + 2(\lambda + \langle w\widehat{\theta}\rangle)w - w^2\widehat{\theta} - Rak^2 \mathrm{L}^{-1}(w\widehat{\theta}^2) = 0. \tag{4.66}$$

where $w$ depends linearly on $\widehat{\theta}$ by relation (4.65) and therefore its solution is contingent on pre-calculation of the inverse bi-Laplacian. Equation (4.49) for $\lambda$ can be substituted explicitly into this equation. The system of optimal equations is then reduced to one spatial equation and one scalar equation, namely (4.66) and (4.56).

A strategy for inverting powers of the Laplacian using the spectral method with Jacobi polynomials and Galerkin projection was presented in Ierley (1997) and details for the stress-free boundaries implementation can be found in the unpublished Appendix B of Ierley & Worthing (2001)[4].

We expand the temperature fluctuation field in the Jacobi polynomials $P_k^{(1,1)}$, namely

$$\widehat{\theta}(x) = (1 - x^2) \sum_{k=0}^{K} \widehat{\theta}_k P_{2k}^{(1,1)}(x),$$

where $x = 2z - 1$ and we only select even polynomials because of the assumed symmetry in the optimal solution. The expansion of $w$ (and similarly $q$) for no-slip boundaries is

$$w(x) = (1 - x^2)^2 \sum_{k=0}^{K} w_k P_{2k}^{(2,2)}(x),$$

and for stress-free boundaries

$$w(x) = (1 - x^2) \sum_{k=0}^{K} (1 - \beta_{2k}\, x^2) w_k P_{2k}^{(1,1)}(x),$$

[4]Available upon request from the papers first author, G. Ierley.

where

$$\beta_j = \frac{2 + j(j+3)}{10 + j(j+3)}.$$

These representations for $w$ and $\widehat{\theta}$ have the boundary conditions built in.

Equation (4.66) is posed as a finite dimensional approximation by taking Galerkin projections of the derivative operators, using LU decomposition to invert L, and tensor contractions to form the cubic terms. The derivative matrices are symmetric and sparse. For example, the bi-Laplacian L is a penta-diagonal matrix. The most expensive operations are calculating the cubic nonlinearity in equation (4.66), such as $w^2\widehat{\theta}$, since the Galerkin projection would seem to require a fourth order contraction with a tensor having elements defined (for no-slip boundaries) by

$$c_{ijkl} = \int_{-1}^{1} dx\,(1-x^2)^6 P_i^{(2,2)}(x)\,P_j^{(2,2)}(x)\,P_k^{(1,1)}(x)\,P_l^{(1,1)}(x).$$

Given that the basis sets have, for some extreme cases, included even polynomials to degree $m = 1800$, this approach is not remotely feasible, even with some reductions based on symmetries and other selection rules.

This difficulty can be partly overcome by performing sequential contractions with two third-rank tensors but the overhead for the initial computation of tensor elements with Gaussian quadrature of order $3m/2$ is still burdensome, and storage scales as $\mathcal{O}(m^3)$.

It is preferable here simply to revert to a pseudospectral treatment of cubic nonlinearities since the operations count and storage requirements are both $\mathcal{O}(m^2)$, a small fraction of the $\mathcal{O}(m^3)$ requirements for matrix inversion at each step of Newton's method.[5] We elected to use a conventional forward transform. There is a potential gain still to be had by switching to the $\mathcal{O}(m(\log m)^2)$ Driscoll & Healy (1994) fast Legendre transformbut the net speedup would be slight. For accuracy and consistency of the inverse transform, it is important to use a kernel consisting of $(1-x^2)P_j^{(1,1)}(x)$ even though this means the coefficients in the resulting expansion then require inversion of a (symmetric) tridiagonal form. (The basis set for $\widehat{\theta}$ diagonalizes the second derivative operator, not the unit operator.)

In devloping a continuation code for this problem, the analytic Jacobian for the optimal equations was derived and used in the multi-dimensional Newton iteration

[5] In principle the rank one updates of quasi-Newton methods can reduce the latter overhead but our experience of these with spectral methods has not proved encouraging.

scheme. This saved a good deal of cpu time over the alternative finite-difference approximation of the Jacobian matrix. Unfortunately, computing the Jacobian matrix is a particularly laborious exercise in tensor manipulations, and the algebra can be checked against a finite difference approximation. The $k$-derivative of $\mathrm{L}^{-1}$ for instance, is

$$\frac{\mathrm{d}}{\mathrm{dk}}(D^4 - 2k^2D^2 + k^4I)^{-1} = \mathrm{L}^{-1}(-4kD^2 + 4k^3I)\mathrm{L}^{-1}.$$

where the $D^4$ and $D^2$ here represent derivative matrices and $I$ is defined by

$$I_{ij} = \int_{-1}^{1} \mathrm{d}x(1-x^2)^4 P_i^{(2,2)}(x) P_j^{(2,2)}(x).$$

# Chapter 5

# Convection at infinite Prandtl number:
# (II) Conservative bounds

## 5.1 Introduction

While the previous chapters have considered full solutions of the optimal equations for CDH bounding problems, this chapter will look at calculating estimates of optimal bounds by using a family of test functions. Indeed, earlier work at extracting scalings from this method has involved considering fixed form test functions as background profiles. In the seminal papers of Constantin & Doering (1995) Doering & Constantin (1994, 1996), a piecewise linear profile, with constant gradient boundary layer and zero gradient interior, was employed as a test function. Using functional analytic estimates on terms in the spectral constraint conservative upper bounds were derived without the need for numerics. Moreover, the derived scalings were invariably found to be optimal in the case of shear flow (see Busse, 1970; Doering & Constantin, 1994) and several problems in convection. In the problem of convection in a porous media such upper bounds were also found to fit tightly over experimental data (see Otero *et al.*, 2004). In each of these problems a numerical treatment of the spectral constraint and optimisation over the balance parameter was only found to improve the prefactor of the upper bound (see Nicodemus, Grossmann & Holthaus,

1997*a*,*b*).

This simple class of test function (pictured on the left of figure 5.1) have also been applied to the problem of infinite Prandtl number convection as described in the previous chapter. The best pure analytic result for no-slip boundary conditions was found to be $Ra^{2/5}$ (Doering & Constantin, 2001)[1] which was also found to be the case if SC-neutrality is enforced numerically in Otero (2002). These estimates are, however, far from the optimal scaling of $Ra^{1/3}$ (Chan, 1971). Our task in this chapter is to investigate the balances in the optimal equations which the simplest test functions fail to capture. We extend the standard one-parameter test functions to two-parameter functions with variable interior-gradient (pictured in figure 5.1). The method of solution will closely follow the method of solution exemplified by Otero (2002).

The discussion of the variant boundary conditions for stress-free convection will also continue. The only known conservative estimate result for this problem is independent of the Prandtl number. In Doering & Constantin (1996) piecewise linear profiles with an interior slope of +1, and standard constant-slope boundary layer, and simple functional estimates yield a $Ra^{1/2}$ upper bound correct for both no-slip and stress-free conditions. Therefore, the expectation is to calculate an exponent lesser than $\frac{1}{2}$ and therefore closer to optimal.

The chapter will begin with a discourse of the structure of the problem to be solved. Then, following Otero (2002), a determinant condition on a matrix of coefficients will be formulated. A short discussion of the solution programme and the presentation of findings will end the chapter.

## 5.2 Formulation

Bearing in mind that the optimal equations depend only on the slope of the background field $\tau'$, it makes sense to write an expression for $\tau'$ only. A direct consequence of the boundary conditions $\tau(0) = 1$, $\tau(1) = 0$ is

$$\int_0^1 \tau' \mathrm{d}z = -1$$

[1]This result uses only functional analytic inequalities to bound the quadratic functional, however, Constantin & Doering (1999) deduce a logarithmic upper bound of the form $Ra^{1/3}(\log Ra)^{2/3}$ using extra PDE information not related to SC-stability.

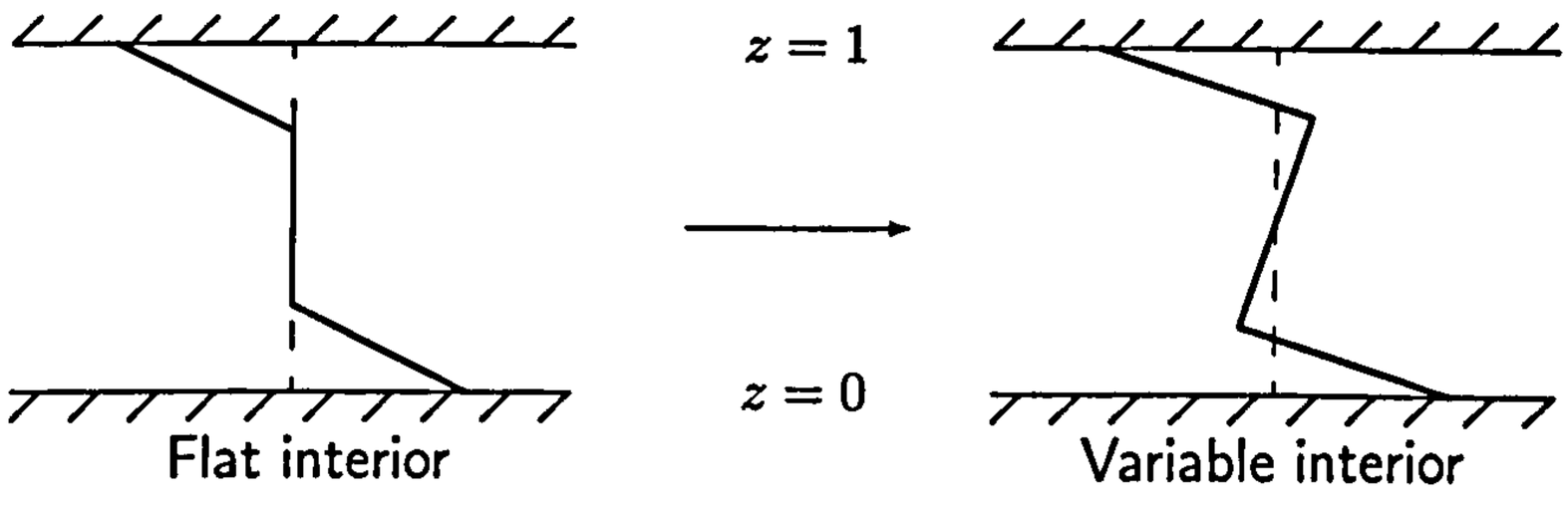


Figure 5.1: Enlarged set of test functions

so that given an interior gradient of $p$, symmetry across the mid-channel (which is at $z = \frac{1}{2}$ in this discussion) and a boundary of thickness $\delta$, the two-parameter test profiles are

$$\tau' = \begin{cases} p - \dfrac{1+p}{2\delta} & \text{for } z \in [0, \delta], \\ p & \text{for } z \in [\delta, 1/2]. \end{cases} \tag{5.1}$$

A sketch of the enlargement of the class of piecewise linear profiles described above is shown in figure 5.1. We assume that the balance parameter has no effect on the scaling of the estimate and set $\lambda = 2$ (this hypothesis will be vindicated in Chapter 6). The conservative estimate of the optimal bound, $Nu \leq \int_0^1 \tau'^2$, is calculated subject to SC-neutrality, as

$$Nu \leq N(\delta, p) := \frac{(1+p)^2}{2\delta} - p(2+p). \tag{5.2}$$

The hope is that the non-negativity of $Q$ in the spectral constraint:

$$Q = \|(D\theta, ik\theta)\|^2 + 2\langle w\theta\tau' \rangle \geq 0 \text{ for any } k \text{ and } \textit{suitable } w,\ \theta.$$

will be enhanced by the inclusion of interior-slope and therefore a larger boundary depth $\delta$ will be admissible, thus decreasing the upper bound. The meaning of *suitable* in the definition of the spectral constraint is contingent on the specific boundary conditions and also the momentum constraint. To recap the boundary conditions are:

$$\begin{aligned} &\text{No-slip} && \theta = w = Dw = q = Dq = 0, \\ &\text{Stress-free} && \theta = w = D^2w = q = D^2q = 0. \end{aligned}$$

Restricting the class of background fields to fixed form test functions necessarily reduces the potency of the bounding procedure over the optimal calculation. A

sub-optimal bound is calculated by selecting a pair $(\delta, p)$ which is SC-stable. In eigenvalue form, SC-stability is a condition on the most positive eigenvalue, denoted by $\overline{\mu}$, of the system:

$$\begin{aligned} 2(D^2 - k^2)\theta - 2w\tau' + Rak^2 q &= \mu\theta, \\ (D^2 - k^2)^2 q + 2\theta\tau' &= 0, \\ (D^2 - k^2)^2 w - Rak^2\theta &= 0. \end{aligned} \tag{5.3}$$

If for any $k \in \mathbb{R}$ we have $\overline{\mu} \leq 0$ then $\tau(z)$ is SC-stable. Profiles which are SC-stable and have $\overline{\mu}(k) = 0$ for some $k$ are said to be SC-neutral. A fact which allows us to restrict attention to the boundary of the admissible set $\{\tau(z) : \overline{\mu}_\tau \leq 0 \quad \forall k \in \mathbb{R}\}$ is the convexity of $Q$ with respect to $\tau'$.

### 5.2.1 Convexity of the admissible set

Let $\tau'(z) = -1 + \phi(y)$ so that $\int_0^1 \phi(z)\mathrm{d}z = 0$ and consider two mean-zero function $\phi_1(z)$ and $\phi_2(z)$ that are both admissible candidates for the spectral constraint. Then

$$\overline{\mu}_{\phi_1} \leq 0 \iff \text{for all } \textit{suitable } w \text{ and } \theta, \quad \|\nabla\theta\|^2 + 2\langle w\theta(\phi_1(z) - 1)\rangle \geq 0$$

and

$$\overline{\mu}_{\phi_2} \leq 0 \iff \text{for all } \textit{suitable } w \text{ and } \theta, \quad \|\nabla\theta\|^2 + 2\langle w\theta(\phi_2(z) - 1)\rangle \geq 0.$$

Now let $0 < a < 1$. Owing to linearity of $\phi$ in the integrals above we see that

$$\|\nabla\theta\|^2 + 2\langle w\theta(a\phi_1(z) + (1-a)\phi_2(z) - 1)\rangle \geq 0 \iff \overline{\mu}_{a\phi_1 + (1-a)\phi_2} \leq 0.$$

Thus the set of admissible functions $\Phi = \{\phi | \overline{\mu}_\phi \leq 0\}$ is convex. In terms of the function space, we need only consider the boundary, $\partial\Phi$, on which $\overline{\mu} = 0$, and seek the minimum distance between the origin and this boundary. The distance function of interest is the Nusselt bound $N(\delta, p)$. It will be assumed that the isospectral surface, $\overline{\mu} = 0$, is smooth and that the minimum is well-defined.

### 5.2.2 Uniformity in $k$

What allows us to write the spectral constraint as a constraint purely on single-mode fields? Thinking back to the original statement of the spectral constraint:

$Q = \|\nabla\theta\|^2 + \lambda\langle w\theta\tau'\rangle \geq 0$ for any $w$ and $\theta$ satisfying the boundary conditions and the momentum equation. If we Fourier expand the fields $w$ and $\theta$ in general we have a multi-mode expansion: $w = \sum_k \mathrm{e}^{\mathrm{i}kx} w_k(z)$ and similarly for $\theta$. Then $Q = \sum_k Q_k$ where

$$Q_k = \|(D\theta_k, \mathrm{i}k\theta_k)\|^2 + \lambda\langle w_k\theta_k\tau'\rangle \geq 0.$$

It is clear that for single-mode fields $Q_k \geq 0 \Rightarrow Q \geq 0$. Given that the spectral constraint must be applied to all fields this means that all single-mode fields must be admissible. Because the boundary conditions and momentum equation are linear no mode mixing occurs and hence all multi-mode fields are admissible fields as $Q = \sum_k Q_k$ and we have already seen that $Q_k \geq 0$. To summarise there is uniformity across $k$:

$$Q \geq 0 \quad \forall w, \theta \iff Q_k \geq 0 \quad \forall k \in \mathbb{R} \text{ and } w(z), \theta(z). \tag{5.4}$$

In actual fact at fixed $Ra$ there is only a finite region $A \subset \mathbb{R}$ for which the the conduction profile is unstable. That is, for $k \notin A$ and $\tau' = -1$ for $0 \leq z \leq 1$ the least damped eigenvalue is always negative, $\overline{\mu} < 0$. This can be attributed to the potency of the term $k^2\|\theta\|^2$ in $Q_k$ for high values of $k$. Of course, the high $k$-cutoff, which we will denote $k^+$, increases with increasing $Ra$.

### 5.2.3 Seeking $\delta_{opt}$

Our intention now is, for fixed $Ra$ and $p$, to find the optimal $\delta$ which both minimises $N$ and ensures the test function is SC-stable. Since $N(\delta, p)$ is monotonic in $\delta$ it suffices to find the maximum $\delta$. A further minimisation of $N$ over the secondary parameter $p$ will be performed at the last step.

The convexity property on $\Phi$ described in Section (5.2.1) implies that for any $k < k^+$ there is a unique $\delta$, $\tilde{\delta}$ say, for which the most positive eigenvalue is zero, $\overline{\mu} = 0$, and for lesser $\delta$ it is negative, $\overline{\mu} > 0$. Finding $\delta$ involves solving system (5.3) with $\mu = 0$. The optimal boundary layer thickness is then

$$\delta_{opt} = \min_{k<k^+} \tilde{\delta}. \tag{5.5}$$

Owing to the monotonicity of $N$ with $\delta$ this minimisation statement can also be written as

$$N_1(p) = \max_{k<k^+} N(\tilde{\delta}, p). \tag{5.6}$$

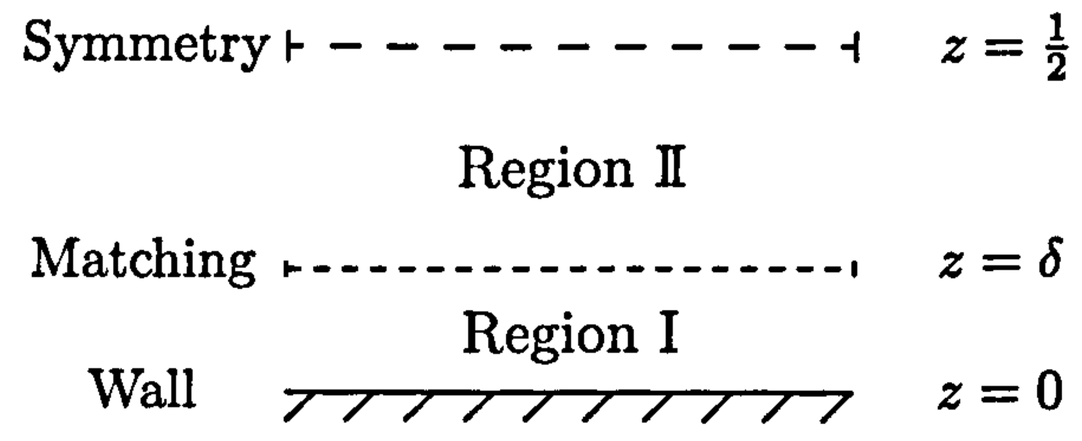


Figure 5.2: Regions of constant $\tau'$ for the two-parameter test functions

Noting that $\tilde{\delta}$ varies with $p$ the final step in the optimisation is a minimisation over the interior gradient. The resulting bound is then

$$Nu \leq \min_{p \in \mathbb{R}} \max_{k<k^+} N(\tilde{\delta}, p). \tag{5.7}$$

The case $p = 0$ is the one-parameter family of solution used by Otero (2002) to extract a $Ra^{2/5}$ scaling. It is hoped that inclusion of positive interior slope will help the positivity of $Q$ such that a larger $\delta_{opt}$ will be valid, thereby improving the scaling of the upper bound.

Solving this problem numerically is a much simpler task than solving the optimal problem owing to the fact that a semi-analytic solution can be sought when $\tau'$ is piecewise constant. The next section deals with deriving the complex valued functions which solve system (5.3) in the two regions (boundary and interior) and posing a determinant condition on a matrix of coefficients.

## 5.3 Solution technique

The method to be discussed below is the best of the range of possible numerical solutions available. Other techniques attempted include a two domain spectral element attack and a finite difference method using shooting parameters for matching boundary and mid-channel conditions. After a little experimentation, it is clear that the best procedure is the reduction of the problem to a determinant condition on a $10 \times 10$ matrix of coefficients, given the speed to code and the abundance of high quality numerical routines for evaluating determinants, eigenvalues and to factor matrices.

So let us begin by considering system (5.3) with $\mu = 0$ and piecewise constant $\tau'$. Within the regions of constant $\tau'$ shown in figure 5.2, the system is a set of linear, constant-coefficient differential equations which can be solved with complex exponentials. One can easily show that the system is tenth order in $w$ and therefore that the solution will be a linear combination of ten exponentials. Moreover, by substituting

$$[\theta, w, q] = [a, b, c]\, \mathrm{e}^{\alpha z}$$

into (5.3) and fixing $\tau'$, the subsequent auxiliary equation reveals that the roots are: two real roots of multiplicity two ($\alpha = \pm k$), and six complex roots of $(\alpha^2 - k^2)^3 = 2Rak^2\tau'$.

All of the variables can be expressed in terms of $w$ so we base our description of the particular solutions associated to each root on $w$ and note that: (1) in the repeated roots case the particular solutions have

$$\theta(z) = 0 \quad \text{and} \quad q(z) = \frac{2\tau'}{Rak^2} w(z), \tag{5.8}$$

and (2) in the complex roots case the particular solutions have

$$\theta(z) = \frac{(\alpha^2 - k^2)^2}{Rak^2} w(z) \quad \text{and} \quad q(z) = -\frac{2\tau'}{Rak^2} w(z). \tag{5.9}$$

Note the difference in sign between the two expressions for $q(z)$. Now define the solution in Region I as

$$w_1(z) = w_{11}(z) + w_{12}(z)$$

where $w_{11}$ is the part of the solution associated to the repeated roots and $w_{12}$ to the complex roots, and similarly for Region II. In Region I we can use the boundary conditions to solve for half of the coefficients and in Region II we assume even symmetry[2] in $w$,

$$Dw = D^3 w = 0 \quad at \quad z = \tfrac{1}{2},$$

to also reduce the coefficients in that region by half.

The coefficients of the solution will be denoted by $c_1, \ldots, c_{10}$. Coefficients $c_1, c_2, c_3$ will be associated to the complex roots and $c_4, c_5$ to the real roots in Region I. While $c_6, c_7, c_8$ will be associated to the complex roots and $c_9, c_{10}$ to the real roots in Region II.

[2]For a discussion of symmetry of the ground-state eigenfunction and why even symmetry is more potent than odd see Appendix C of Otero (2002).

### 5.3.1 Real roots

The solutions in Region II are independent of boundary condition, thus $w_{21}$ and $w_{22}$ are the same for no-slip and stress-free. By insisting on even symmetry we find that

$$w_{21} = c_9 \cosh(k\tilde{z}) + c_{10}\tilde{z}\sinh(k\tilde{z}). \tag{5.10}$$

where $\tilde{z} = z - \frac{1}{2}$. For no-slip boundary condition the repeated-roots Region I solution is

$$w_{11} = c_4(\sinh(kz) - kze^{-kz}) + c_5 z \sinh(kz), \tag{5.11}$$

while for stress-free boundary conditions, this is

$$w_{11} = c_4 \sinh(kz) + c_5 z \cosh(kz). \tag{5.12}$$

### 5.3.2 Complex roots

By making the transformation $\beta^2 = k^2\alpha^2$ the complex roots can be written down more explicitly as

$$\beta^2 - 1 = \begin{cases} \sqrt[3]{\frac{2|\tau'|Ra}{k^4}}e^{i(2j+1)\pi/3} & \text{for } \tau' < 0, \\ \\ \sqrt[3]{\frac{2|\tau'|Ra}{k^4}}e^{i(2j)\pi/3} & \text{for } \tau' > 0, \end{cases} \tag{5.13}$$

where j=1,2,3. The positive square root is selected when finding $\beta$ in expression (5.13). We use $\alpha_1, \alpha_2, \alpha_3$ to denote the Region I complex roots and $\alpha_6, \alpha_7, \alpha_8$ to denote the Region II complex roots.

The Region II part of the solution is for either boundary condition

$$w_{22} = c_6 \cosh(\alpha_6\tilde{z}) + c_7 \cosh(\alpha_7\tilde{z}) + c_8 \cosh(\alpha_8\tilde{z}). \tag{5.14}$$

For stress-free boundary conditions, the Region I solution is

$$w_{12} = c_1 \sinh(\alpha_1 z) + c_2 \sinh(\alpha_2 z) + c_3 \sinh(\alpha_3 z), \tag{5.15}$$

while for no-slip this part of the solution is rather unwieldy

$$\begin{aligned} w_{12} = {} & c_1(\sinh(\alpha_1 z) - \frac{\alpha_1}{\alpha_3}\sinh(\alpha_3 z)) + c_2(\sinh(\alpha_2 z) - \frac{\alpha_2}{\alpha_3}\sinh(\alpha_3 z)) \\ & + c_3(\cosh(\alpha_1 z) - \frac{(f_1 - f_3)}{(f_2 - f_3)}\cosh\alpha_2 z + \frac{(f_1 - f_2)}{(f_2 - f_3)}\cosh\alpha_3 z) \end{aligned} \tag{5.16}$$

but we have made the expression slightly tidier by setting $f_i = (\alpha_i^2 - k^2)^2$, for $i = 1, 2, 3$. Putting everything together we have a solution for $w$ in terms of ten coefficients $c_1, \ldots, c_{10}$ and six complex roots. Region I and II solutions for $\theta(z)$ and $q(z)$ can be constructed using the rules in expression (5.8) and (5.9).

### 5.3.3 Matching conditions

The job of constructing the semi-analytic solutions is finished. It only remains to specify ten jump conditions to match the solution in Region I to that in Region II:

$$\begin{aligned} [\theta]_\delta &= [D\theta]_\delta = 0 \\ [w]_\delta &= [Dw]_\delta = [D^2 w]_\delta = [D^3 w]_\delta = 0 \\ [q]_\delta &= [Dq]_\delta = [D^2 q]_\delta = [D^3 q]_\delta = 0 \end{aligned} \tag{5.17}$$

where the jump across $z = \delta$ has been denoted by $[f]_\delta = f_2(\delta) - f_1(\delta)$. Each of these jump conditions depend linearly on all of the coefficients and hence (5.17) may be written in matrix form:

$$\mathbf{M}\,\mathbf{c} = \mathbf{0}, \qquad \text{for } \mathbf{c} = [c_1, \ldots, c_{10}]^T$$

### 5.3.4 Determinant method

Section (5.2.3) described how to obtain a conservative upper bound from these test functions. How does that correspond to this solution method? At fixed $Ra$, $p$ and $k$ a zero of the determinant, at $\delta = \breve{\delta}$ say, implies the existence of a solution to equations (5.3) with $\mu = 0$. If $\breve{\delta}$ is the smallest $\delta$ for which $\det \mathbf{M} = 0$ then $\breve{\delta} = \tilde{\delta}$ and therefore the least damped eigenvalue is zero ($\overline{\mu} = 0$). The upshot of this is that equation (5.5) can be restated as a determinant condition:

$$\delta_{opt} = \min_{k<k^+} \{\delta : \det \mathbf{M} = 0\}. \tag{5.18}$$

and, likewise, equations (5.6) and (5.7) can be rewritten replacing $\overline{\mu} = 0$ with $\det \mathbf{M} = 0$. The method of solution is best represented by the mini-max problem for the upper bound:

$$Nu \leq \min_{p \in \mathbb{R}} \max_{k<k^+} \{N(\delta) : \delta \text{ smallest s.t. } \det \mathbf{M} = 0\} \tag{5.19}$$

For fixed $Ra$ the primary task is to locate $\delta_{opt}$ the global maximum of $\tilde{\delta}$ (for which $\det \mathbf{M}$ and its first derivative are both zero), and then to follow this point by continuation. A secondary minimisation over the interior gradient $p$ is also included in the continuation as a subsidiary Newton iteration loop. Therefore, beginning at low $Ra$ the optimal point can be traced smoothly[3] in $Ra$ up to the asymptotic regime at low cost. The subtlety here is that row and column operations must be applied to $\mathbf{M}$ in order to scale out all of the explicit $Ra$-dependence to facilitate a solution to high $Ra$ with only double precision computer arithmetic. The problem of resolution at high $Ra$ is not one of dynamical range of terms but of cancellation of similarly sized terms. At about $Ra = 10^{20}$ double precision arithmetic begins to fail and multiple-precision numerical techniques are then required to move past this point.

An attempt was made to extract the limiting exponent by a symbolic determinate, with various levels of truncation of the entries of $\mathbf{M}$. An expansion of the trigonometric terms out to $\delta^3$ makes the determinant vanish identically, so that a nontrivial determinant expansion must keep terms at least one degree higher. Unfortunately, doing so leads to so complex an algebraic set of manipulations we have not been able to distill from this the essence of the balance determination. This supports the notion that the numerical solution should become ill-resolved due to cancellation of terms of moderate size.

## 5.4 Results

As we proceed to discuss the results of the computation it will be helpful to define some notation. Optimal parameters will henceforth be denoted by subscript *opt*. A polynomial dependence for the upper bound and the wavenumber on $Ra$ will be assumed, so $N_{opt} \sim Ra^{\gamma_1}$ and $k_{opt} \sim Ra^{\gamma_2}$. The exponents $\gamma_1$ and $\gamma_2$ will be calculated locally be evaluating $\mathrm{dlog}(\cdot)/\mathrm{dlog}(Ra)$ pointwise.

Because $\lambda$ is fixed at 2, the optimal test functions bifurcates from the conduction profile at $\frac{1}{2}Ra_c$. In the next paragraph the behaviour of the optimal test functions close to bifurcation will be discussed. Later the asymptotic findings for no-slip and stress-free boundary conditions will be studied separately. At the end of this section

[3]The validity of this smoothness assumption will be established *ex post facto*.

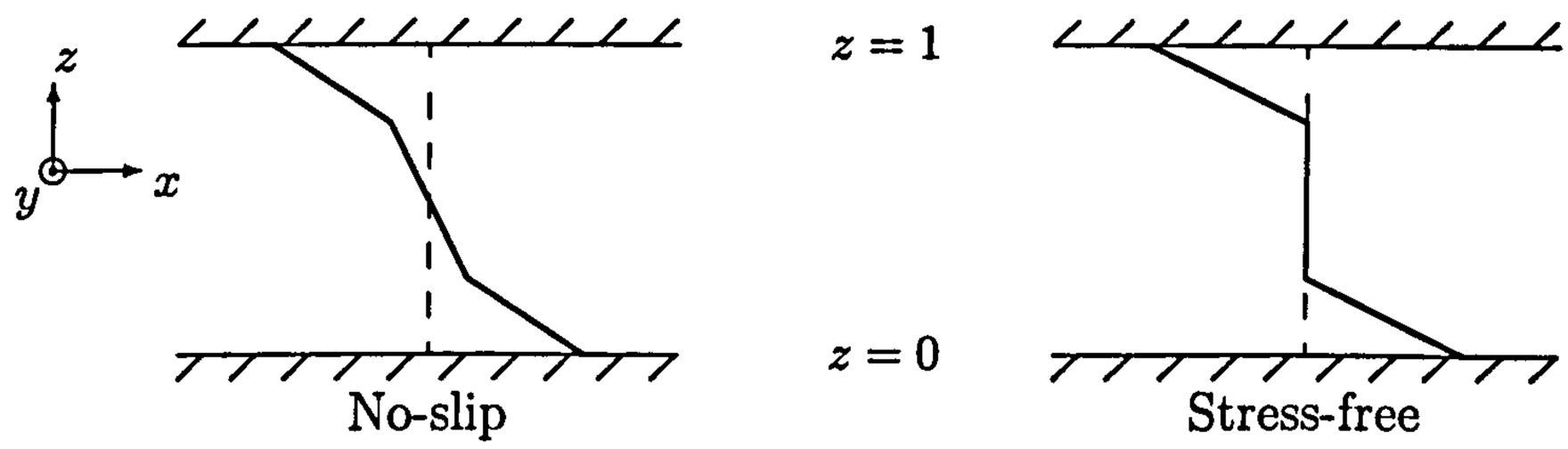


Figure 5.3: The form of the optimal test function at low $Ra$ ($10^2 - 10^3$) for no-slip and stress-free boundary conditions.

supplementary evidence will be presented in order to confirm the validity of the numerics and then comparison will be made between the test function results and the optimal solutions calculated in Chapter 4.

### 5.4.1 Low $Ra$ behaviour

A smooth transition from the conduction profile ($\tau' = -1$) to the path of the optimal solution through the $(\delta, p)$-family can occur in two ways. Either the interior of the function opens up a negative gradient smoothly connecting back to $-1$ at the bifurcation point or an interior with zero gradient emerges out of the bifurcation. The two types of behaviour are pictured in figure 5.3. Our calculations show that in the no-slip case the former scenario leads to the smallest upper bound on $Nu$, while in the stress-free case the smaller upper bound emerges from the latter scenario.

### 5.4.2 No-slip scalings

Recall that the objective in extending the test function approach of Otero (2002) to a $(\delta, p)$-family was to bring into correspondence the conservative bound method, for which the best no-slip bound scales like $Ra^{2/5}$, with the optimal scaling of $Ra^{1/3}$ and in so doing reveal what particular feature of the background field is critical to the optimal calculation. We will find that the 'optimal features' of $\tau(z)$ can not be found using the $(\delta, p)$-family of test functions. The scaling of the upper bound *is* improved to $Ra^{7/20}$ but it still removed from the optimal scaling of $Ra^{1/3}$.

Figure 5.4 shows the local exponent $\gamma_1$ in $N = Ra^{\gamma_1}$ and, as an inset plot, the rate of convergence to 7/20 as $Ra \to \infty$. Note that this convergence is extremely slow

and that even using multiple-precision numerics there is still only three decimal place accuracy at $Ra = 10^{30}$. The optimal interior gradient settles to a positive value, shown in figure 5.6, and the behaviour of the optimal wavenumber is $k \sim Ra^{1/4}$, shown in figure 5.5, which is identical to the behaviour of the 1-$k$ solution of Chapter 4. Since convergence is very slow we have used Shanks extrapolation[4] to resolve the limiting value of $p_{opt}$.

[4]We iterate the vector of $p_{opt}$ data, which is equi-spaced in $\log Ra$, using the Shanks transform $S'_n = S_n - (S_n - S_{n-1})^2/(S_n - 2S_{n-1} + S_{n-2})$.

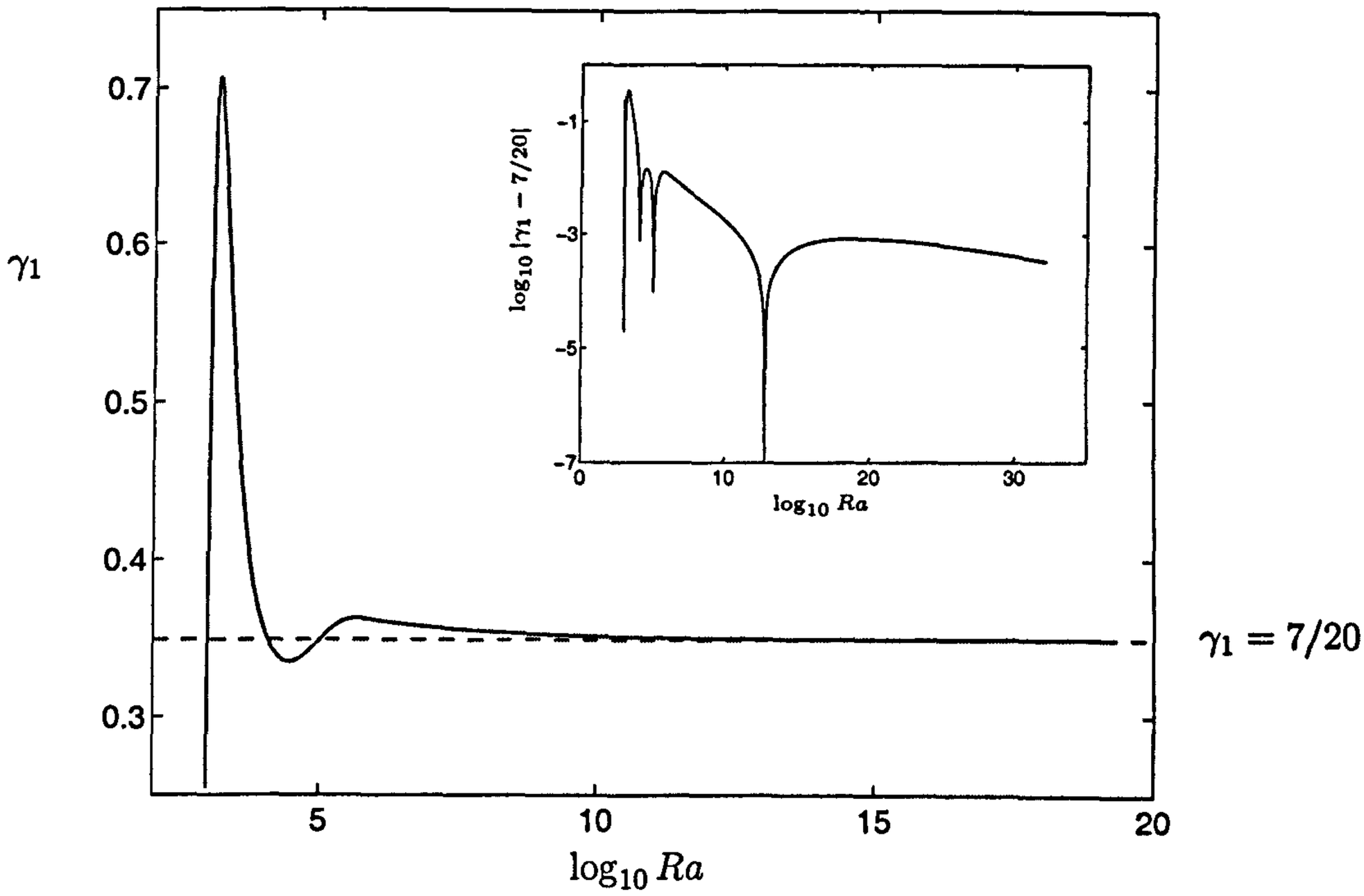


Figure 5.4: [No-slip] The exponent $\gamma_1$ of the upper bound $N_{opt}$ with a limiting value of 7/20. The inset plot shows the residual of the local exponent and 7/20 calculated using multiple-precision numerics.

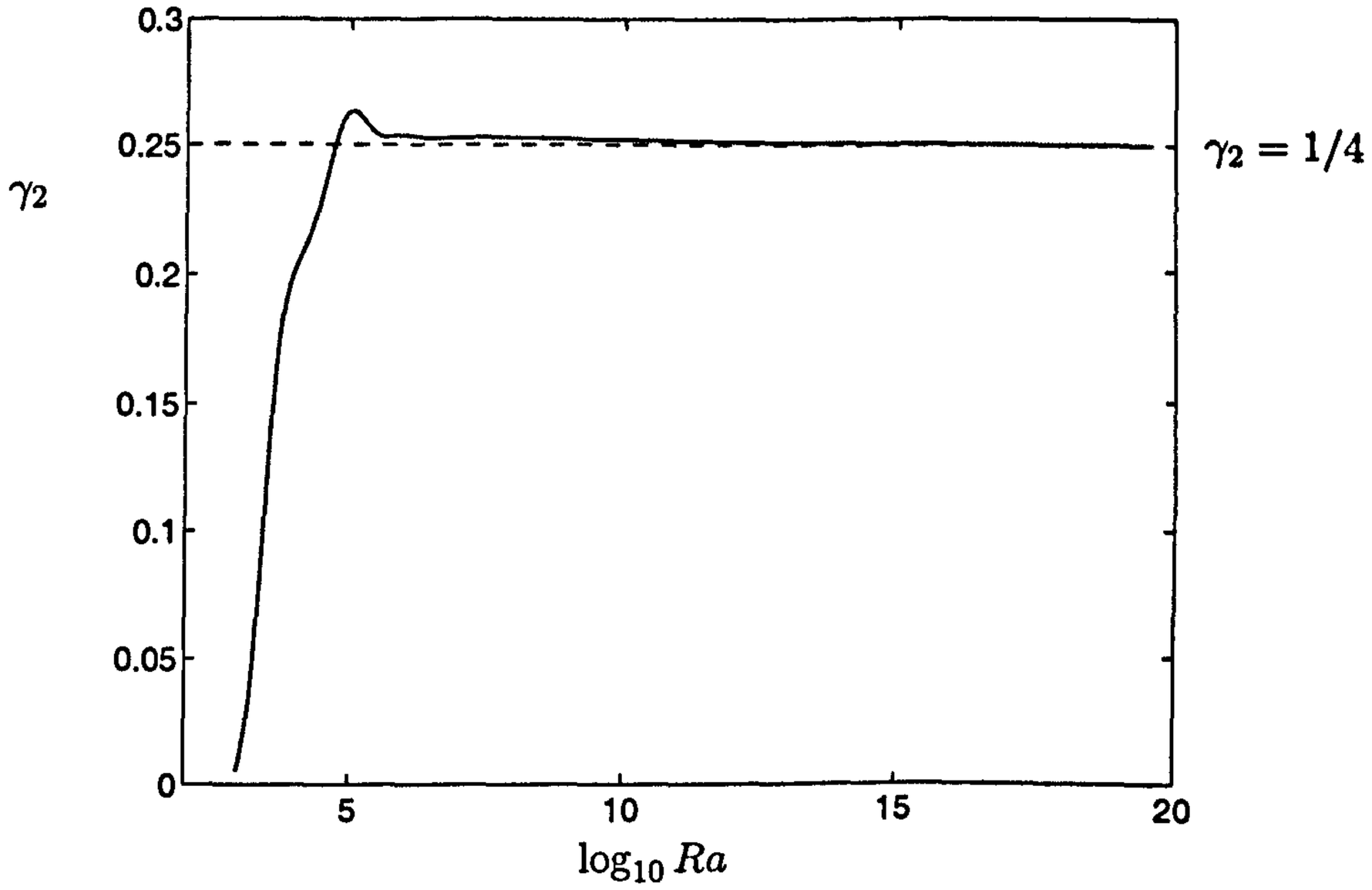


Figure 5.5: [No-slip] The exponent $\gamma_2$ for the optimal wavenumber $k_{opt}$

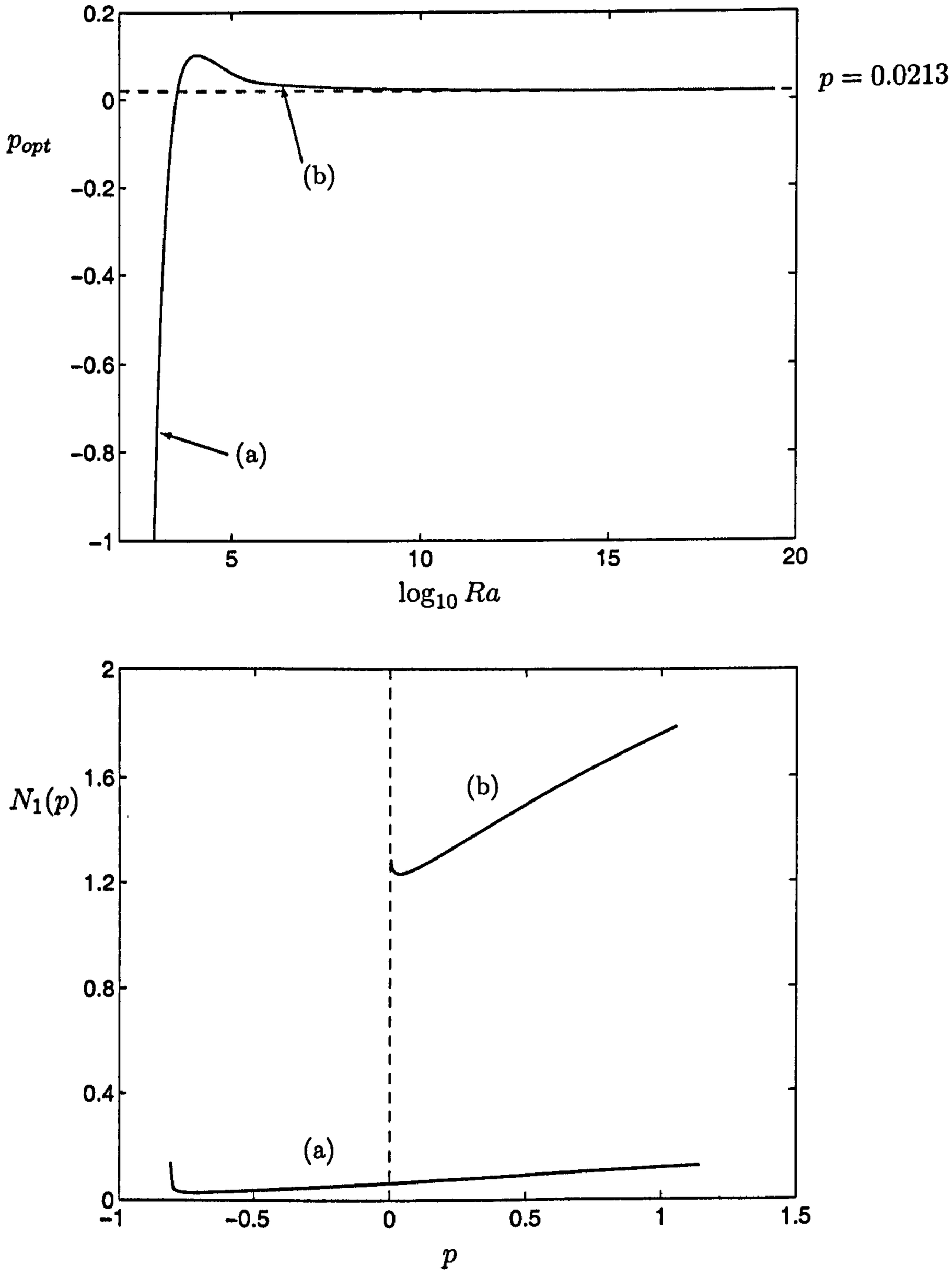


Figure 5.6: [No-slip] The optimal interior gradient with a limiting value of $p = 0.0213$. Two particular points in $Ra$ have been selected for comparison of the value of $N_1$ as a function of $p$.

### 5.4.3 Stress-free scalings

Ironically, although the multi-$k$ analysis of the optimal problem for stress-free boundary conditions is rather non-standard (as illustrated in Chapter 4), the computation of the conservative bound was easier than the equivalent calculation for no-slip boundary conditions. Indeed, in figure 5.7 the convergence to a limiting exponent of 5/12 is considerably faster than for no-slip and the resolution required to follow the solution to $Ra = 10^{35}$ was 32 digits (quad-precision) compared to 96 digits ('duodecuple'-precision) for no-slip.

In figure 5.8 the optimal interior-gradient is shown to tend to a limiting value of $p = 0.103$. Also pictured is the small region of $Ra$ past $Ra = \frac{1}{2}Ra_c$ where a zero-gradient interior is favoured before a positive interior-gradient emerges. This is evident from the plot of $N_1(p)$ where a non-trivial minimum is observed in curve $(b)$ but not curve $(a)$. The optimal wavenumber, shown in figure 5.9, is seen to scale like $Ra^{1/4}$ in common with no-slip.

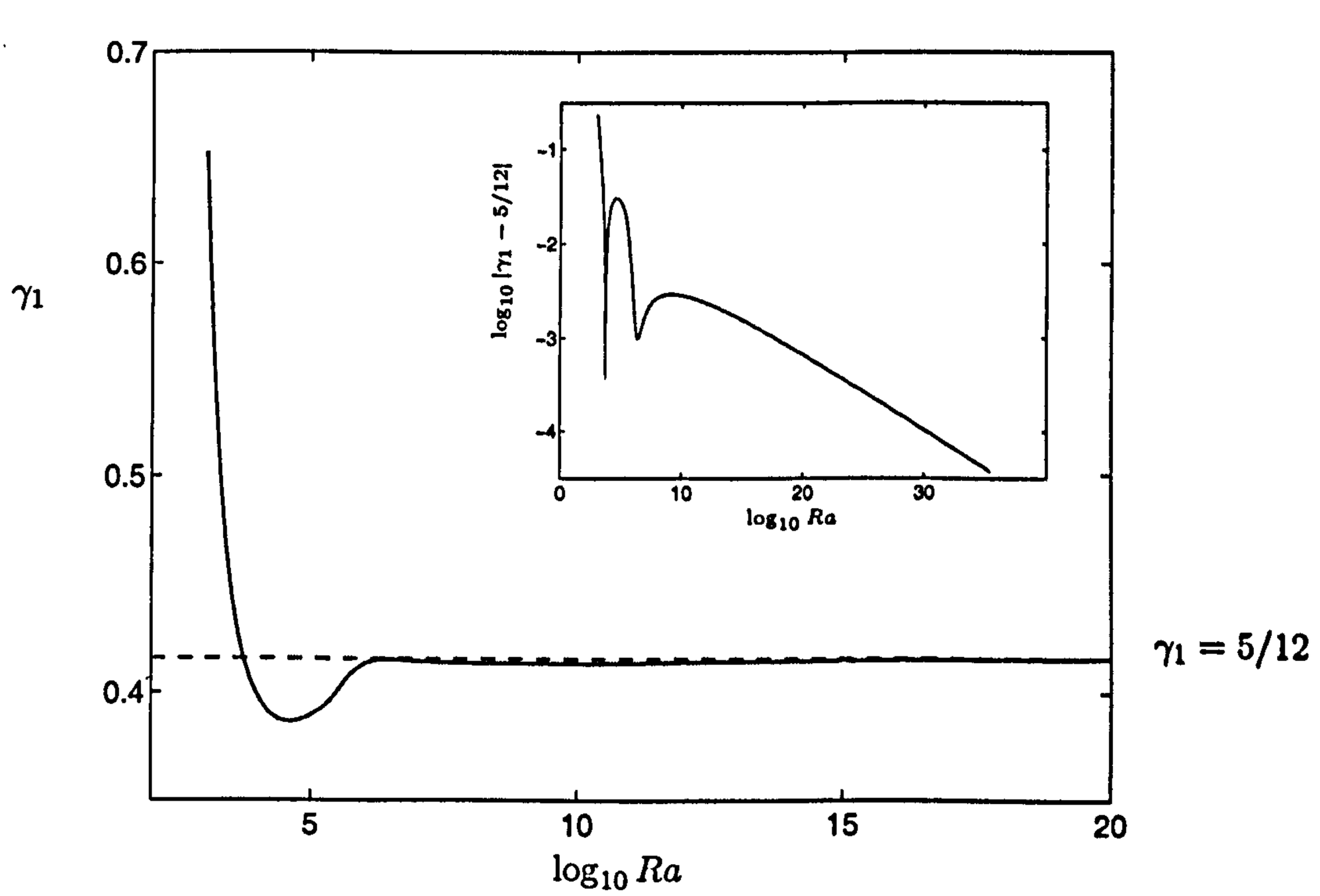


Figure 5.7: [Stress-free] The exponent $\gamma_1$ of the upper bound with a limiting value of 5/12. The inset plot shows the residual of the local exponent and 5/12 calculated using multiple-precision numerics.

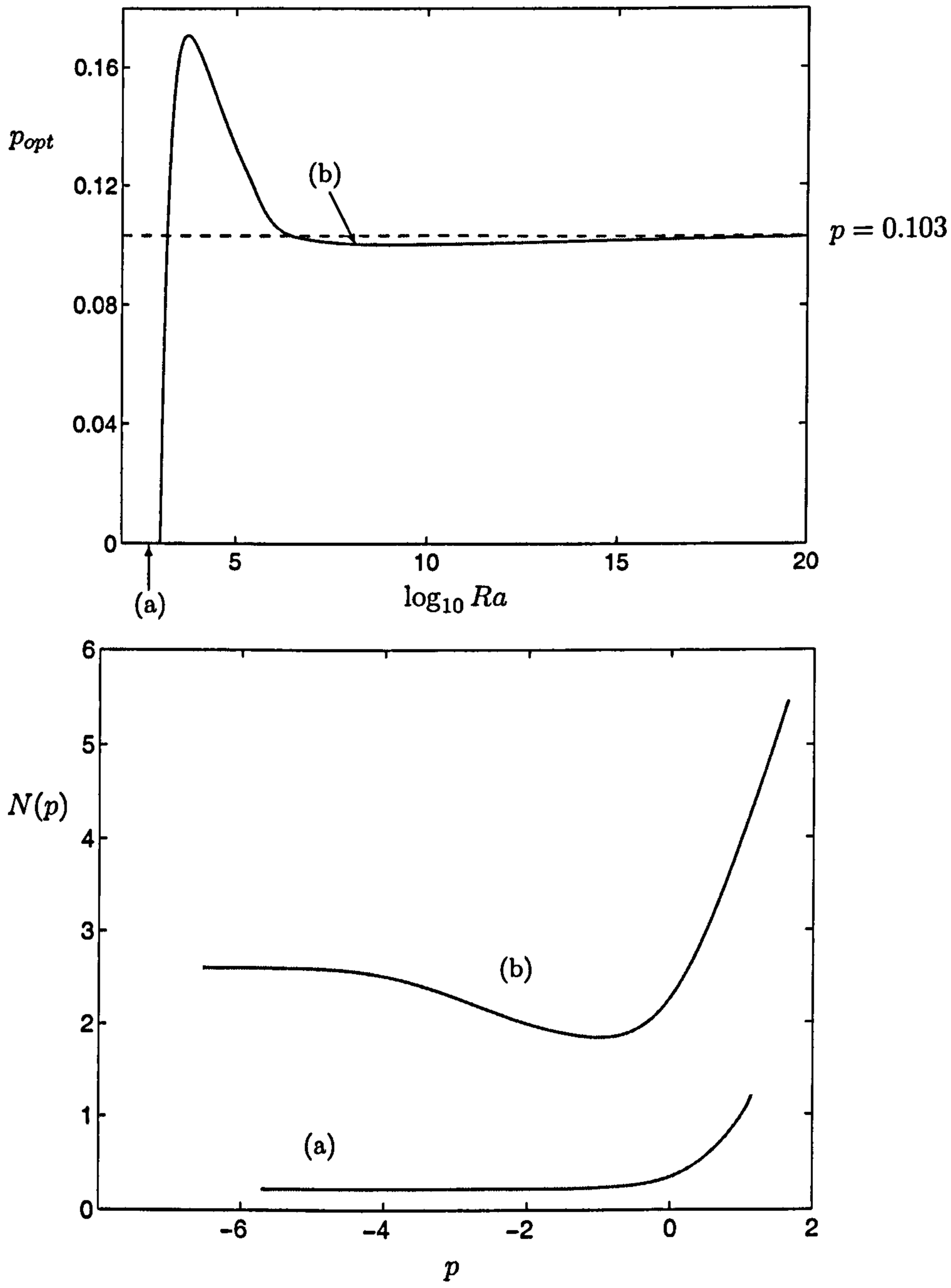


Figure 5.8: The optimal interior gradient with a limiting value of $p = 0.103$. Two particular points in $Ra$ have been selected for comparison of the value of $N_1$ as a function of $p$.

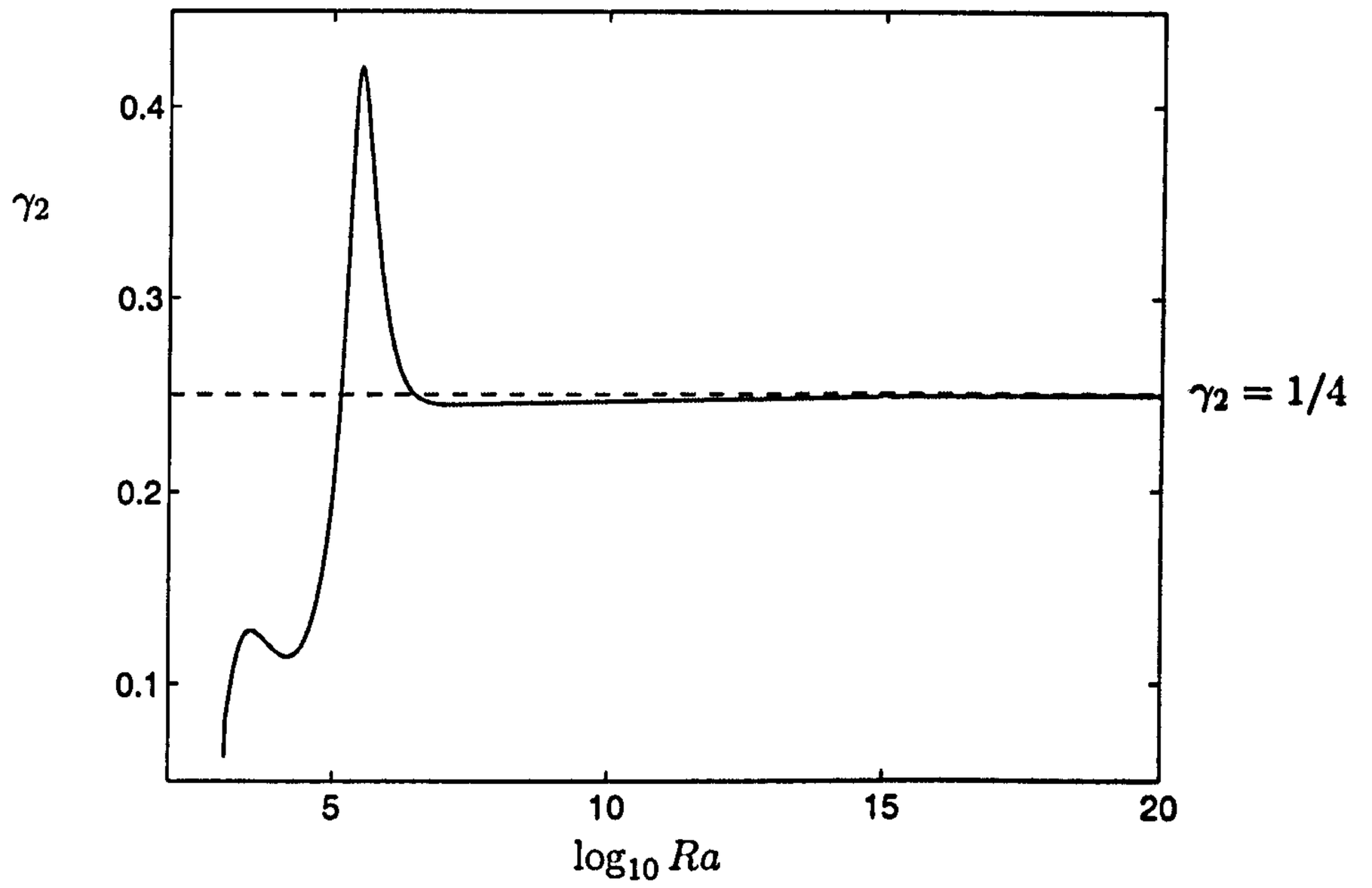


Figure 5.9: [Stress-free] The exponent $\gamma_2$ for the optimal wavenumber $k_{opt}$

### 5.4.4 Consistent numerics

Although in principle the determinant method of solution is the most efficient (memory and cpu-time wise), the correspondence with a method which directly calculates the spectrum of the spectral constraint eigenvalue problem is not entirely clear without a couple of subsidiary checks. Two problems may arise during computation. Firstly, if there is a discontinuity in the slope of the envelope of the eigenvalues due to crossing of eigenvalues the method outlined here may not sense the change in the highest eigenvalue. This has been investigated by plotting the value of the determinant for $\delta$ less than the contested $\delta_{opt}$ at fixed $p$, $k$, and $Ra$. It was found that the determinant increased in magnitude in an unbounded manner and the conclusion was that no other $\delta$ made $\det \mathbf{M}$ zero and hence to $\delta_{opt}$ there corresponds a zero of the lowest eigenvalue.

The second possible anomalous behaviour of this method is the possibility of multiple maxima in the envelope of eigenvalues associated to the spectral constraint. This would correspond to a 1-$k$ solution becoming multi-$k$ as is seen in the optimal solution and also reported by Nicodemus *et al.* (1997*b*) when using two-parameter piecewise quadratic test functions to calculate a conservative bound in the shear flow problem. Of course, a new maximum of the spectral constraint eigenvalue problem would also be accompanied by a new maximum in $N(\tilde{\delta}, p)$ over $k$. Tracking the global maximum amongst several local maxima would obviously be a more sensitive procedure than that discussed in this Chapter. In fact, for both boundary conditions the graph of $N(\tilde{\delta}, p)$ for a relatively high value of $Ra$ shows that the solutions are manifestly 1-$k$ (see figure 5.10). Only a single maximum between zero and the cutoff point $k^+$ is evident in both cases.

These two subsidiary tests certify that $N_{opt}(Ra)$ is indeed a true upper bound on the Nusselt number of the flow.

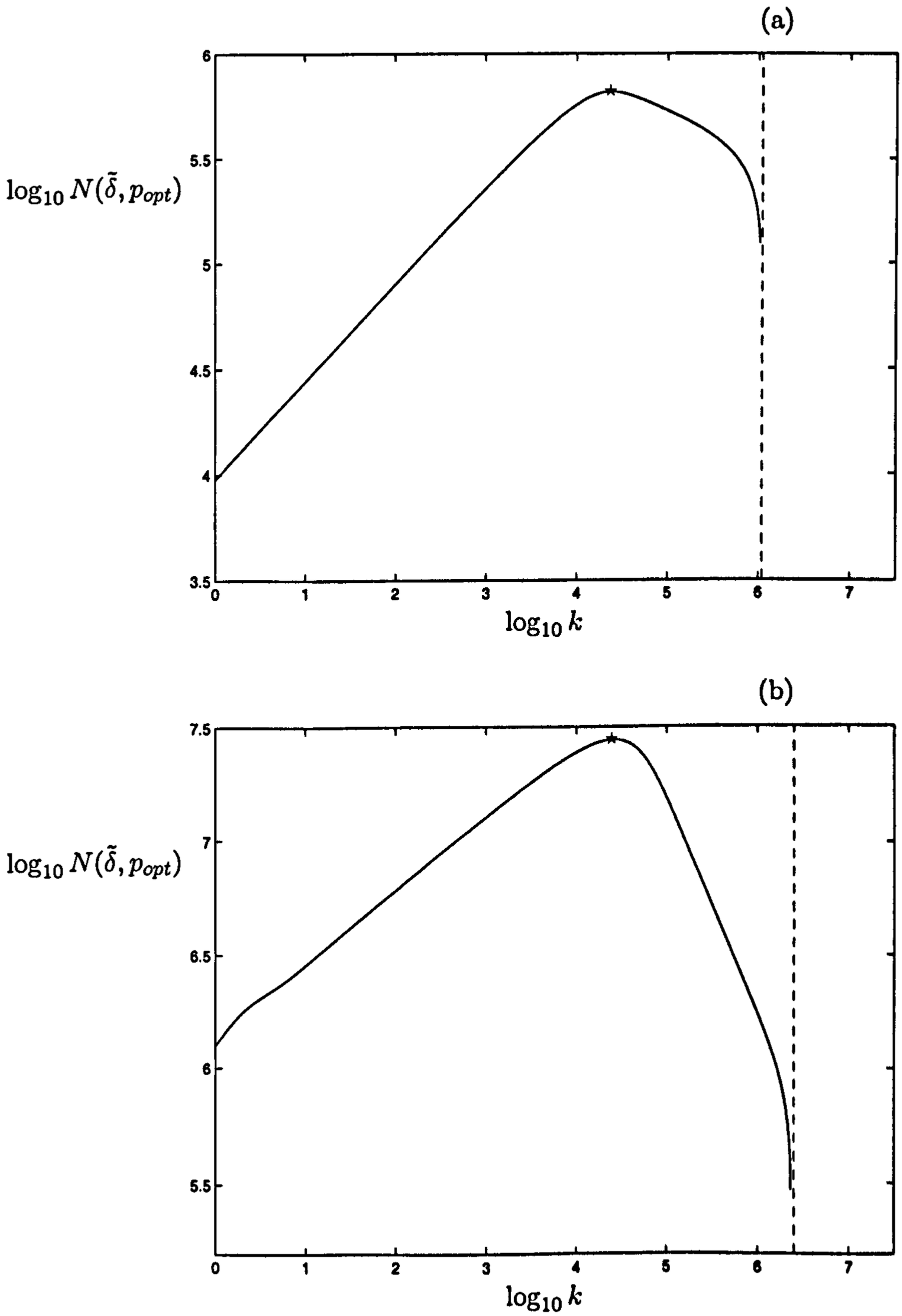


Figure 5.10: Plot of $N$ as a function of $k$ for fixed $p = p_{opt}$ and $Ra$, prior to maximisation over $k$ to find the optimal boundary layer thickness $\delta_{opt}$ (see section 5.3.4). Frame $(a)$ is for no-slip conditions at $Ra = 10^{19}$ and (b) for stress-free conditions at $Ra = 10^{20}$. Dotted lines represent the cutoff value $k^+$ past which conduction state is always stable. The starred points represent the maximum and hence the optimal values of $k$ and $\delta$ which yield the upper bound on $Nu$.

### 5.4.5 Comparison with optimal profiles

In figures 5.11 and 5.13 we compare and contrast the form of the background field, $\tau(z)$, for optimal solutions taken from Chapter 4 with the optimal $(\delta, p)$-functions at the same $Ra$. Are the $(\delta, p)$-family an adequate approximation to the ideal? We will try to answer this question by comparing two views of the background field as shown in figure 5.11. Remember that the mid-channel is located at $z = 1/2$ and that $\tau(0) = 1$. In figures 5.12 and 5.13 the left plot shows the closeness of fit for the interior of the slope and the right plot shows the boundary-layer fit. Their axes limits correspond to the size of the slender dashed boxes in figure 5.11.

The comparison of depth of boundary layer seems adequate for both boundary conditions. For stress-free, the interior slope is very flat across the channel and is therefore quite well approximated by the test function. This would suggest that for stress-free the $(\delta, p)$-family have captured the salient features of the optimal background field and perhaps that the optimal asymptotic scaling has been attained. For no-slip, the story is not at all similar for the interior approximation. The optimal background has more prominent over-shoot than stress-free and the interior slope is relatively insignificant, and the $(\delta, p)$-family fails to capture this irregular shape.

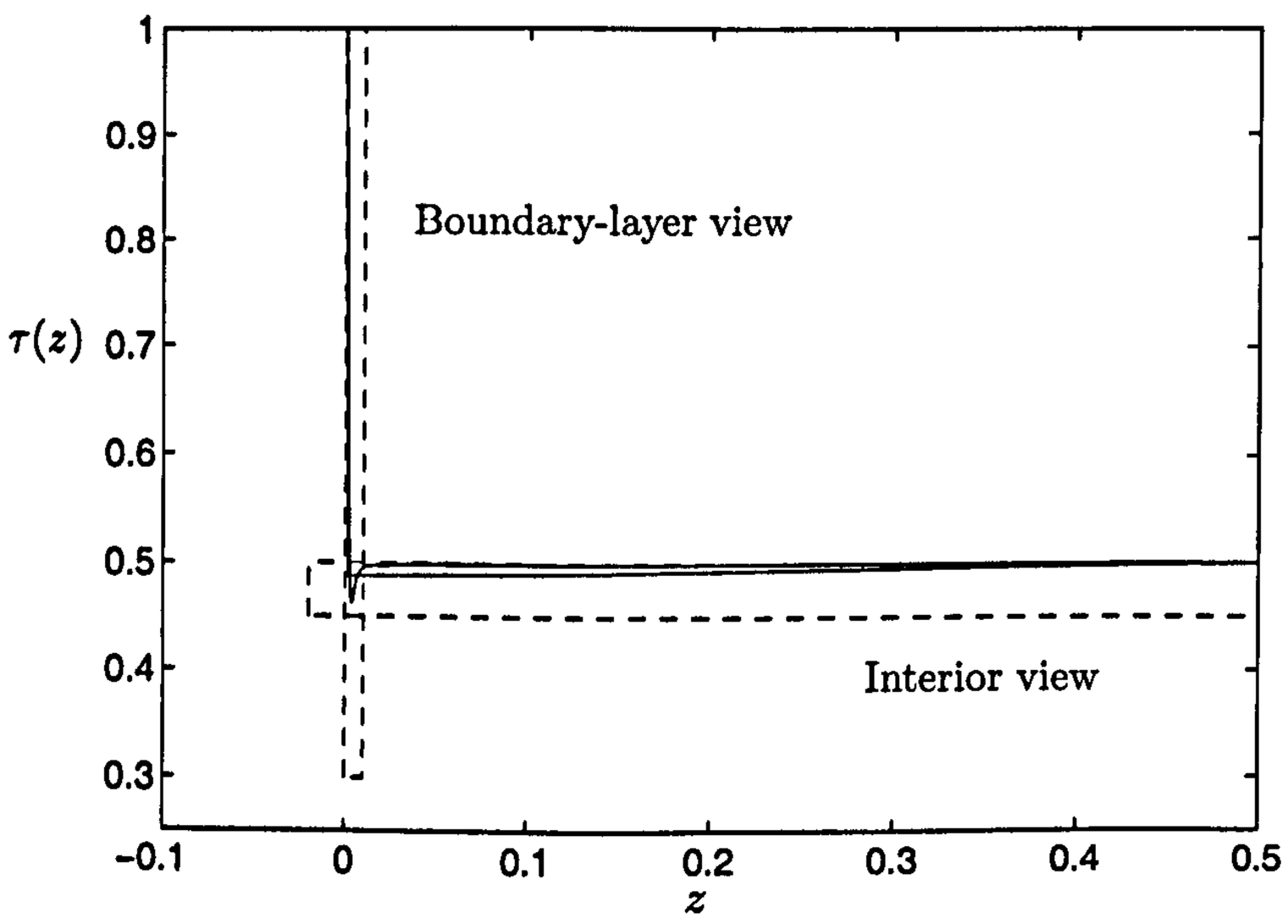


Figure 5.11: Specifying two views of the background field.

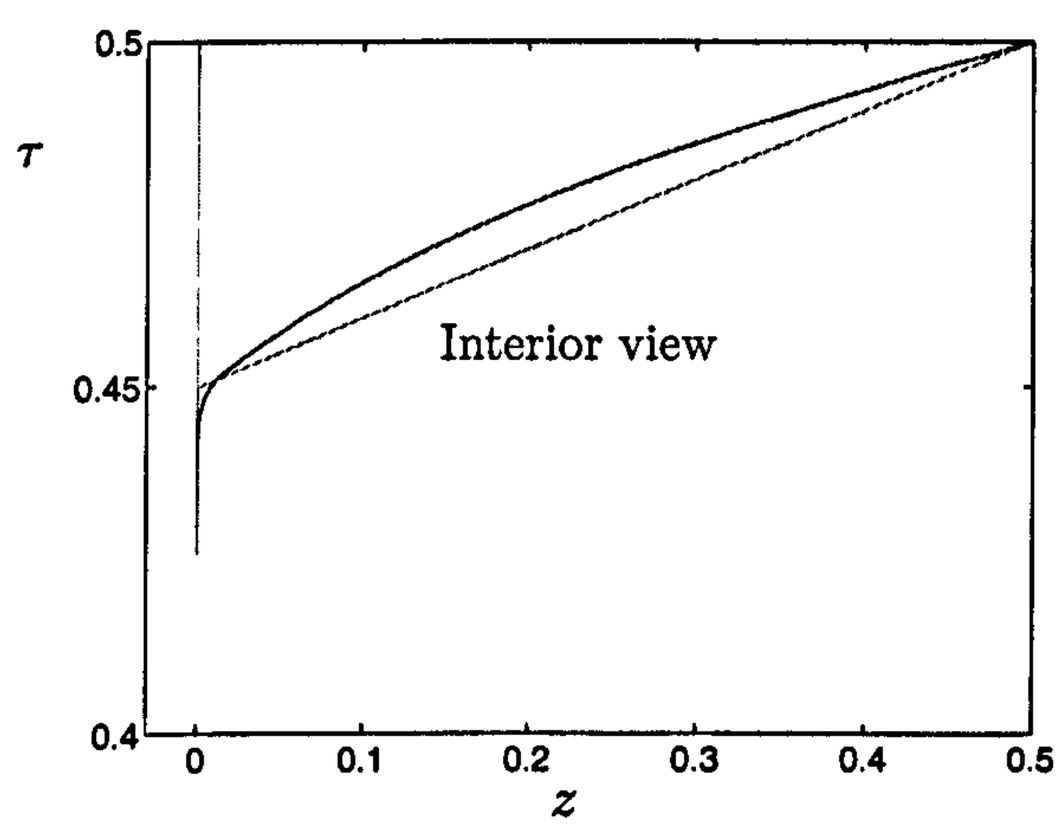


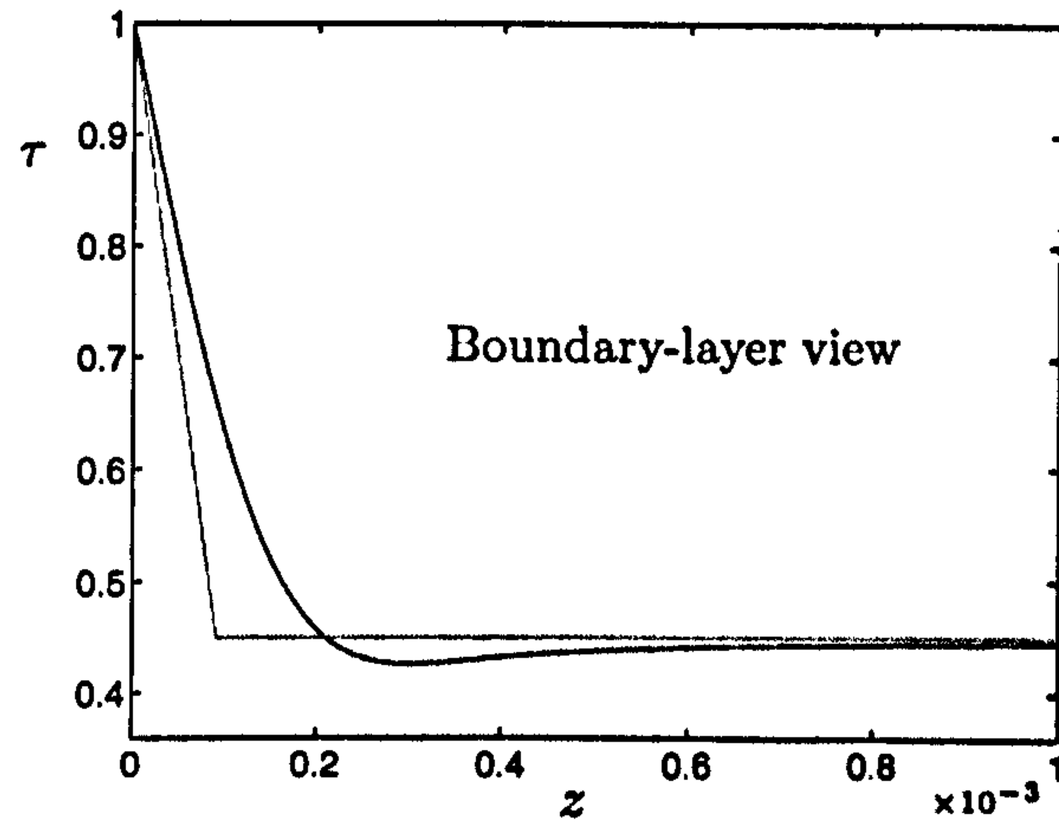


Figure 5.12: Comparing the stress-free optimal solution with the test function at $Ra = 10^{11}$. At this value of $Ra$ the optimal solution is 3-$k$.

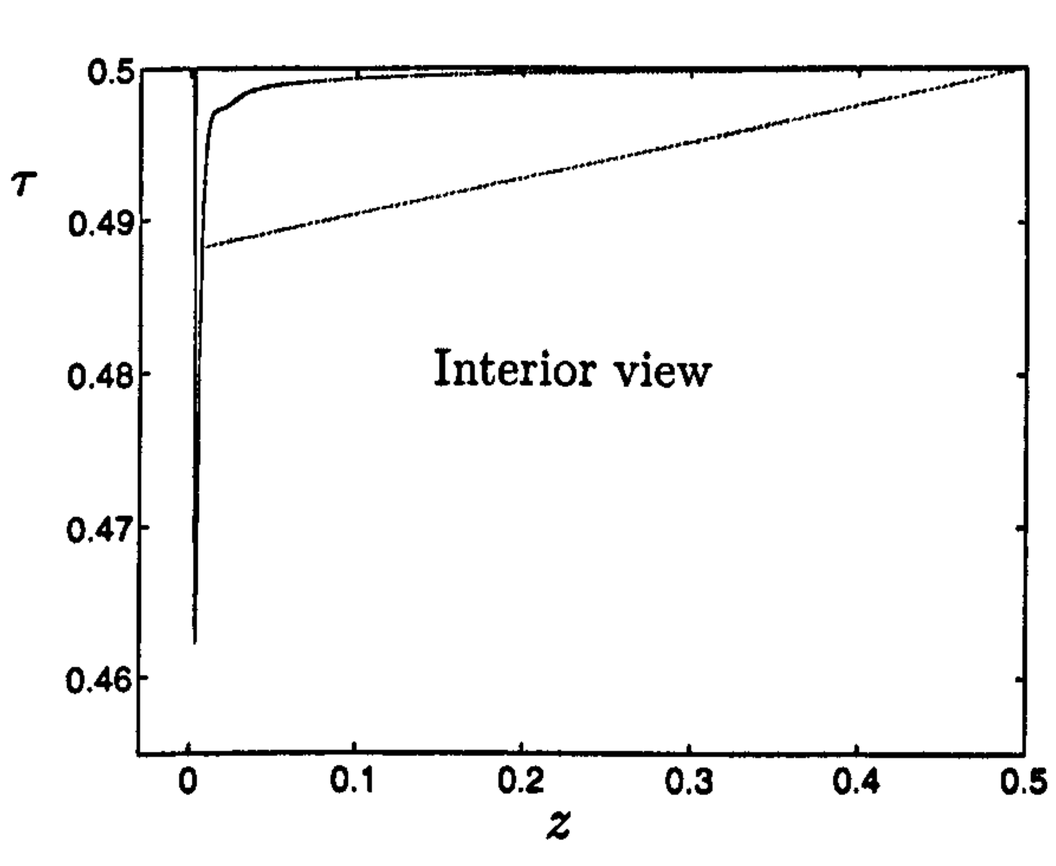


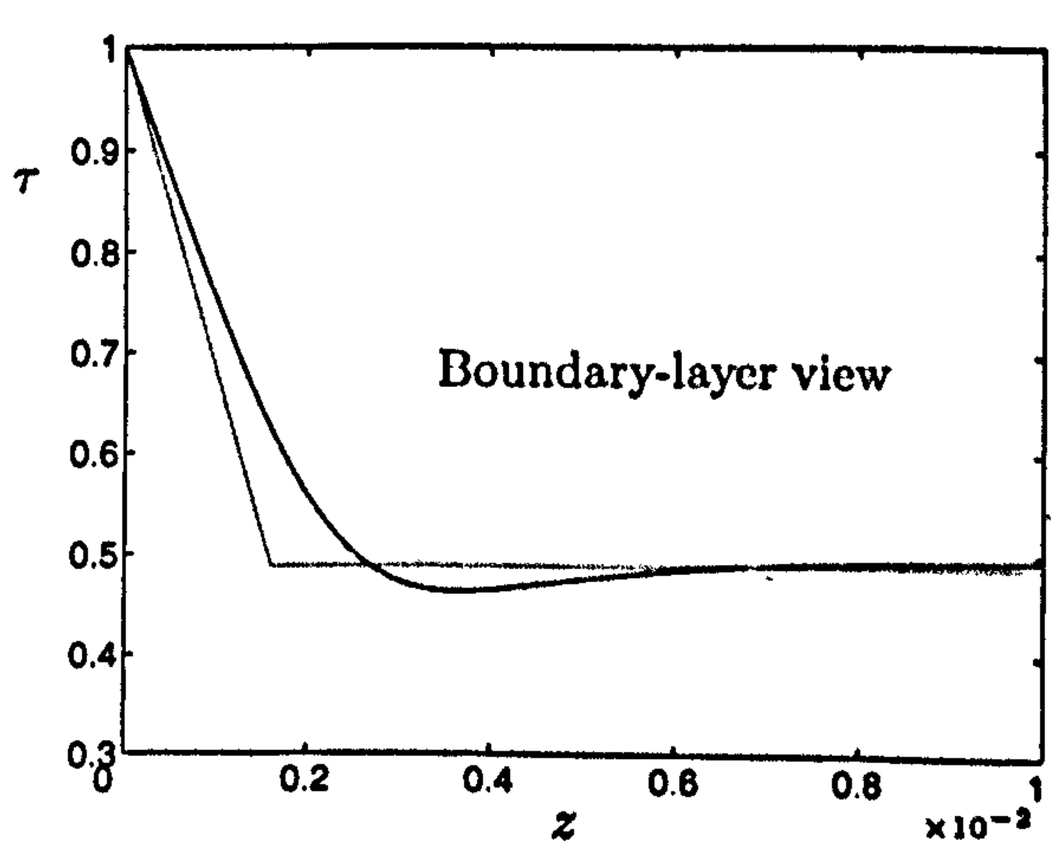


Figure 5.13: Comparing the no-slip optimal solution with the test function at $Ra = 4 \times 10^9$. At this value of $Ra$ the optimal solution is 4-$k$.

## 5.5 Discussion

To conclude, it is clear that there is no one-size-fits-all family of test functions with the power to produce optimal scaling for both boundary conditions covered here. The $(\delta, p)$-family is suited to stress-free but not to no-slip conditions. More thought needs to be given to constructing test functions suitable to attaining the optimal scaling for no-slip boundary conditions. It is not at all clear that sticking with piecewise linear profiles will enable one to to reach the goal of a $Ra^{1/3}$ scaling. The evidence in the interior view of figure 5.12 suggests that higher order polynomials should be used to approximate the over-shoot and second boundary layer structure.

We end this Chapter with plots, figures 5.14 and 5.15, of the conservative upper bounds calculated in this Chapter and the optimal upper bounds of Chapter 4 scaled by the optimal asymptotic scalings. These figures represent the climax of this research project. As a final parting comment on Chapters 4 and 5 we note that the no-slip problem while being accessible to the traditional multi-$k$ asymptotic analysis pioneered by Busse (1969*b*) is ill-suited to a conservative bound analysis using $(\delta, p)$-family of test functions. Conversely, the stress-free problem seems well-suited to the $(\delta, p)$-family but may not be soluble by traditional multi-$k$ analysis.

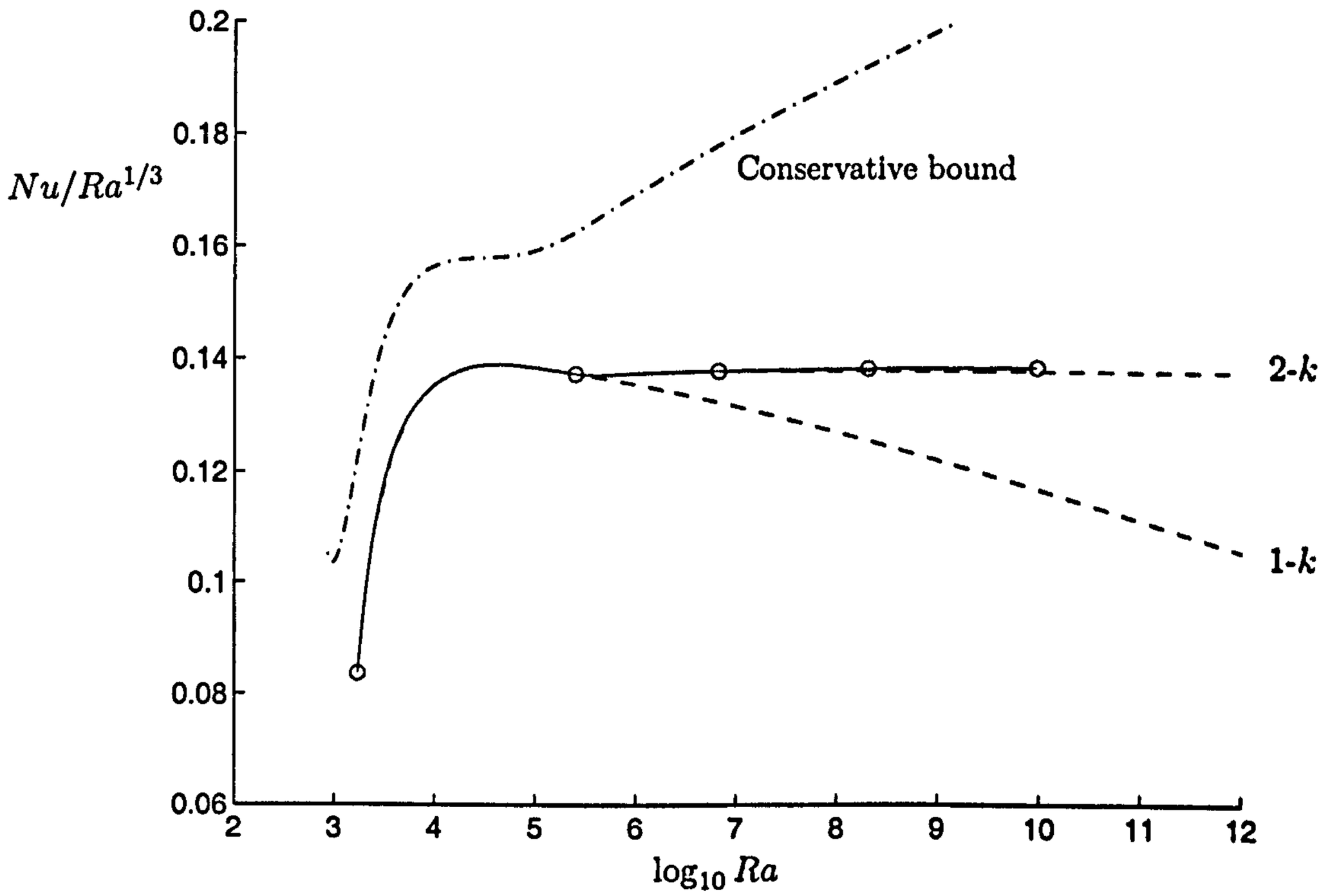


Figure 5.14: [No-slip] A comparison of the conservative bound and the optimal bound calculated in Chapter 4 scaled by the optimal asymptotic scaling of $Ra^{1/3}$. The dot-dash curve is the conservative upper bound which scales as $Ra^{7/20}$. The solid curve is the optimal bound and the circles represent wavenumber bifurcation points for the optimal solution. Dashed lines show the behaviour of the 1-$k$ and 2-$k$ bounds extended beyond the points after which they are no longer valid upper bounds.

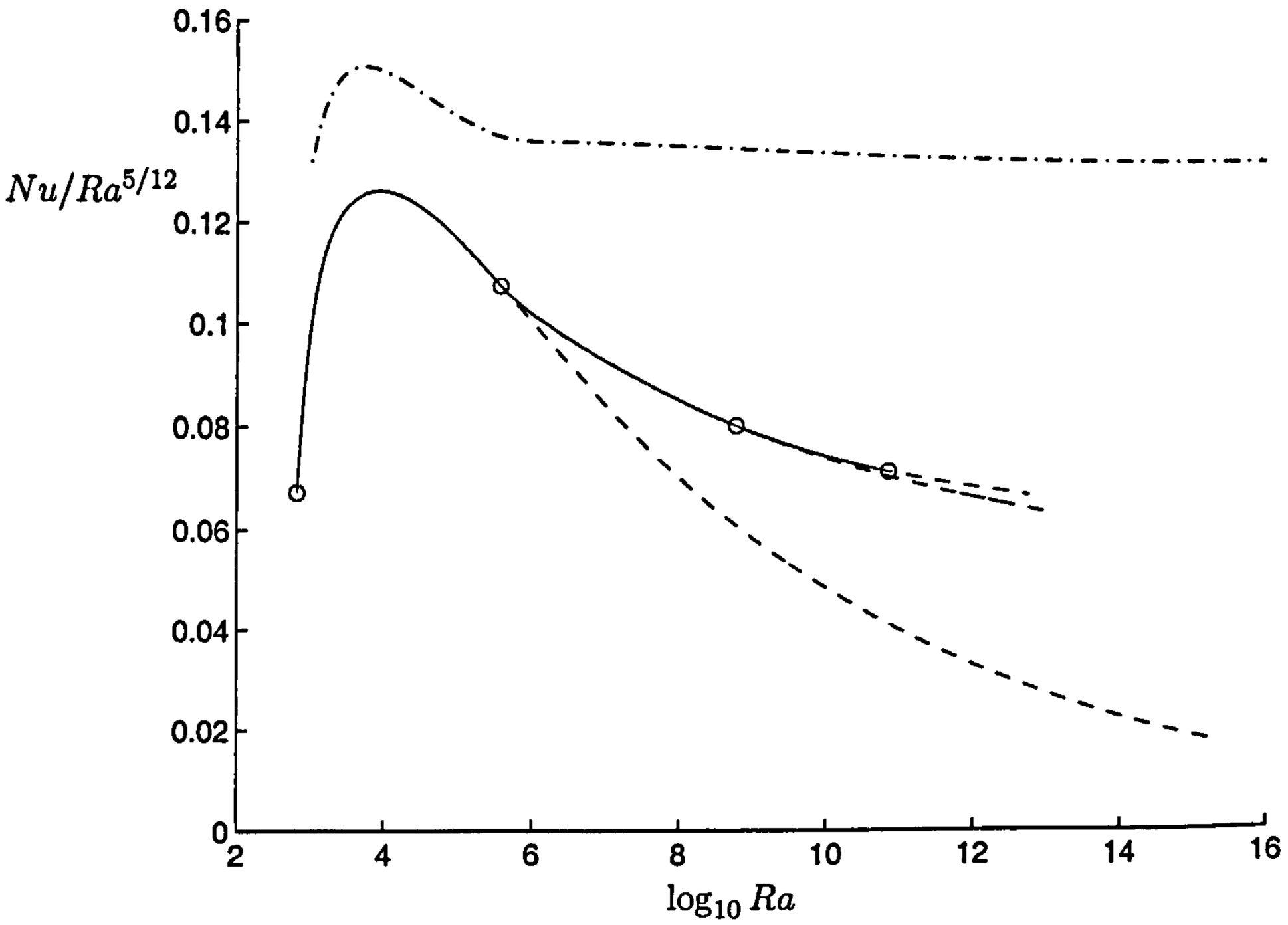


Figure 5.15: [Stress-free] A comparison of the conservative bound and the optimal bound calculated in Chapter 4 scaled by the best guess for the optimal asymptotic scaling of $Ra^{5/12}$ (in the absence of any extra knowledge of the asymptotic behaviour for the optimal solution). The dot-dash curve is the conservative upper bound which scales as $Ra^{5/12}$. The solid curve is the optimal bound and the circles represent wavenumber bifurcation points for the optimal solution. Dashed lines show the behaviour of the 1-$k$, 2-$k$ and 3-$k$ bounds extended beyond the points after which they are no longer valid upper bounds.

# Chapter 6

# Miscellaneous results

This Chapter contains two short results which are intended to be complementary to the material in Chapters 2 to 5. The first result relates to the balance parameter and is applicable to all Chapters, while the second is an empirical result relating to the PCF bounding problem.

## 6.1 Balance parameters

In this section we will address the issue of whether optimisation over the balance parameter, first introduced by Nicodemus *et al.* (1997*a*), can have any significant effect on the upper bounds. Most importantly can the choice of balance parameter produce a change in the asymptotic scaling exponent or does it only affect the numerical prefactor? We analyse the two standard CDH bounding problems considered in this thesis: plane Couette flow and infinite Prandtl number convection in the limit of large control parameter ($Re$ or $Ra$).

### 6.1.1 The generic form of CDH problems

We will first show that the two bounding problems considered in this thesis have the same form except that in the infinite Prandtl number problem there is an associated point-wise constraint. To show this let us begin by considering the plane Couette flow Lagrangian in Chapter 2

$$D = \frac{\lambda^2}{4(\lambda-1)}\langle(\phi' + Re)^2\rangle + Re^2 - \mathcal{H}_{(\phi,\lambda)}(\widehat{\nu}) \tag{6.1}$$

where $\mathcal{H}_{(\phi,\lambda)}(\widehat{\nu}) = \langle|\nabla\widehat{\nu}|^2\rangle + \lambda\langle\phi'\widehat{\nu}_1\widehat{\nu}_3\rangle$. The spectral constraint requires that $\mathcal{H}_{(\phi,\lambda)}(\widehat{\nu}) \geq 0$ for any divergence-free $\widehat{\nu}$ satisfying Dirichlet boundary conditions. The Reynolds number dependence is contained in the boundary conditions for $\phi(z)$. If we transform $\phi \longrightarrow \phi/Re$ the background now satisfies

$$\phi(\pm\tfrac{1}{2}) = \mp\tfrac{1}{2}$$

and a corresponding scaling of $\widehat{\nu}$ brings equation (6.1), once divided through by $Re^2$, into the form

$$\widetilde{D} = \frac{\lambda^2}{4(\lambda-1)}(\|\phi'\|^2 - 1) - \widetilde{\mathcal{H}}_{(\phi,\lambda)}(\widehat{\nu}). \tag{6.2}$$

The quadratic functional now hides the $Re$-dependence as follows

$$\widetilde{\mathcal{H}}_{\phi}(\widehat{\nu}) = \langle|\nabla\widehat{\nu}|^2\rangle + R\langle\phi'\widehat{\nu}_1\widehat{\nu}_3\rangle \tag{6.3}$$

where $R = \lambda\, Re$. We know from Chapter 2 that the optimal scaling for this problem is $\widetilde{D} = \mathcal{O}(Re)$. Given any function $\phi$ there exists a critical point $R = R_c$ below which the spectral constraint is satisfied and for $R > R_c$ the spectral constraint does not hold. The calculation of the critical Reynolds number is therefore independent of the balance parameter. For the particular $\phi$ under consideration the best possible bound available will be achieved by at once maximising $Re$ and minimising the prefactor $\lambda^2/4(\lambda-1)$: the optimal $\lambda$ will be contained in the interval $[1,\infty)$.

Now let us consider the Lagrangian in the infinite Prandtl number problem

$$N = \frac{\lambda^2}{4(\lambda-1)}(\|\tau'\|^2 - 1) - \mathcal{H}_{(\tau,\lambda)}(w,\theta), \tag{6.4}$$

where $\mathcal{H}_{(\tau,\lambda)}(w,\theta) = \langle|\nabla\theta|^2\rangle + \lambda\langle\tau' w\theta\rangle$. The spectral constraint $\mathcal{H}_{(\tau,\lambda)}(w,\theta) \geq 0$ must be fulfilled by all single-mode fields $(w,\theta)$ satisfying the pointwise constraint $\nabla^4 w + Ra\nabla_H^2\theta = 0$ and boundary conditions in figure 4.1. Equation (6.4) already has a strong similarity to equation (6.2), if we let $w \longrightarrow Ra^{1/2}w$ and $\theta \longrightarrow Ra^{-1/2}\theta$ then the parametric dependence also moves to the spectral constraint

$$\widetilde{\mathcal{H}} = \langle|\nabla\theta|^2\rangle + R\langle\tau' w\theta\rangle \geq 0 \quad \text{for all } \textit{suitable } (w,\theta) \tag{6.5}$$

where as before $R = \lambda\, Ra$. Therefore, the same argument for a critical $R$ independent of the choice of $\lambda$ also holds for this convection problem.

### 6.1.2 A scaling assumption

Consider a family of functions $\phi(R)$ that marginally satisfy the spectral constraint (SC-neutral functions parametrised by $R$). Optimisation over the balance parameter which remains is set aside until later. Here we may be considering functions like the two-parameter piecewise linear profiles used in Chapter 5 or optimal profiles with no optimisation over $\lambda$ carried out. Now assume that we know the scaling of the upper bound and that it has the form of a power-law scaling

$$\|\phi'\|^2 \sim R^\gamma. \tag{6.6}$$

In the following discussion we will show that this scaling assumption implies that the optimal choice of $\lambda$ is a constant and we will give a formula for its derivation.

### 6.1.3 Theorem: $\lambda = \mathcal{O}(1)$

The family of functions $\phi(R)$ yields the upper bound

$$\tilde{D} \leq \frac{\lambda^2}{4(\lambda-1)}(\|\phi'\|^2 - 1) \tag{6.7}$$

where the optimal $\lambda$ is as yet unknown. Assuming that to first order $\|\phi'\|^2 = cR^\gamma$ we can differentiate the right hand side (6.7) with respect to $\lambda$:

$$\frac{\lambda^2-2\lambda}{4(\lambda-1)^2}cR^\gamma + \frac{\lambda^2}{4(\lambda-1)}\frac{\mathrm{dR}}{\mathrm{d}\lambda}\gamma cR^{\gamma-1}$$

and set this to zero to find its maxima. Noting that $R = \lambda Re$, in which case $\mathrm{d}R/\mathrm{d}\lambda = Re$, we have

$$\frac{\lambda-2}{\lambda-1}R^\gamma + \gamma Re\lambda R^{\gamma-1} = 0,$$

which implies that

$$\gamma = \frac{2-\lambda}{\lambda-1}$$

or rearranging

$$\lambda = \frac{2+\gamma}{1+\gamma}. \tag{6.8}$$

To summarise this proves that the optimal choice for $\lambda$, given the asymptotic hypothesis (6.6), is an $\mathcal{O}(1)$ constant and is calculated by formula (6.8).

Owing to the similarities of the plane Couette flow and infinite Prandtl number convection bounding problems the formula for the optimal asymptotic value of $\lambda$ is

the same. For PCF $\gamma = 1$ and therefore the optimal $\lambda = 3/2$ by equation (6.8); which agrees with the prediction in Kerswell (1997). For infinite Prandtl number convection with no-slip boundary conditions $\gamma = 1/3$ and therefore the optimal $\lambda = 7/4$. These limiting values are confirmed by the numerical calculation of the corresponding optimal solution in Chapter 2 and Chapter 4.

This result depends on the exact manner in which the $\lambda$ and $Re$ (or other control parameter) dependence appears in the spectral constraint. More complex bounding problems, in which the spectral constraint is not parametrised by a single variable, here $R = \lambda Re$, are not covered by this result.

It can be shown that this result would also hold true if the upper bound scaled like $Ra^{\gamma_1}(\log Ra)^{\gamma_2}$ for some constants $\gamma_1$ and $\gamma_2$. Equation (6.8) would still be true to leading order with first correction being a constant multiple of $(\log Ra)^{-1}$. The rate of convergence of $\lambda$ to its limiting value, would then be logarithmic instead of polynomial and signs of convergence might be hard to spot in numerical data spanning twenty decades of $Ra$. We note this because the optimal $\lambda$ in the 1-$k$ no-slip problem experiences a logarithmically slow convergence rate.

### 6.1.4 Conservative bounds and balance parameters

The optimal choice of balance parameter discussed here is not globally optimal for all $Re$. It is only an asymptotic result owing to the analysis depending on knowledge of the slope of the bound with control parameter. To connect smoothly to energy stability the balance parameter $\lambda$ takes the value 1 at $Re = Re_c$. The balance parameter then converges to its limiting value at the same rate as the upper bound exponent converges to $\gamma$.

This result also holds true for trial functions estimates of the optimal upper bound. In the first paper to include the balance parameter, Nicodemus *et al.* (1997*a*), employing the simplest one-parameter test functions, the authors showed that the optimal asymptotic balance parameter was $\lambda = 3/2$ for the shear flow problem which led to improvement of the prefactor of the upper bound estimate by 27/32. In fact, this asymptotic limit is correct for any family of test functions; Nicodemus *et al.* (1997*b*) also calculated an upper bound estimate using two-parameter piecewise quadratic profiles with a numerical treatment of the spectral constraint and found

the same asymptotic behaviour for $\lambda$.

## 6.2 Empirical mean profiles

In this section we study the effect of stipulating the shape of the turbulent mean profile on the shear flow bounding problem. Our objective in imposing a turbulent mean was to investigate the internal consistency of the von Kármán–Prandtl logarithmic friction law for the dissipation, or equivalently drag, with asymptotic behaviour as $Re \to \infty$,

$$D \sim \frac{Re^3}{(\log Re)^2}$$

in units of $\nu^3/h^4$. Using a simple one-parameter background field with zero interior gradient we will show that imposition of a certain empirical mean profile leaves the optimal asymptotic scaling of the upper bound unchanged not adding any logarithmic factors.

The traditional empirical mean profile is parametrised by the friction units $u_\tau$ and $Re_\tau$. The change in the mean velocity away from the wall is denoted $U(z)$, which, to be consistent with Chapter 2, is $U = \frac{1}{2}Re - \overline{u_1}$. In the non-dimensionalisation of Chapter 2 the wall shear is

$$\tau = -\left.\frac{\partial \overline{u_1}}{\partial z}\right|_{z=\frac{1}{2}}$$

which (on taking the power integral of the Navier–Stokes equation) is computed to be $\tau = D/Re$. The friction velocity length scale is then defined by $u_\tau^2 = \tau$, which implies that $u_\tau = \sqrt{D/Re}$, and the friction Reynolds number is $Re_\tau = \sqrt{D/Re}$. Now we can define the empirical mean profile $U^+ = U/u_\tau$, in the coordinate $z^+ = Re_\tau(z+\frac{1}{2})$, by,

$$U^+ = \begin{cases} z^+ & \text{for } 0 \le z^+ \le d^+ \\ a \ln z^+ + b & \text{for } d^+ < z^+ \le Re_\tau \end{cases}$$

where $a$ and $b$ are fitting parameters routinely taken to be 2.5 and 5.5 respectively. This description leads to a meeting point of the inner (viscous sublayer) and logarithmic outer region at $d^+ \approx 11$. For simplicity we are considering a mean profile without a *buffer* layer between the viscous and inertial sublayers. A sketch of this mean profile is presented in figure 6.1.

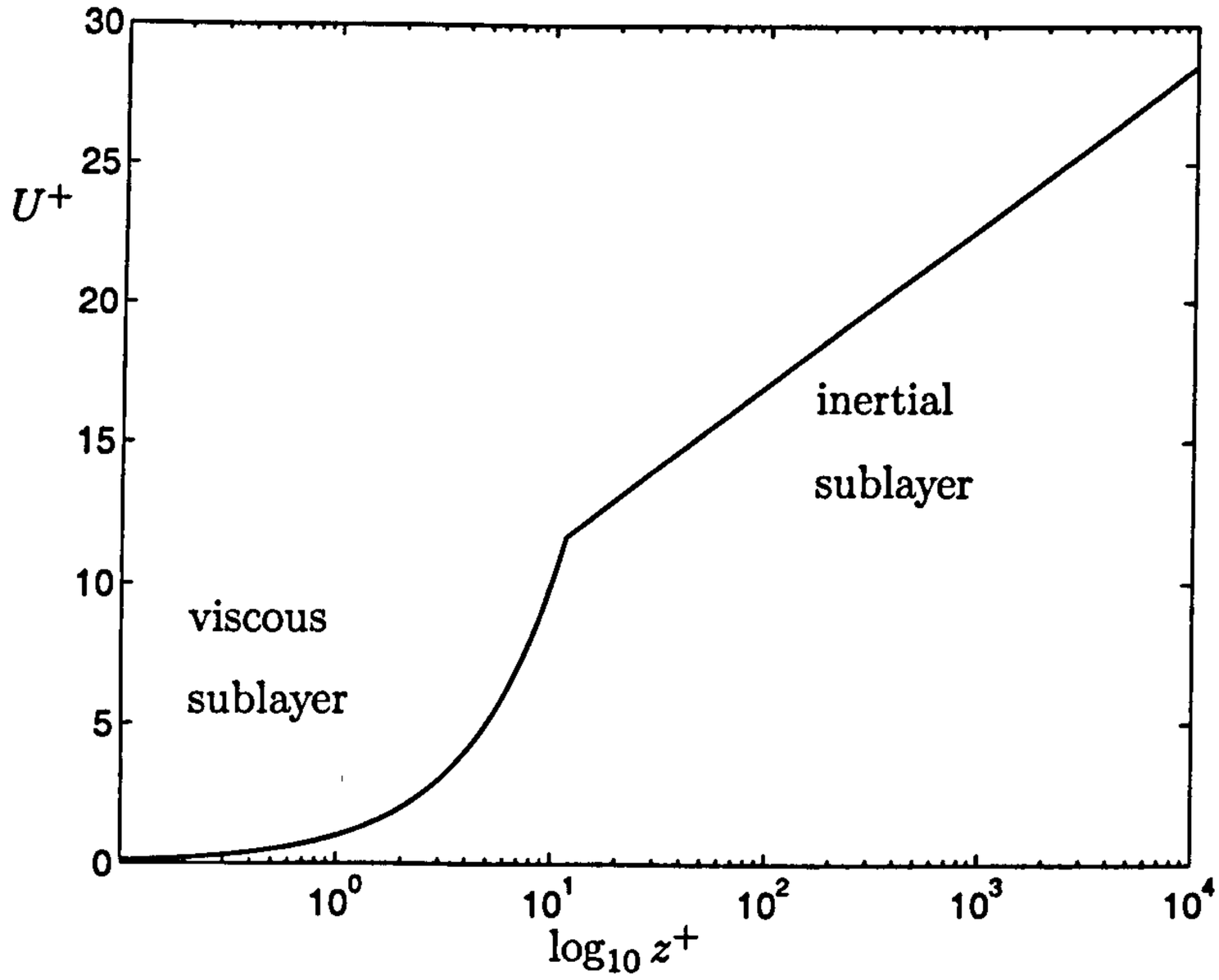


Figure 6.1: Empirical mean profile $U^+$.

Note that in the standard problem it is found that $D = \mathcal{O}(Re^3)$ and hence in that case the friction Reynolds number scales as $Re$ ($Re_\tau \sim Re$). We disregard what actually happens mid-channel to the velocity profile and concentrate instead on satisfying the law of the wall at the boundary. As $Re \to \infty$ presumably the well mixed centre of the channel will have little effect on the slope of the mean profile. Estimates of integrals related to $U^+$ will be made with this approximation in mind. Because the mean velocity is assumed odd across the channel we need only enforce that $\phi + \overline{\nu_1} = -\frac{1}{2}Re + U$ for $z \in [0, \frac{1}{2}]$, where $U$ is the change in the mean velocity away from the wall.

### 6.2.1 Imposing a mean profile

Consider the original CDH problem with one-dimensional uni-directional background field $\phi(z)\widehat{x}$ with $\boldsymbol{u} = \boldsymbol{\nu} + \phi(z)\widehat{x}$. Using the Lagrange multiplier $\chi(z)$, with boundary conditions $\chi(\frac{1}{2}) = \chi(0) = 0$, for imposing the mean velocity profile $U(z) = U^+(z)u_\tau$, the extended Lagrangian is

$$\begin{aligned}\mathcal{L} = \langle|\nabla \boldsymbol{u}|^2\rangle &- \langle a\boldsymbol{\nu} \cdot \left[\boldsymbol{u}_t + \boldsymbol{u} \cdot \nabla \boldsymbol{u} + \nabla p - \nabla^2 \boldsymbol{u}\right]\rangle \\ &- \langle \chi''(z) \left[\phi + \overline{\nu_1} + \tfrac{1}{2}Re - U(z)\right]\rangle.\end{aligned} \tag{6.9}$$

The novel feature is that the fluctuation field and background are connected via $\phi + \overline{\nu_1} = -\frac{1}{2}Re + U$. The non-dimensional scheme in Chapter 2 has the control parameter dependence $Re$ on the boundary conditions $\phi(\pm\frac{1}{2}) = \mp\frac{1}{2}Re$. In terms of $\phi$ and $\boldsymbol{\nu}$ the Lagrangian is

$$\begin{aligned}\mathcal{L} = \langle \phi'^2 - \chi''\phi - \{(a-1)|\nabla\boldsymbol{\nu}|^2 + a\nu_1\nu_3\phi' \\ - (a-2)\nu_1\phi'' + \chi''\nu_1 - \chi''(\tfrac{1}{2}Re - U)\}\rangle.\end{aligned} \tag{6.10}$$

The variation derivatives of $\mathcal{L}$ have an extra $\chi''$ terms as follows

$$\frac{\delta\mathcal{L}}{\delta\boldsymbol{\nu}} = 2(a-1)\nabla^2\boldsymbol{\nu} - a\phi' \begin{bmatrix}\nu_3\\0\\\nu_1\end{bmatrix} - \nabla p + \left[(a-2)\phi'' - \chi''\right]\widehat{\boldsymbol{x}} = \mathbf{0},$$

$$\frac{\delta\mathcal{L}}{\delta\chi''} = \phi + \overline{\nu_1} - (\tfrac{1}{2}Re - U) = 0.$$

Splitting field $\boldsymbol{\nu}$ into mean and fluctuating parts, $\boldsymbol{\nu} = \overline{\nu_1}\widehat{\boldsymbol{x}} + \widehat{\boldsymbol{\nu}}$, then $\delta\mathcal{L}/\delta\boldsymbol{\nu}$ separates into the two parts

$$\frac{\delta\mathcal{L}}{\delta\widehat{\boldsymbol{\nu}}} = 2(a-1)\nabla^2\widehat{\boldsymbol{\nu}} - a\phi' \begin{bmatrix}\widehat{\nu}_3\\0\\\widehat{\nu}_1\end{bmatrix} - \nabla p = \mathbf{0},$$

$$\frac{\delta\mathcal{L}}{\delta\overline{\nu_1}} = 2(a-1)\overline{\nu_1}'' + (a-2)\phi'' - \chi'' = 0.$$

The first is the familiar $\widehat{\boldsymbol{\nu}}$ variational from the standard problem and the second now contains a $-\chi''$ term. Using the boundary conditions we can integrate the second expression twice, as long as we stipulate that $\chi(\pm\frac{1}{2}) = 0$, to find that

$$\overline{\nu_1} = -\frac{a-2}{2(a-1)}(\phi + Rez) - \frac{\chi}{2(a-1)}.$$

Now let's drop $\chi''$ and impose the constraint explicitly by substituting $\overline{\nu_1} = (\frac{1}{2}Re - U) - \phi$ into (6.10). In terms of the mean fields and $\widehat{\boldsymbol{\nu}}$ the Lagrangian becomes:

$$\begin{aligned}\mathcal{L} &= \langle \phi'^2 - (a-1)\overline{\nu_1}'^2 + (a-2)\overline{\nu_1}\phi''\rangle - \mathcal{G}_\phi(\widehat{\boldsymbol{\nu}}) \\ &= \langle U'^2 - aU'(\phi' - U')\rangle - \mathcal{G}_\phi(\widehat{\boldsymbol{\nu}})\end{aligned} \tag{6.11}$$

where $\mathcal{G} = (a-1)\langle|\nabla\widehat{\boldsymbol{\nu}}|^2\rangle + a\langle\phi'\widehat{\nu}_1\widehat{\nu}_3\rangle$. An upper bound is therefore available to us if $\phi$ fulfils the spectral constraint: $\mathcal{G} \geq 0$ for all divergence-free single-mode fields satisfying Dirichlet boundary conditions.

Now substitute $U = \sqrt{D/Re}\,U^+$ into expression (6.11)

$$D \leq \left\langle \frac{D}{Re} U^{+\prime 2} - a\sqrt{\frac{D}{Re}} U^{+\prime} \left( \phi' - \sqrt{\frac{D}{Re}} U^{+\prime} \right) \right\rangle - \mathcal{G}_\phi(\widehat{\nu}),$$

and collecting terms

$$D \left( 1 + \frac{1}{Re} \langle (a-1) U^{+\prime 2} \rangle \right) - a \left( \frac{D}{Re} \right)^{\frac{1}{2}} \langle U^{+\prime} \phi' \rangle + \mathcal{G}_\phi(\widehat{\nu}) \leq 0,$$

and solving for $D$ amongst SC-stable background fields $\{\phi \mid \mathcal{G}_\phi \geq 0\}$ we find

$$D \leq \inf_{a,\phi} \frac{a^2 \langle U^{+\prime} \phi' \rangle^2}{\left[ 1 + \frac{1}{Re} \langle (a-1) U^{+\prime 2} \rangle \right]^2 Re}. \tag{6.12}$$

Let us investigate the scaling of this upper bound on $D$ using the simplest one-parameter piecewise linear trial function. (These are the piecewise linear functions zero-valued in the interior and changing from $\pm\frac{1}{2}Re$ at the boundary to zero in a small distance $\delta$ from the wall.) If $\delta_0$ is the width of the viscous sublayer for the profile $U^+$ then for some $\delta < \delta_0$ the spectral constraint will be satisfied (from Doering & Constantin, 1994, and others we know that the behaviour of the optimal trial function is $\delta \sim Re^{-1}$ ). Since $U^+ = z^+ = (z + \frac{1}{2})(D/Re)^{\frac{1}{2}}$ in the viscous sublayer we can calculate the numerator of expression (6.12) as follows:

$$\langle U^{+\prime} \phi' \rangle = \int_{\frac{1}{2}-\delta}^{\frac{1}{2}} \sqrt{\frac{D}{Re}} \frac{Re}{\delta} \mathrm{d}z = \sqrt{D\,Re},$$

and this integral is uniform in $\delta \leq \delta_0$.

Now we can make $\delta$ as small as we like without changing the value of $\langle U^{+\prime} \phi' \rangle$ and in so doing we guarantee SC-stability, therefore the infimum over $a$ is attained for $a \to \infty$ and we have

$$D \leq \frac{Re^2 D}{\langle U^{+\prime 2} \rangle^2}. \tag{6.13}$$

The calculation of the denominator is more sensitive to the exact manner in which the mean profile connects on to the value of the velocity at the centre-line. However, the contribution will certainly be sub-dominant in this mid-channel region so we

neglect its contribution. Given $\delta_0 \sim \sqrt{D/Re}$

$$\begin{aligned}\langle U^{+\prime 2}\rangle &= \int_{\frac{1}{2}-\delta}^{\frac{1}{2}} \frac{D}{Re}\mathrm{d}z + \int_{z>0}^{\frac{1}{2}-\delta} \left(\frac{11}{1+2z}\right)^2 \mathrm{d}z \\ &= \mathcal{O}\left(\sqrt{\frac{D}{Re}}\right)\end{aligned}$$

and using the fact that $D_{lam} = Re^2$ is a lower bound. Substituting this scaling result into (6.13) we find that $D = \mathcal{O}(Re^3)$ in units of $\nu^3/h^4$ or $D = \mathcal{O}(1)$ in units of $U^3/h$. Therefore, to summarise, the form of the empirical mean profile $U(z) = u_\tau U^+(z)$ is not inconsistent with a $1/(\log Re)^2$ factor in the asymptotic scaling of the global energy dissipation rate. We still obtain a Kolmogorov type scaling result in which the dissipation rate is not assumed to vanish as $\nu \to 0$ (or $Re \to \infty$).

# Chapter 7

# Conclusions

We began this thesis by describing the germination of the Howard–Busse method from the seed of Malkus's theories of turbulent convection. The discovery of an asymptotic multi-wavenumber method of solution by Busse, for Howard's problem with incompressibility, launched the theory into many new directions other than turbulent convection (Busse's 1978 review is a testament to this). Howard determined in his review article of 1972 that the optimum theory could be made more potent if direct estimates of a rigorous upper bound, or computation methods for solving the problems Euler–Lagrange equations, could be devised. The Constantin–Doering–Hopf method is the answer to the former requirement. This thesis work is, it is hoped, an answer to the second requirement that constructive methods for numerical solution of the optimal equations be available.

Kerswell's deduction in 1998 that the CDH method was a complementary, or dual, method for the HB method has provoked a pooling of tools in this subject. A numerical solution of the full CDH problem can be directly compared to Busse's asymptotic multi-$k$ solutions. In Chapter 2 we perform the first numerical solution of Busse's plane Couette variational problem. We show that the spectral constraint of the CDH method assists the solution programme by enabling clear branch switching between multi-mode solution branches — this feature is unique to the CDH technique and is not available to a solution by the HB method alone. Direct comparison is made between Busse's asymptotic solution and our numerical solution, calculated to high enough $Re$ such that asymptotic behaviour sets in; namely, one observes self-

similarity in the $k$-bifurcation diagram. Our solution supports Busse's predictions even at low $Re$ and our upper bound prefactor is only 17% lower than he predicts which is happily within published error estimates. The upper bound we present is a 20% reduction on the previous best published bound of Nicodemus *et al* (1998a).

Busse's assumption that the optimal fields are streamwise independent, and therefore two-dimensional, is used in the full solution of the optimal equations in Chapter 2. However, in Chapter 3 we show that at two well separated points in $Ra$ this assumption is correct, and is almost certainly uniformly valid. It is clear that to improve upon the upper bound in Chapter 2 addition information must be incorporated into the variational functional. A strategy for doing this is set out in the rest of Chapter 3. We consider a weak form of Malkus's second theory; that the turbulent mean profile is marginally linearly stable; and formulate a direct extension of the PCF variational problem. The Euler–Lagrange equations are slightly more involved for this problem because of the non-self-adjointness of the Orr–Sommerfeld equation. Our preliminary results show that standard optimal solutions of Chapter 2 are linearly stable. In future work we plan to find a path from the solution branch in Chapter 2 to the LS-neutral branch of solution using continuation methods.

In Chapters 4 and 5 we considered a novel bounding problem —infinite Prandtl number convection— with a pointwise linear time-independent momentum constraint. This problem was particularly of interest due to the dissymmetry between the HB approach estimation for $Nu$ of $\mathcal{O}(Ra^{1/3})$, and the CDH approach invoking conventional functional estimates of $\mathcal{O}(Ra^{2/5})$. Interestingly, the CDH method together with some unconventional extra information yields an improved estimate of the form $\mathcal{O}(Ra^{1/3}(\log Ra)^{2/3})$ while Chan's $n$-$k$ asymptotic solution have associated $Nu$ which scale as $f(n)\left[Ra^{1/3}(\log Ra)^{2/3}\right]^{1-10^{-n}}$; where the asymptotic scaling of $Ra^{1/3}$ is arrived at by optimising over $n$, the number of boundary layers. This intrigue set the scene for the work contained in Chapters 4 and 5. In Chapter 4 we solved the optimal equations for both no-slip and stress-free boundary conditions. The no-slip solution supported Chan's asymptotic exponent of 1/3. In Chapter 5 enhanced test-functions were employed to calculate conservative estimates but again as in earlier research the elusive 1/3 exponent was not within our grasp. Worthy future investigation could focus on the role of the over-shoot observed in the mean

temperature just outside of the thermal boundary layer. The variant stress-free boundary condition was also studied and the optimal and conservative bound solution were found to exhibit subtly different properties from the no-slip problem. The numerical evidence enabled Kerswell to solve the 1-$k$ and 2-$k$ asymptotic problems. The intrigue of Chan's infinite Prandtl number convection problem thus lives on.

In the last Chapter two small results were described. The first of these states that the balance parameter is always an $\mathcal{O}(1)$ number for the bounding problems studied here. Therefore, it cannot have an effect on the asymptotic scaling of the upper bound, and a formula for its asymptotic value in terms of the asymptotic upper bound exponent is stated. The second result in Chapter 6 attempts to imposes an empirical mean velocity profile on the standard PCF problem in order to improve the scaling of the dissipation rate bound. The hope was to try to induce logarithmic factors in the dissipation bound, however, the imposition of the mean failed to alter the asymptotic scaling of $D = \mathcal{O}(Re^3)$.

As well as the future directions of the work discussed in the previous paragraphs there are a number of problems of special interest in bounding theory at present for which our methods could be fruitfully applied. Problems for which additional constraints can easily be included; such as two-dimensional convection with stress-free boundaries including the enstrophy constraint; are logical starting points. Problems which reduce to near two-dimensionality, such as pipe flow for which the axial symmetry implies only integer wavenumbers in the axial direction and hence a $(2+\epsilon)$-dimensional solution space. Then one can pose the question: are upper bounds for two-dimensional fluid flows more potent than for three-dimensional ones?

# Bibliography


BOYD, J. P. 2001 *Chebyshev and Fourier Spectral Methods*, 2nd edn. Dover.

BUSSE, F. H. 1968*a* Eine neuartige Methode zur theoretischen Behandlung turbulenter Transportvorgänge. *Z. Angew. Math. Mech.* **48**, T187–T190.

BUSSE, F. H. 1968*b* On the mean field problem of thermal convection. *Tech. Rep.* 8. Max-Planck-Institut für Physik und Astrophysik.

BUSSE, F. H. 1969*a* Bounds on the transport of mass and momentum by turbulent flow. *Z. Angew. Math. Phys.* **20**, 1–14.

BUSSE, F. H. 1969*b* On Howard's upper bound for heat transport by turbulent convection. *J. Fluid Mech.* **37**, 457–477.

BUSSE, F. H. 1970 Bounds for turbulent shear flow. *J. Fluid Mech.* **41**, 219–240.

BUSSE, F. H. 1978 The optimum theory of turbulence. *Adv. Appl. Mech.* **18**, 77–121.

BUSSE, F. H. 1996 Bounds for properties of complex systems. In *Nonlinear Physics of Complex Systems - Current Status and Future Trends* (ed. J. Parisi, S. Müller & W. Zimmermann). Springer-Verlag.

CHAN, S. K. 1971 Infinite Prandtl number turbulent convection. *Stud. Appl. Math.* **50** (13-49).

CHANDRASEKHAR, S. 1961 *Hydrodynamic and hydromagnetic stability*. Oxford: Clarendon Press.

CONSTANTIN, P. & DOERING, C. R. 1995 Variational bounds on energy-dissipation in incompressible flows: II. Channel flow. *Phys. Rev.* E **51**, 3192–3198.

CONSTANTIN, P. & DOERING, C. R. 1999 Infinite Prandtl number convection. *J. Stat. Phys.* **94**, 159–172.

CONSTANTIN, P., HALLSTROM, C. & PUTKARADZE, V. 2001 Logarithmic bounds for infinite Prandtl number rotating convection. *J. Math. Phys.* **42**, 773–783.

DOERING, C. R. & CONSTANTIN, P. 1992 Energy dissipation in shear driven turbulence. *Phys. Rev. Lett.* **69**, 1648–1651.

DOERING, C. R. & CONSTANTIN, P. 1994 Variational bounds on energy dissipation in incompressible flows: Shear flow. *Phys. Rev.* E **49**, 4087–4099.

DOERING, C. R. & CONSTANTIN, P. 1996 Variational bounds on energy dissipation in incompressible flows: III. Convection. *Phys. Rev.* E **53**, 5957–5981.

DOERING, C. R. & CONSTANTIN, P. 1998 Bounds for heat transport in a porous layer. *J. Fluid Mech.* **376**, 263–296.

DOERING, C. R. & CONSTANTIN, P. 2001 On upper bounds for infinite Prandtl number convection with or without rotation. *J. Math. Phys.* **42**, 784–795.

DOERING, C. R. & GIBBON, J. D. 1995 *Applied Analysis of the Navier–Stokes Equations*. Cambridge University Press.

DOERING, C. R. & HYMAN, J. M. 1997 Energy stability bounds on convective heat transport: numerical study. *Phys. Rev.* E **55**, 7775–7778.

DOERING, C. R., SPIEGEL, E. A. & WORTHING, R. A. 2000 Energy dissipation in a shear layer with suction. *Phys. Fluids* **12**, 1955–1968.

DRAZIN, P. & REID, W. H. 1981 *Hydrodynamic stability*. Cambridge University Press.

DRISCOLL, J. & HEALY, D. 1994 Computing fourier transforms and convolutions on the 2-sphere. *Adv. in Appl. Math.* **15**, 202–250.

FOIAS, C., MANLEY, O., ROSA, R. & TEMAM, R. 2001 *Navier–Stokes Equations and Turbulence*. Cambridge University Press.

FOMIN, S. V. & GELFAND, I. M. 2000 *Calculus of Variations*. Dover.

FRISCH, U. 1995 *Turbulence: The Legacy of A. N. Kolmogorov*. Cambridge University Press.

GEBHARDT, T., GROSSMANN, S., HOLTHAUS, M. & LÖHDEN, M. 1995 Rigorous bound on the plane-shear-flow dissipation rate. *Phys. Rev.* E **51**, 360–365.

HOPF, E. 1941 Ein allgemeiner endlichkeitssatz der hydrodynamik. *Mathematische Annalen* **117**, 764–775.

HOWARD, L. N. 1963 Heat transport by turbulent convection. *J. Fluid Mech.* **17**, 405–432.

HOWARD, L. N. 1972 Bounds on flow quantities. *Ann. Rev. Fluid Mech.* 4, 473–494.

HOWARD, L. N. 1990 Limits on the transport of heat and momentum by turbulent convection with large scale flow. *Stud. Appl. Math.* **83**, 273–285.

IERLEY, G. R. 1997 A class of sparse spectral operators for inversion of powers of the Laplacian in N dimensions. *J. Sci. Comput.* **12** (1), 57–63.

IERLEY, G. R. & WORTHING, R. A. 2001 Bound to improve: a variational approach to convective heat transport. *J. Fluid Mech.* **441**, 223–253.

JOSEPH, D. D. 1976 *Stability of Fluid Motions I*. Springer-Verlag.

KERSWELL, R. R. 1997 Variational bounds on shear-driven turbulence and turbulent Boussinesq convection. *Physica* D **100**, 355–376.

KERSWELL, R. R. 1998 Unification of variational principles for turbulent shear flows: the background method of Doering–Constantin and Howard–Busse's mean-fluctuation formulation. *Physica* D **121**, 175–192.

KERSWELL, R. R. 1999 Variational principle for the Navier–Stokes equations. *Phys. Rev.* E **59**, 5482–5494.

KERSWELL, R. R. 2000 Lowering dissipation bounds for turbulent shear flows using a smoothness constraint. *Phys. Lett* A **272**, 230–235.

KERSWELL, R. R. 2001 New results in the variational approach to turbulent Boussinesq convection. *Phys. Fluids* **13**, 192–209.

KERSWELL, R. R. 2002 Upper bounds on general dissipation functionals in turbulent shear flows: revisiting the 'Efficiency' functional. *J. Fluid Mech.* **461**, 239–275.

KERSWELL, R. R. & SOWARD, A. M. 1996 Upper bounds for turbulent Couette flow incorporating the poloidal power constraint. *J. Fluid Mech.* **328**, 161–176.

MALKUS, W. V. R. 1954*a* Discrete transitions in turbulent convection. *Proc. Roy. Soc.* **225**, 185–195.

MALKUS, W. V. R. 1954*b* The heat transport and spectrum of thermal turbulence. *Proc. Roy. Soc.* **225**, 196–212.

MALKUS, W. V. R. 1956 Outline of a theory for turbulent shear flow. *J. Fluid Mech.* **1**, 521–.

NICODEMUS, R., GROSSMANN, S. & HOLTHAUS, M. 1997*a* Improved variational principle for bounds on energy dissipation in turbulent shear flow. *Physica* D **101**, 178–190.

NICODEMUS, R., GROSSMANN, S. & HOLTHAUS, M. 1997*b* Variational bound on energy dissipation in plane Couette flow. *Phys. Rev.* E **56**, 6774–6786.

NICODEMUS, R., GROSSMANN, S. & HOLTHAUS, M. 1998*a* The background flow method. Part 1. Constructive approach to bounds on energy dissipation. *J. Fluid Mech.* **363**, 281–300.

NICODEMUS, R., GROSSMANN, S. & HOLTHAUS, M. 1998*b* The background flow method. Part 2. Asymptotic theory of dissipation bounds. *J. Fluid Mech.* **363**, 301–323.

NICODEMUS, R., GROSSMANN, S. & HOLTHAUS, M. 1999 Towards lowering dissipation bounds for turbulent flows. *Eur. Phys. J.* B **10**, 385–396.

OTERO, J. 2002 Bounds for the heat transport in turbulent convection. PhD thesis, University of Michigan.

OTERO, J., DONTCHEVA, L. A., JOHNSTON, H., WORTHING, R. A., KURGANOV, A., PETROVA, G. & DOERING, C. R. 2004 High-Rayleigh-number convection in a fluid-saturated porous layer. *J. Fluid Mech.* **500**, 263–281.

OTERO, J., WITTENBERG, R. W., WORTHING, R. A. & DOERING, C. R. 2002 Bounds on Rayleigh–Bénard convection with an imposed heat flux. *J. Fluid Mech.* **473**, 191–199.

PLASTING, S. C. & KERSWELL, R. R. 2003 Improved upper bound on the energy dissipation in plane Couette flow: The full solution to Busse's problem and the Constantin–Doering–Hopf problem with one-dimensional background field. *J. Fluid Mech.* **477**, 363–379.

POPE, S. B. 2000 *Turbulent Flows*. Cambridge University Press.

RHEINBOLDT, W. C. & BURKARDT, J. V. 1983*a* ALGORITHM 596 a program for a locally parameterized continuation process. *ACM Trans. Math. Software* **9**, 236–241.

RHEINBOLDT, W. C. & BURKARDT, J. V. 1983*b* A locally parametrized continuation process. *ACM Trans. Math. Software* **9**, 215–235.

SOTIN, C. & LABROSS, S. 1999 Three-dimensional thermal convection in an isoviscous, infinite Prandtl number fluid heated from within and from below: applications to the transfer of heat through planetary mantles. *Phys. Earth Planet. Int.* **112**, 171–190.

TENNEKES, H. & LUMLEY, J. 1972 *A First Course in Turbulence*. MIT Press, Cambridge, MA.

VITANOV, N. K. 1998 Upper bound on the heat transport in a horizontal fluid layer of infinite Prandtl number. *Phys. Lett.* A **248**, 338–346.

VITANOV, N. K. 2000*a* Convective heat transport in a fluid layer of infinite Prandtl number: upper bounds for the case of rigid lower boundary and stress-free upper boundary. *Eur. Phys. J.* B **15**, 349–355.

VITANOV, N. K. 2000*b* Upper bounds on convective heat transport in a rotating fluid layer of infinite Prandtl number: Case of intermediate Taylor numbers. *Phys. Rev.* E **62**, 3581–3591.

VITANOV, N. K. 2000*c* Upper bounds on the heat transport in a fluid layer of infinite Prandtl number, rigid lower boundary and stress-free upper boundary. *Phys. Rev.* E **61**, 956–959.

VITANOV, N. K. & BUSSE, F. H. 1997 Bounds on the heat transport in a horizontal fluid layer with stress-free boundaries. *Z. angew. Math. Phys.* **48**, 310–324.